INVESTIGATION OF CHEMICAL AND ADSORPTION PROPERTIES OF CARBON NANOTUBES: BUILDING A BRIDGE FOR TECHNOLOGICAL APPLICATIONS OF CARBON NANOTUBES

by

Dmitry Kazachkin

Specialist, Chemistry, Novosibirsk State University, 2000

Master of Science, Chemical Engineering, University of Pittsburgh, 2006

Submitted to the Graduate Faculty of

Swanson School of Engineering in partial fulfillment

of the requirements for the degree of

Doctor of Philosophy

University of Pittsburgh

2009

UNIVERSITY OF PITTSBURGH

SWANSON SCHOOL OF ENGINEERING

This dissertation was presented

by

Dmitry Kazachkin

It was defended on

December 12, 2008
and approved by

J. Karl Johnson, Professor, Department of Chemical and Petroleum Engineering, University of Pittsburgh

Götz Veser, Professor, Department of Chemical and Petroleum Engineering, University of Pittsburgh

Radisav D. Vidic, Professor, Department of Civil and Environmental Engineering,

University of Pittsburgh

Dissertation Director: Eric Borguet, Professor, Department of Chemistry, Temple University and Adjunct Professor, Department of Chemical and Petroleum Engineering, University of Pittsburgh

INVESTIGATION OF CHEMICAL AND ADSORPTION PROPERTIES OF CARBON NANOTUBES: BUILDING A BRIDGE FOR TECHNOLOGICAL APPLICATIONS OF CARBON NANOTUBES

Dmitry Kazachkin, Ph.D.

University of Pittsburgh, 2009

In the present work, the results of investigations of the chemical, adsorption and optical properties of carbon nanotubes (CNTs) will be presented. A brief introduction describes CNTs, how they are produced, and how they are purified. Experimental investigations of the effect of air/HCl purification on the introduction of oxygen functionalities will be reported. It was established that air/HCl purification results in the introduction of oxygen containing functionalities to single wall carbon nanotubes (SWCNTs) produced by the HiPco (high pressure carbon monoxide) method. The introduced oxygen functionalities decompose at ~670 K detected as masses 18 (H_2O), 28 (CO) and 44 amu (CO_2) in the mass spectrum. The exact chemical nature of those functionalities requires more detailed investigation.

Low-temperature (100 K) adsorption of acetone on carbon black, as-produced and air/HCl purified SWCNTs allowed the accessibility of different adsorption sites in SWCNTs to be established. A key variable was the vacuum-annealing temperature. The energetics of interaction of acetone with different adsorption sites was determined. The most energetic adsorption sites were found to be endohedral adsorption sites.

The interaction of solvents with carbonaceous materials was studied under different conditions: sonication, reflux, and exposure to solvent vapors over a range of pressures. It was shown that the binding energy of molecules with SWCNTs depends on the interaction conditions: the higher the temperature and pressure during the contact of molecules with SWCNTs, the higher the adsorption energy of molecules on/in SWCNTs. This finding suggests a "pressure gap" effect for nanoporous carbonaceous materials.

Infrared studies of CNTs suggest that molecules adsorbed inside of endohedral channels are invisible to IR. This result is in contrast with experimental findings by other authors. Additional research, both experimental and theoretical, must be done to identify factors responsible for the screening of molecules adsorbed inside SWCNTs.

TABLE OF CONTENTS

LIST OF TABLES

LIST OF FIGURES

GLOSSARY

CNT – Carbon Nanotubes

S(D, M)WCNT – Single (Double, Multi) Walled Carbon Nanotubes

FTIR – Fourier Transform Infrared

HOPG – Highly Oriented Pyrolitic Graphite

MS – Mass Spectroscopy

RGA – Residual Gas Analyzer; the same as a Mass Spectrometer in given context

SSA – Specific Surface Area (m^2/g)

TGA – Thermo Gravimetric Analysis

TPD – Temperature Programmed Desorption

XPS – X-ray Photoelectron Spectroscopy

UV-vis-NIR – Ultraviolet-visible-near infrared absorption spectroscopy

ACKNOWLEDGEMENTS

First, I would like to acknowledge the help of my research advisor - Professor Eric Borguet. For me Professor Borguet was more than advisor. His help and constructive critique allowed making me a good progress.

I appreciate the help and support of my family: my parents who supported me all these years, my spouse, Miraslava, who believed in me and sacrificed the best years of her life helping me to pass this part of the way. My son, Alexander, who inspired me by his joy, energy, and ability to make discoveries every day!

I acknowledge the help of all Borguet group members. The support of Professor Radisav Vidic and Professor J. Karl Johnson, who backed me up at the University of Pittsburgh, is greatly appreciated.

I would like to say thank you to all dissertation committee members. I appreciate your patience and flexibility.

The help of our collaborators, theoretical chemists - Professor Stephan Irle and PhD student Yoshifumi Nishimura from Nagoya University - is difficult to underestimate. The explanation of experimental findings made in this work would not be complete without their thoughtful input.

Financial support from National Science Foundation (NSF), Department of Energy (DOE), and Applied Sensor Research & Development Corporation (ASRD) is acknowledged.

1.0 INTRODUCTION

It is possible that ancient steelmakers knew the secret of CNT synthesis - traces of CNTs have been found in the legendary Damascus steel.[1] Perhaps the presence of CNTs was the origin of the unique properties of Damascus steel.[1] The first experimental detection of CNTs with electron microscopy was in 1952.[2] Nowadays, CNTs are attracting increasing attention.[3-9] Carbon nanotubes are promising materials for the development of CNT based devices and materials – chemical sensors,[10-17] materials for storage of chemicals,[5, 18-20] membranes for gas separation,[21-23] composite materials with unique properties (electrically conductive, thermally stable, mechanically strong),[5, 8, 9, 24] and electronic devices (nanowires, electron emitters, etc.)[5]. The unique mechanical properties of CNTs made the concept of a space elevator feasible.[25] The author is confident that the advanced properties of CNTs will allow their use for more applications in the near future.

1.1 IMPORTANCE OF THE WORK

Technological applications of CNTs are not possible without a detailed knowledge of their chemistry. The development of CNT based chemical detectors that are sensitive to specific molecules requires information on the interaction of CNTs with these molecules.[10-13, 15-17] The

synthesis of composite materials (e.g., modified polymers) and incorporating CNTs often requires the use of organic solvents. Sonication is often used to facilitate dispersion of CNTs in solvents.[8, 26-29] However, sonication can induce chemical interaction of CNTs with solute molecules[30, 31] due to temperature and pressure changes.[32] Understanding of the interaction of CNTs with solvents under different conditions will benefit future applications of solvents for CNT processing.

1.2 THE GOAL AND SCOPE OF THE WORK

In the present work, the results of investigations of simple molecule interactions (e.g., acetone, ethanol, etc.) with CNTs and other carbonaceous materials will be reported. Experiments on the interaction of different solvents with SWCNTs under cryogenic conditions provide information on the energetics of adsorption of simple molecules on different sites: external walls (exohedral), grooves, interstitial channels, and internal walls (endohedral sites) (Figure 1). This information is important to understand the mechanism of molecular binding to different adsorption sites. Theoretical consideration for molecules adsorbed on different CNT sites will be provided. Interactions, especially reversible interactions, of molecules with different carbon nanotubes sites is important for understanding CNT based sensors, and for the creation of storage materials based on CNTs (capturing and release of molecules).

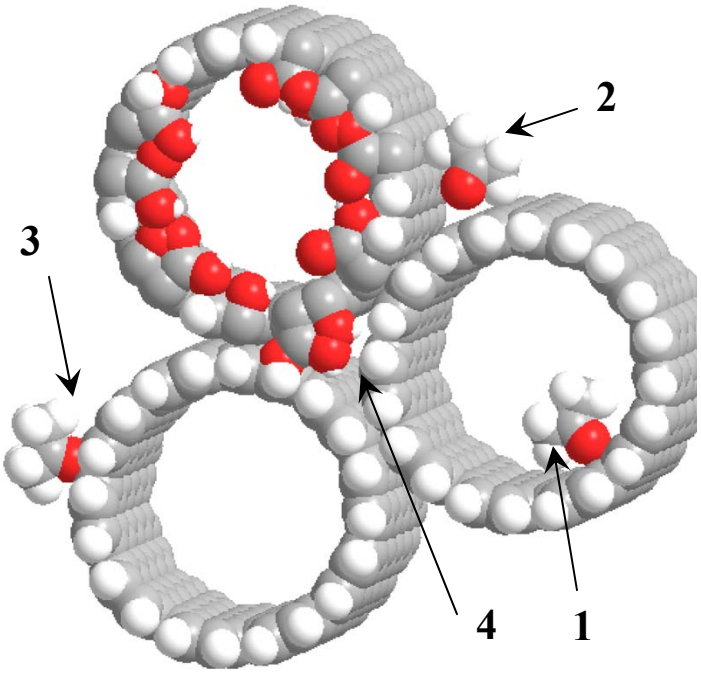

Figure 1: Model of nanotube (10, 10) bundle with different adsorption sites shown – endohedral (1), grooves (2), external walls (3), and interstitial (4) (red – oxygen, white – hydrogen, grey – carbon atoms).

The interaction of CNTs with solvents under reflux, sonication, and exposure to solvents vapors at elevated pressures and temperatures is helpful to understand the mechanisms of interaction of CNTs with molecules. Such investigations may reveal chemical reactivity of CNTs to different solvents. Information of this kind is important for technological processing of CNTs.

2.0 EQUIPMENT AND EXPERIMENTAL SETUP

2.1 EQUIPMENT

In this section the equipment used for the experimental work and its technical characteristics will be described. The reader should address individual chapters of the thesis to find out more details about procedures used for preparation of samples, pretreatments and experimental conditions.

2.1.1 Temperature Programmed Desorption (TPD) with Mass Spectrometry (MS) detection system

The Temperature Programmed Desorption with Mass Spectroscopy detection (TPD-MS) system[33] in the present work is used primarily for studying the chemical species leaving the surface of materials upon heating. The TPD technique can address the following issues:

a. Identify molecular fragments leaving the surface of materials upon thermal decomposition;
b. Detect multiple adsorption sites for adsorbed molecules and determine the binding energy for each adsorption site (multiple peaks in TPD spectrum);
c. Establish the kinetics of desorption processes (simulation of the desorption profiles);
d. Ascertain whether irreversible chemical transformations took a place upon adsorption.

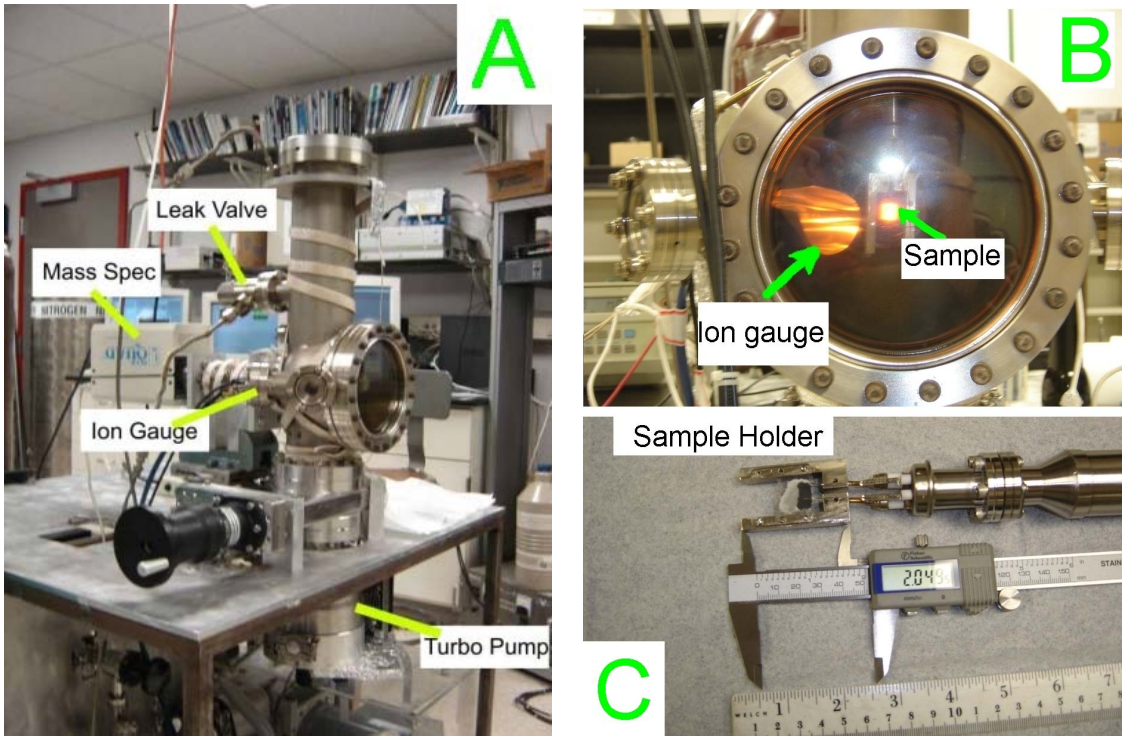

Figure 2: Vacuum chamber for TPD studies (A). The vacuum chamber (B) with a sample holder (C) inside. The part B shows the sample holder with W-grid heated to 1400 K. In the part C the sample holder with CNTs deposited on a CaF_2 pellet pressed into the W-grid is shown. IR transparent materials (e.g., CaF_2, NaCl, KBr) were used in some FTIR experiments.

The TPD-MS experiments are performed in a stainless steel ultrahigh vacuum chamber with a base pressure better than 10^{-9} Torr (Figure 2). Samples are deposited either by drop-and-dry method on a W-grid (AlfaAesar, 100 mesh, 0.002" wire diameter) or by pressing the sample directly into the W-grid. The W-grid is fixed by nickel clamps connected to copper wires cooled via a liquid nitrogen Dewar. The overall design of the sample holder allows cooling of the sample to cryogenic temperatures (<100 K) and heating up to 1400 K. Gases are dosed to the sample, preconditioned to the desired temperature, by backfilling the chamber through a leak valve (Varian). After the desired dose is achieved and the base pressure is recovered, the TPD spectrum is recorded while heating the sample at a constant ramp (typically 2 K/sec). The total

pressure is monitored with an ion gauge. To heat the sample, direct current from a power supply (Kepco 10-100) is driven through the W-grid. Temperature is monitored by means of a K-type thermocouple (Omega) spot-welded to the W-grid. The residual gas analyzer (RGA 300, Stanford Research Systems) is used to monitor the desorption species. Custom Labview programs are used to control the temperature, monitor the dosing, and to record TPD-MS spectra.

2.1.2 Infrared system (FTIR)

Infrared spectroscopy is used to study surface functionalities introduced to CNTs during materials preparation stages. Also, adsorbed species dosed from the gas phase to the surface of CNTs are studied with FTIR technique. Infrared spectra are recorded with an infrared spectrometer (Tensor 27, Bruker) equipped with a Mercury Cadmium Telluride (MCT) detector. A vacuum stainless steel system was used for FTIR measurements (Figure 3). The design of sample holder used in FTIR studies was analogous to the design of the sample holder used in TPD studies and allowed cooling of samples to ~100 K

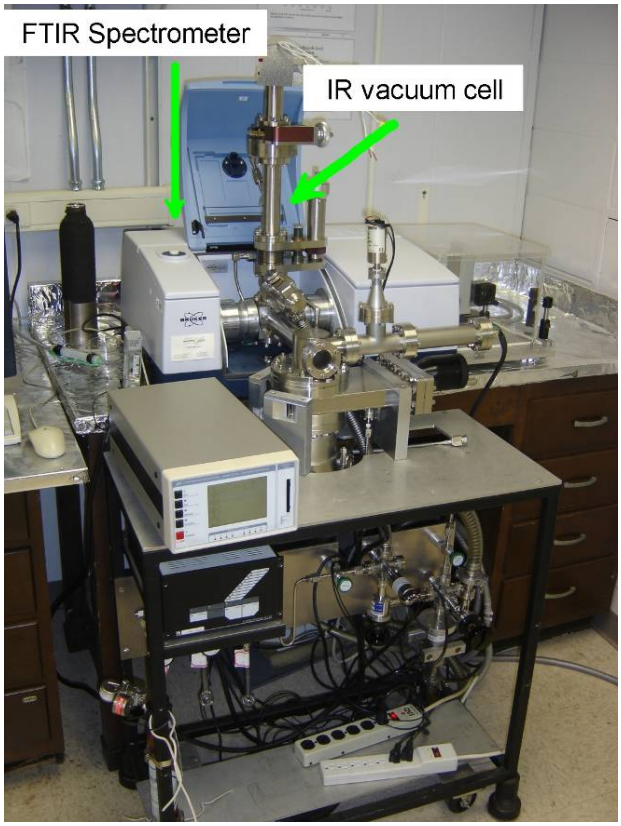

Figure 3: Vacuum IR system. Custom made IR vacuum cell is inserted into sample compartment of FTIR spectrometer (Tensor 27, Bruker).

and heating to 1400 K. Typical base pressure before the FTIR experiments was better then 10^{-8} Torr. The vacuum FTIR cell was equipped with differentially pumped KBr windows. Spectra were recorded by collecting 900-10,000 scans (depending on S/N ratio required) in the range of 400-6000 cm^{-1} at a resolution of 4-8 cm^{-1}.

2.1.3 Volumetric adsorption system

A surface area analyzer (Micrometrics, ASAP 2020) was used for characterization of the porous structure and total surface area of samples under investigation. The Brunauer, Emmett and Teller (BET) method provided with instrument was used for the data processing.[34]

2.1.4 Thermo-gravimetric analysis (TGA)

The objective of the TGA experiment was the evaluation of residual catalyst content (Fe, Ni, Co). The TGA analysis was performed using a Pyris 6 Thermogravimetric Analyzer (PerkinElmer) or a Hi-Res 2950 (TA Instruments). During the analysis pre-purified air (Airgas), controlled by mass-flow controller, was metered at 20 cc min^{-1} through the TGA sample compartment while ramping the temperature from ambient to 1173 K at 10 K min^{-1}.

2.2 PRECAUTIONS: EXPERIMENTAL CONCERNS AND SAFETY ISSUES

There are certain precautions should be taken while working with materials and equipment described in this thesis.

The effect of CNTs on living organisms are still being debated.[35, 36] For the present moment, it is rational to avoid penetration of CNTs into the body. Avoid skin contact with CNTs by using gloves. Avoid inhaling of CNTs - work under the hood, try to operate CNTs in solutions, use respirators and safety dust goggles. Address Materials Safety Data Sheets (MSDS) before using any chemicals.

The use of electrical equipment requires a common sense and an understanding of the principles described in manuals provided by equipment producers. Laboratory procedures should be consulted to understand the operation of each piece of equipment better.

3.0 WHAT ARE CARBON NANOTUBES?

Carbon nanotubes are an allotropic modification of carbon that can be represented as a sheet of graphene (single layer of graphite) rolled into a cylinder.[3, 4, 7, 8] The carbon atoms of carbon nanotubes are in the sp^2 hybridization state. Depending on the number of concentric walls in a carbon nanotube the following classification is used: single (SWCNTs), double (DWCNTs) and multi-wall (MWCNTs). The layers in DW and MWCNTs are attracted to each other due to van der Waals forces (similar to layers of graphene in graphite). Depending on coefficient n and m of the chiral vector ($R=n\mathbf{a_1}+m\mathbf{a_2}$), where $\mathbf{a_1}$ and $\mathbf{a_2}$ are the unit cell vectors (Figure 4), carbon nanotubes can be armchair (n=m), zigzag (n, m=0 or n=0, m), or achiral (all other cases). Knowing the coefficients of the chiral vector (n, m) it is possible to calculate the diameter, d, of carbon nanotubes:

$$d = \sqrt{3}a_{C-C}(m^2 + nm + n^2)^{1/2} / \pi \sim 7.8\,\overset{0}{\text{Å}} * (m^2 + nm + n^2)^{1/2},$$

where $\mathbf{a}_{C\text{-}C}$ the length of C-C bond (1.42 Å).

By knowing the coefficients of the chiral vector (n, m) it is possible to predict the electronic properties of carbon nanotubes: if $2n + m = 3q$, where q is an integer the nanotube is metallic and if $2n+m \neq 3q$ then the nanotube is semiconducting.[3, 4] According to calculations based on statistically equal probability to synthesize carbon nanotube with any chiral vector (n, m), it is found that only ~1/3 of all nanotubes is metallic.[4] Currently, there is no known way to

synthesize selectively carbon nanotubes of uniform electronic properties (metallic or semi-conducting). Methods of nanotubes separation are being actively investigated.[37, 38]

The mechanical properties of carbon nanotubes surpass the properties of many known structural materials. For example, the Young's modulus of SWCNTs is ~ 1 TPa (10^{12} Pa)[39] and exceeds the Young's modulus of steel ~0.2 TPa[40].

The thermal conductivity of individual SWCNT (10, 10) was predicted to be 6600 W/m K at room temperature and 37000 W/m K at 100 K[41]. For comparison, the thermal conductivities of Cu and Ag are 401 and 429 W/m K, respectively.[42]

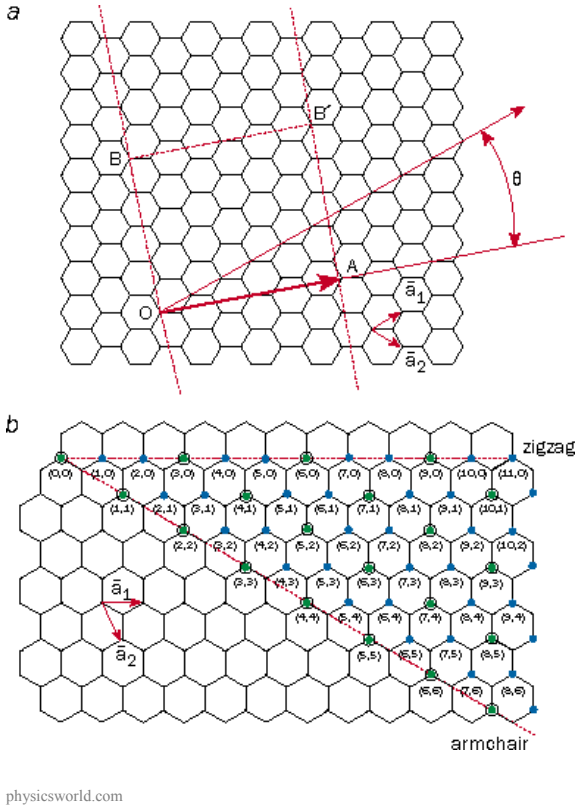

Figure 4: The chiral vector R is defined by unit vectors [a_1, a_2] on the honeycomb lattice of a graphene sheet.[4] The coefficients (n, m) define how many times the corresponding unit vector contribute to the chiral vector R.

Typical diameters of SWCNTs produced either by HiPco method[43], laser ablation, or arch-discharge are on the order of 1-2 nm, with a typical length of several microns (1-5 μm)[43] that corresponds to the aspect ratio (length/diameter) of ~1000. Nanotubes of several millimeters in length were reported.[44] The specific surface area (SSA) depends on pretreatment and for SWCNTs varies in ~400-1600 m^2/g range.[45-47]

Carbon nanotubes have unique electronic properties. It was established that conductance of MWCNTs is quantized.[48] MWCNTs conduct current ballistically and do not dissipate heat; the current density was measured to be 10^7 A/cm^2.[48] For SWCNTs experimentally the maximum measured current density was 10^9 A/cm^2.[49]

3.1 PRODUCTION OF CARBON NANOTUBES

There are several principal methods for carbon nanotube production: arc-discharge,[50] laser ablation,[51] chemical vapor deposition (CVD),[52] and catalytic growth in the gas phase (e.g., HiPco method)[43]. Some exotic methods of carbon nanotubes production were reported such as production of MWCNTs from grass,[53] or non-catalytic method of SWCNTs production from silicon carbide.[54]

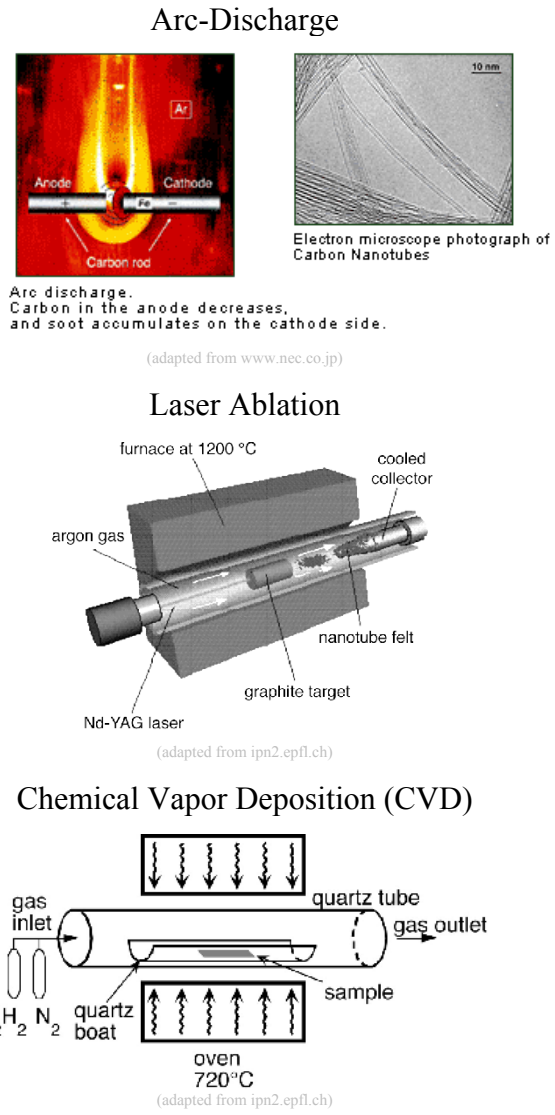

Figure 5: Schematic of experimental setups used for different nanotube production methods (see text for details).

In the arc-discharge method, CNTs are produced from graphite electrodes that are evaporated by plasma (usually inert gas, e.g., He or Ar) (Figure 5). Plasma is produced by running high currents (~100 Amp) through electrodes separated by an inert atmosphere. During the arc-discharge process, material from the anode evaporates producing CNTs that deposit on the cathode. Both single-[55] and multi-wall[56] CNTs can be produced by the arc-discharge method. For SWCNT production a catalyst[1] is required,[55]

[1] NASA researchers claim development of arc-discharge method of SWCNT production without using catalyst. Details of the process are not disclosed (http://ipp.gsfc.nasa.gov/ft-tech-nanotech.html).

while there procedures exist for production of MWCNTs that do not require catalyst (MER corporation).

In the laser ablation method CNTs are produced by ablation of preheated (~1200 °C) carbon target with an intense laser pulses (Figure 5).[51] For the production of SWCNTs by the laser ablation method a catalyst is required (Co, Ni, Y).[51, 57]

In the method of chemical vapor deposition (CVD) for CNT production, a feedstock based on carbon containing chemicals (e.g., C_2H_2, CH_3OH, etc.) passes over preheated (~1000 °C) heterogeneous catalyst (Co, Ni supported over, e.g., silica or alumina). Carbon containing chemicals decompose over catalyst particles producing CNTs.[58, 59]

The High Pressure carbon monoxide (HiPco) decomposition process[43] is somewhat similar to CVD. In the HiPco process metal carbonyls ($Fe(CO)_5$ or $Ni(CO)_4$) are injected into the reactor along with CO in the gas phase. The reaction mixture has a pressure of ~30-50 atm. and temperature of ~900-1100 °C.[60] Formation of CNTs proceeds through a thermal disproportionation of CO on metal clusters formed from metal carbonyls. Single wall carbon nanotubes produced by HiPco process have a narrow diameter distribution (maximum at ~1.0 nm).[43, 61, 62]

3.2 PURIFICATION OF CARBON NANOTUBES

One of the concerns of production, and subsequent applications, of CNTs is the purity of the final product. As-produced carbon nanotubes contain admixtures of carbonaceous impurities (fullerenes, graphitic impurities) and catalytic particles.[63] For many applications, such as

electronics, and biological applications (drug delivery), it is highly desirable to have CNTs of high purity. Hence, the development of CNT purification methods is very important.

Fullerenes and polyaromatic carbons can be removed by rinsing in CS_2, followed by filtration.[64] Air oxidation was suggested to remove non soluble carbonaceous impurities, on the basis that carbon nanotubes are more stable towards oxidation than carbonaceous impurities.[63, 65] Several methods for liquid phase oxidative purification of CNTs were proposed using HNO_3,[66] H_2O_2/H_2SO_4,[67] $Fe/H_2O_2/HCl$ ("Fenton")[68]. Oxidative purification in the presence of acids can allow removal of carbonaceous impurities and metal impurities in one step. In the case when air oxidation is used for removal of carbonaceous impurities, a second step is required (acid treatment) for removal of catalyst particles. From the technological point of view single step processes are more advantageous.

Challenges to purification of CNTs exist. One of these challenges is how to prevent the loss of CNTs during purification of carbon nanotubes, especially oxidative purification. Oxidative treatment of CNTs in air in the presence of metal particles leads to combustion of CNTs along with carbonaceous impurities.[61, 62] Another problem is how to avoid cutting of carbon nanotubes in oxidative media; oxygen can attack the side walls of CNTs, destroying the tubular structure of CNTs and finally lead to the shortening of CNTs.[67]

In this work the effect of air/HCl purification on the introduction of oxygen functionalities will be considered. Air/HCl purification was chosen for the study, because results reported in the literature on the nature of chemical functionalities introduced are scarce and inconsistent.[69-71]

4.0 EFFECT OF AIR/HCL PURIFICATION OF SINGLE WALL CARBON NANOTUBES PRODUCED BY HIPCO METHOD ON THE NATURE OF SURFACE FUNCTIONALITIES

Results reported in this chapter require additional research to be done before submitting for publication.

Abstract

Oxygen functionalities formed during air/HCl purification of single wall carbon nanotubes (SWCNTs) were studied by a combination of temperature programmed desorption (TPD-MS) and infrared spectroscopy (FTIR). The air/HCl purification introduces oxygen functionalities to SWCNTs. According to TPD-MS the dominant species desorbing below 600 K are H_2O and CO_2. These species are observed both for the as-produced and purified SWCNTs and might be associated with desorption of species adsorbed from ambient. Oxygen functionalities introduced decompose at ~670 K in TPD-MS spectra with release of H_2O, CO, and CO_2 as the dominant species. A second maximum for CO release at 1130-1180 K is observed for both the as-produced and purified SWCNTs. Hydrogen-deuterium exchange experiments carried out in the liquid phase upon sonication and in the gas phase upon exposure of SWCNTs to water (H_2O or D_2O) vapors show easy H-D proton exchange for species desorbing below 600 K, while for species desorbing with a maximum at 670 K there is only limited H-D proton exchange suggesting limited accessibility of those species for water molecule protons. FTIR spectroscopy

detected a decrease in intensity of multiple bands upon SWCNT heating that could be associated with desorption/decomposition of hydrocarbons and oxygen functionalities. No thermal decomposition of species containing organic carbonyl (C=O) bond was detected by FTIR for either the as-produced or purified SWCNTs. Functionalities with a mobile proton introduced by air/HCl purification are tentatively assigned to OH groups.

4.1 INTRODUCTION

As-produced SWCNTs contain a substantial fraction of catalyst particles (e.g., SWCNTs produced by the HiPco[43] method contain ~20 wt.% of Fe), as well as carbonaceous impurities that should be removed for the study of pure CNTs and many CNT applications.[72] Multiple purification routes have been proposed[46, 71, 73-76]. One popular method, air/HCl purification, is a two stage procedure that preferentially burns carbon impurities in a flow of air in a first step, and dissolves metal catalyst particles in HCl solution in a second step.[46, 61, 62, 69, 77, 78] In the course of air/HCl purification oxygen containing functionalities were reportedly introduced.[69, 70, 78]

The presence of oxygen containing functionalities at the surface of CNTs is important for many reasons. The presence of oxygen containing functionalities assists in the dispersion of SWCNTs in polar solvents.[79] Oxygen containing functionalities improve the miscibility and adhesion of CNTs in polymer matrices.[29] The presence of oxygen containing functionalities can increase the sensitivity of CNT based sensors,[11, 80] increase the specific capacitance of capacitors,[81] and reduce the electrical conductivity of CNTs.[73, 82, 83] Oxygen functionalities with a mobile proton (e.g., OH groups) are of particular importance because they can serve as

coordination centers for metal cations, opening the way for production of highly dispersed metal particles at the surface of nanotubes,[84] e.g., for catalyst production. Furthermore, oxygen containing functionalities with a mobile proton can be easily converted chemically to other functionalities.[27, 85-87]

The chemistry of oxygen functionalities introduced by air/HCl treatment has been studied but the results reported are inconsistent.[69-71] In the FTIR study Feng et al. detected carboxylic (C=O, 1700 cm^{-1}) and ether (C-O, 1150 cm^{-1}) functionalities both for as-produced and air/HCl purified HiPco SWCNTs.[70] Carboxylic groups in carbonaceous materials decompose by 700 K,[88-92] and ether groups decompose at ~1100 K,[88, 91, 92] Feng et al. proposed that those bands (~1150 and ~1700 cm^{-1}) can also be assigned to intrinsic modes of SWCNTs, because these bands slightly decreased in intensity after annealing to 1300 K, but neither of these bands disappeared completely.[70] Kim et al. observed similar bands in the 800-1760 cm^{-1} region for SWCNTs produced by arc-discharge and annealed to 1673 K.[93] Based on the results of theoretical calculations Kim et al. assigned those bands to the first and second-order IR modes intrinsic to SWCNTs.[93] Kim et al. also suggested that oxygen functionalities (C=O and C-O) might contribute into intensity of the bands observed (C=O ~1720 cm^{-1}, and C-O ~1100 cm^{-1}) in 800-1760 cm^{-1}.[71, 93] Papers by other authors reported multiple IR active vibrations theoretically predicted for SWCNTs in 1000-1600 cm^{-1} region, but no vibrations around 1700 cm^{-1}.[94-96]

There is general agreement regarding certain effects of air/HCl purification. It is established that air/HCl treatment of SWCNTs leads to microporosity and specific surface area increase.[46, 47] The Fe content for SWCNTs (HiPco) purified by air/HCl treatment varies in the 0.4-6 wt.% range.[46, 47, 61, 70, 78] Air/HCl purification does not introduce significant amount of new defects to as-produced SWCNTs.[47, 70, 71, 97]

Air/HCl purification introduces oxygen functionalities, but there is no agreement on the chemical nature and amount of those functionalities. Results of XPS studies on SWCNTs purified by air/HCl show that the air oxidation step introduces a limited amount of C-O-C and/or -OH groups, while after HCl treatment a significant signal (~20% of C1s signal) from C=O groups (COOH and C=O) could be observed.[46] Strong et al. reported 0, 7.9, and 1 at.% of oxygen for as-produced, air oxidized, and for air/HCl treated SWCNTs (HiPco), respectively.[78] The objective of the present study is to determine the chemical nature and thermal stability of oxygen functionalities introduced by air/HCl purification. We will report the amount of oxygen functionalities introduced to SWCNTs by different oxidative purification methods elsewhere.[98] The nature of oxygen functionalities is probed by FTIR. The thermal stability and decomposition products of oxygen functionalities are explored by TPD coupled to mass spectroscopy (TPD-MS).

The results reported here suggest that air/HCl purification introduces oxygen containing functionalities that were absent on the as-produced SWCNTs. The introduced oxygen containing functionalities decompose upon heating under high vacuum at ~670 K with release of H_2O, CO, and CO_2 as the dominant species. Based on the results of FTIR and TPD measurements we tentatively assign the introduced functionalities to hydroxyl groups (OH).

4.2 EXPERIMENTAL

4.2.1 Sample purification

As-produced (non-purified) SWCNTs generated by the HiPco[43] method (Lot# R0559) were purchased from CNI (Houston, TX). To remove residual catalyst (Fe) and amorphous carbon particles, a two-step purification procedure was used.[61, 62] First, non-purified SWCNTs were placed in a plug-flow reactor made of a pyrex U-tube and treated at 570 K for 1 hour in a flow of pre-purified air (Airgas) saturated with a water vapor, prepared by bubbling room temperature air through ultra-pure water (Easypure II, Barnstead). Second, the oxidized SWCNTs were transferred from the U-tube reactor to a flask and sonicated for 3 hours in 6 M HCl (Fisher Scientific) using a laboratory ultrasonic bath (Bransonic 2200). The solution containing SWCNTs was filtered using a 2 μm filter (Whatman). The sample on the filter was rinsed with 6 M HCl and then ultra-pure water to wash out HCl until pH neutrality was reached. The filter was then dried overnight (~16 hours) at 60 °C in ambient air. The yield of purified SWCNTs was evaluated to be ~6-9 wt.%.

4.2.2 Sample preparation for vacuum studies

The as-produced SWCNTs were deposited in powder form on a W-grid (AlfaAesar, 0.001" (for FTIR) or 0.002" (for TPD)) either by a direct pressing method or by drop-and-dry method. For the direct pressing method, a sample was placed on a stainless steel block and evenly distributed with a stainless steel blade on an area of ~5x5 mm. After that the W-grid (~25x12 mm) was

placed on top of the sample, covered with another stainless steel block, and the sample was hydraulically pressed into the W-grid. After that the W-grid with pressed-in sample was clamped to a vacuum sample holder, a thermocouple (K-type) was spot-welded to the W-grid. Finally, the sample holder was placed into a vacuum chamber and evacuated.

For the drop-and-dry method, ~0.5-1 mg of the as-produced or the purified SWCNTs were sonicated in 5 ml of water (H_2O or D_2O) for 3 hours before deposition. During sonication the temperature of the SWCNT suspension in water typically increased up to 50-60 °C after 3 hours. Immediately, after sonication samples were deposited on the W-grid by drop-and-dry method in an air flow at T_{max}~60 ºC. Before sample deposition the W-grid was clamped to the vacuum sample holder and thermocouple was spot-welded. After deposition sample was placed into a vacuum chamber and pumped down to 10^{-9}-10^{-8} Torr.

4.2.3 Thermo-gravimetric analysis (TGA)

The objective of the TGA experiment was the evaluation of residual iron content. The TGA analysis was performed using a Pyris 6 thermogravimetric analyzer (PerkinElmer). About 3-8 mg of analyzed sample powder were used for the analysis. During the analysis pre-purified air (Airgas), controlled by mass-flow controller, was metered at 20 cc min^{-1} through the TGA sample compartment while ramping the temperature from ambient to 1173 K at 10 K min^{-1}.

4.2.4 Temperature programmed desorption studies

The TPD-MS studies were performed in a stainless steel ultrahigh vacuum chamber equipped with residual gas analyzer RGA 300 (SRS, CA) (Figure 2).[99] The base pressure in the TPD vacuum chamber before experiments was ~10^{-8} Torr.

Analogous designs of the sample holder were used for both FTIR and TPD-MS studies: that design allowed sample cooling to ~100 K and controlled heating up to 1300-1400 K.

For the TPD-MS study the sample was cooled to ~100 K and then was heated at 2 K sec^{-1} to 1300 K with simultaneous monitoring of all the species released in a range of 1-100 amu. Typically 120 spectra (1-100 amu) were collected while heating a sample from 100 to 1300 K: one data point per 10 K. Actual temperature corresponding to a given data point was calculated based on known initial temperature (typically 95-100 K), known heating rate (2 K sec^{-1}), and the time at which data point (1-100 amu) was collected. As the time to scan from 1 to 100 amu is 5 sec then the temperature difference between collection of first point (1 amu) and last point (100 amu) is 10 K. Data in the 100-300 K range were recorded for control purposes: water physically adsorbed from background desorbs in a range of 160-170 K in case of proper thermocouple connection to the W-grid and good thermal contact of the W-grid with a sample.

4.2.5 Infrared studies

The FTIR measurements were performed in a vacuum chamber embedded into the sample compartment of Tensor 27 infra-red spectrometer (Bruker) (Figure 3).[70, 100] The base pressure in the FTIR vacuum chamber before experiments was typically ~10^{-8} Torr.

For FTIR measurements the sample was cooled down to 100-110 K, flash heated to 300 K, and then a background spectrum was collected. Then the sample was steadily heated at 2 K sec^{-1} and held at 500 (for 5 min), 700 (5 min), 900 (3 min), and 1300/1400 K (1 min). After annealing, the sample was allowed to cool to 100-110 K, the temperature allowed to stabilize, and a spectrum was collected. For the control purposes some FTIR experiments were performed with monitoring of desorbing upon annealing species with the mass-spectrometer.

4.3 RESULTS

4.3.1 TGA Results

The air/HCl purification procedure allows significant removal of residual iron catalyst; from 21.3 wt.% for the as-produced SWCNTs to 0.9 wt.% after purification (Figure 6). The purity obtained is similar or better to that reported in the literature for the air/HCl purification.[46, 47, 61, 70, 78] Though, the yields obtained are 7-10 % of original sample mass, that is equivalent to 9-12 % in terms of carbon related compounds. The TGA profiles for the purified and as-produced

SWCNTs are different. The TGA profile for the as-produced SWCNTs shows a weight gain between 400 and 560 K, most likely due to oxidation of Fe to Fe_2O_3.[77, 78] The weight gain is followed by the catalytic oxidation[47, 77] of the as-produced SWCNTs with a maximum oxidation rate at 685 K (Figure 6). The TGA profile for the purified SWCNTs shows ~4 wt.% weight loss in a range of 300-400 K, presumably due to evaporation of physisorbed water and decomposition of surface functionalities (Figure 6). Weight loss due to combustion of carbonaceous material is observed in the range of 700-1100 K (Figure 6).

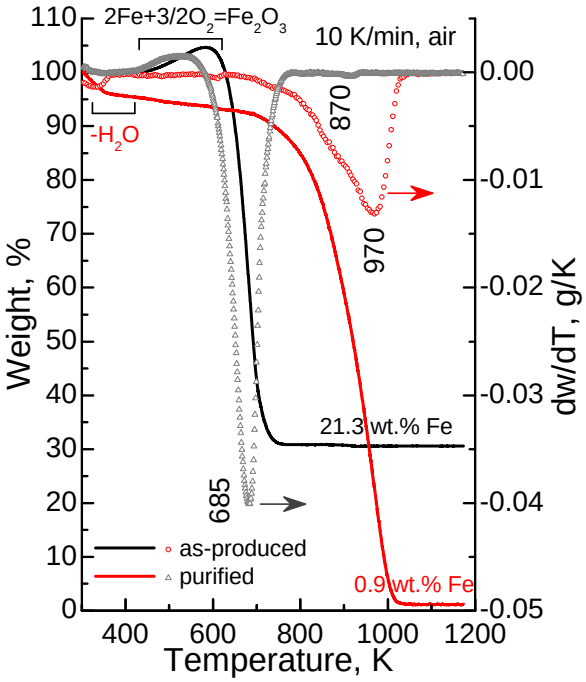

Figure 6: Results of thermo-gravimetric analysis (TGA) in air flow of as-produced (TGA -, DGA △) and purified (TGA -, DGA ○) SWCNTs. Initial iron content of ~21 wt.% in as-produced SWCNTs can be reduced to ~0.9 wt.% after air-HCl purification.

To summarize, according to the TGA analysis, air/HCl purification procedure allowed removal of 95% of the residual iron catalyst (Figure 6). Thermal stability in air of purified SWCNTs (970 K) exceeds that for as-produced SWCNTs (685 K). Purified SWCNTs are more hydrophilic than as produced and retain adsorbed water.

4.3.2 TPD-MS Results

The examples of the full TPD spectra for the as-produced SWCNTs or purified SWCNTs are shown in the Figure A1 and profiles of the selected masses (18, 28, and 44 amu) are shown in Figure 7. Those fragments can be assigned to H_2O (18 amu), CO (28 amu), and CO_2 (44 amu). The intensities of H_2O and CO_2 for the as-produced SWCNTs deposited by direct pressing increase in the entire temperature range and do not have a pronounced maxima below 1000 K (Figure 7A). For as-produced SWCNTs deposited by drop-and-dry, the CO_2 signal showed the same behavior, while the signal for water was relatively more intense having maxima at 500 K and at ~700 K (Figure 7B). The intensity of CO for both as-produced and purified samples increased in the entire temperature range with pronounced peak at 1180 (Figure 7A and B).

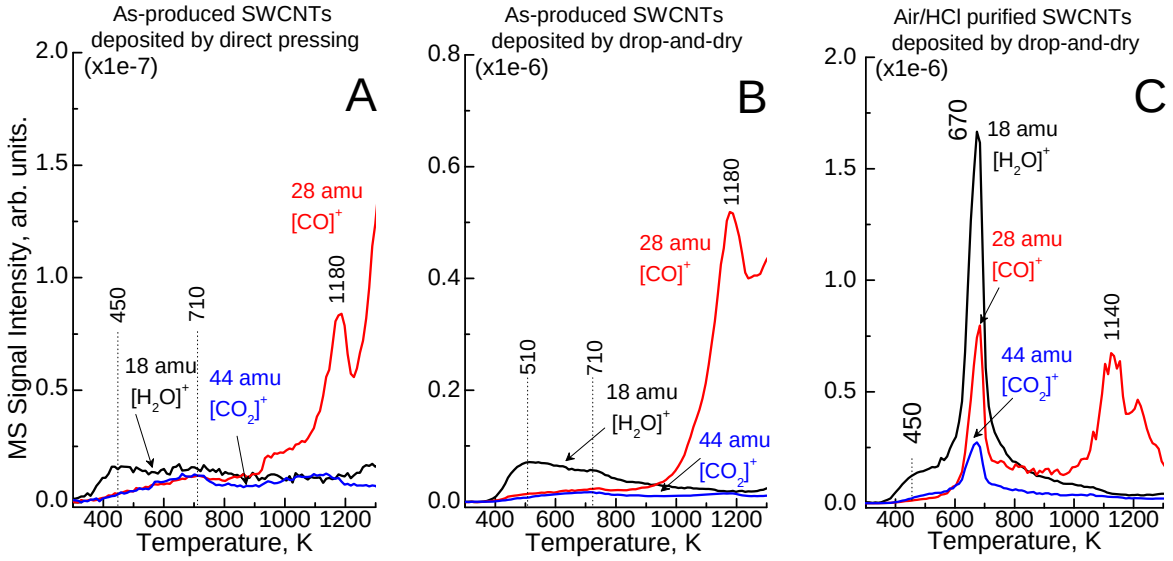

Figure 7: TPD profiles of 18 amu [H_2O], 28 amu [CO], and 44 amu [CO_2] extracted from full TPD spectra of **A.** As-produced SWCNTs deposited by direct pressing; **B.** As-produced SWCNTs sonicated in H_2O deposited by drop-and-dry, and **C.** Air/HCl purified SWCNTs sonicated in H_2O and deposited by drop-and-dry. The air/HCl purified SWCNTs show distinct peak with maximum at ~670 K.

The same desorption fragments can be observed for as-produced SWCNTs and for air/HCl purified SWCNTs (Figure A1). H_2O desorption starts from ~400 K as a broad peak (Figure 7B). The maxima of H_2O, CO and CO_2 release for air/HCl purified SWCNTs was at 670 K (Figure 7B), while as-produced SWCNTs sample had no pronounced maxima for either H_2O or CO_2 (Figure 7A). The analysis of full TPD spectrum showed that mass 17 amu (OH) profile follows the same pattern as mass 18 amu with the ratio corresponding to H_2O (see Figure 8) suggesting molecular water desorption. The signal intensity of CO (28 amu) was at least 3 times greater than that of CO_2 (44 amu) suggesting that CO is not a fragment of CO_2.

The TPD peak at 670 K, associated with simultaneous release of H_2O, CO, and CO_2 (Figure 7B), can originate from the decomposition of oxygen functionalities at the surface of SWCNTs. Also it can originate from decomposition of oxygen functionalities blocking the entrances to endohedral sites of SWCNTs,[101, 102] with further release of species trapped inside SWCNTs (H_2O (18 amu), N_2 (28 amu), etc.). In order to elucidate the origin of the observed peaks and their chemical nature several control experiments were performed.

The first control experiment was designed to find out whether during the purification procedure gases can be trapped inside SWCNTs. For that purpose SWCNTs were oxidized in a mixture of 20 vol.% O_2/He with subsequent sonication in HCl and re-dispersion of the sample in H_2O before deposition under 20 vol.% O_2/He environment. The experiment revealed no release of He (4 amu) during heating the O_2/He-HCl purified SWCNTs (Figure A2). No trapping of He was established (Figure A2) suggesting free access of He in and out of SWCNT endohedral sites. It does not exclude the possibility that bigger molecules such as H_2O, N_2 and O_2 may have limited access to SWCNTs endohedral sites: a signal from 32 amu (presumably from O_2) was observed, but its intensity was ~1000 less than the intensity of signals 18, 28, and 44 amu (Figure

A2). Based on the result of the first control experiment no encapsulation of atmospheric molecules (H_2O, N_2, and O_2) was observed during the air/HCl treatment.

The second control experiment had the aim to determine if the water release is due to decomposition of oxygen functionalities containing a mobile proton and if these functionalities are accessible to molecules in the gas phase. For that purpose we performed control experiments involving H-D exchange in the liquid phase upon sonication of SWCNTs in D_2O (ICON, 99.9 at.% D) and in the gas phase upon sample exposure to D_2O vapors. These experiments showed that H-D exchange proceeds both upon sonication in D_2O and upon SWCNTs exposure to D_2O vapors.

For purified SWCNTs sonicated in D_2O and H_2O, the signals for 20 amu (D_2O), 19 amu (HDO), 18 amu (H_2O, OD), and 17 amu (OH) are shown in Figure 8. The signals were normalized[2] to the mass 44 amu (CO_2); the intensity of the signal from CO_2 should not be affected by sonication media (D_2O or H_2O) and was used as an internal standard. Profiles for 20, 19, 18, and 17 amu masses from as-produced sample are shown for comparison and were not normalized. The small signal from mass 20 amu (D_2O) and differences in TPD profiles for water (D_2O, HDO, H_2O) related fragments might be explained by exchange (D to H) with water from ambient air during sample deposition.

[2] Normalization was done by division of mass 20, 19, 18, 17 amu by maximum signal intensity of mass 44 amu (CO_2) releasing at ~670 K for the corresponding sample (either sonicated in H_2O or D_2O).

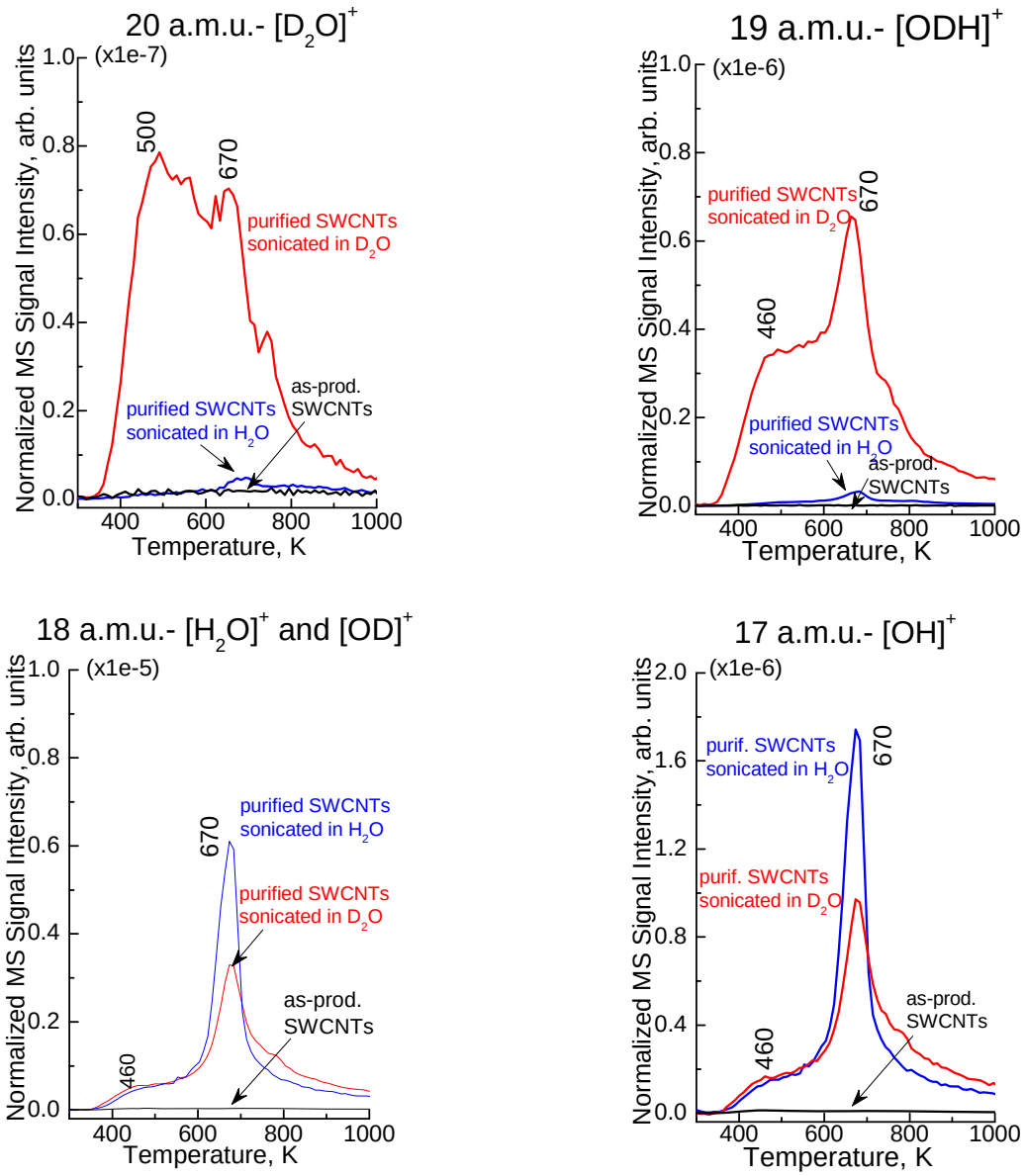

Figure 8: TPD profiles for masses 20, 19, 18, and 17 amu for the as-produced (black line) SWCNTs (deposited by direct pressing) and purified SWCNTs (deposited by drop-and-dry) sonicated in H_2O (blue line) and D_2O (red line). Signals from purified sample were normalized based on CO_2 (44 amu) signal. Sonication of the sample in D_2O resulted in partial H-D exchange.

The H-D exchange experiment was also performed with water molecules dosed from the gas phase. The first objective was to minimize the H-D exchange with water vapor from ambient air that was likely occurring during drop-and-dry deposition of SWCNTs sonicated in D_2O onto the W-grid. The second objective was to check if there are any accessibility

limitations caused by bundling of SWCNTs after deposition. To proceed with H-D exchange in the gas phase, the sample sonicated in H_2O was placed in a vacuum chamber, evacuated to $<10^{-7}$ Torr. Then the vacuum chamber was 3 times refilled with 7.6 Torr of D_2O and kept for 10 min under D_2O vapors at ambient temperature. The vacuum chamber was then evacuated to $\sim10^{-8}$ Torr for TPD-MS experiments. The TPD analysis of water related fragments showed that there is H-D exchange in the gas phase (Figure 9) and profiles for water fragments were similar as for SWCNTs sonicated in D_2O (Figure 8). The results suggest that H-D exchange proceeds easily for the water TPD peak evolving below 600 K (Figure 9), while for the peak evolving at ~650-670 K there is only partial H-D exchange. In the case of unrestricted proton exchange between water molecules in the gas phase and mobile protons at the surface of SWCNTs, the ratio between different water fragments (D_2O, HDO, H_2O, OD, OH) desorbing from the SWCNT surface should be the same in the whole temperature range and equal to the ratio of water fragments in the gas phase before TPD experiment (Figure 9). From Figure 9A one can see that the ratio between water fragments changes with temperature; as temperature increases species containing H become to dominate over species containing D. All protons that are at the surface of SWCNTs can exchange with protons of water in the gas phase, but species that decompose at ~670 K exchange in less extent than species that decompose at lower temperatures. To conclude, the oxygen containing functionalities that decompose at 670 K contain a mobile proton and these oxygen containing functionalities have the limited accessibility for a proton of water molecules in the gas phase.

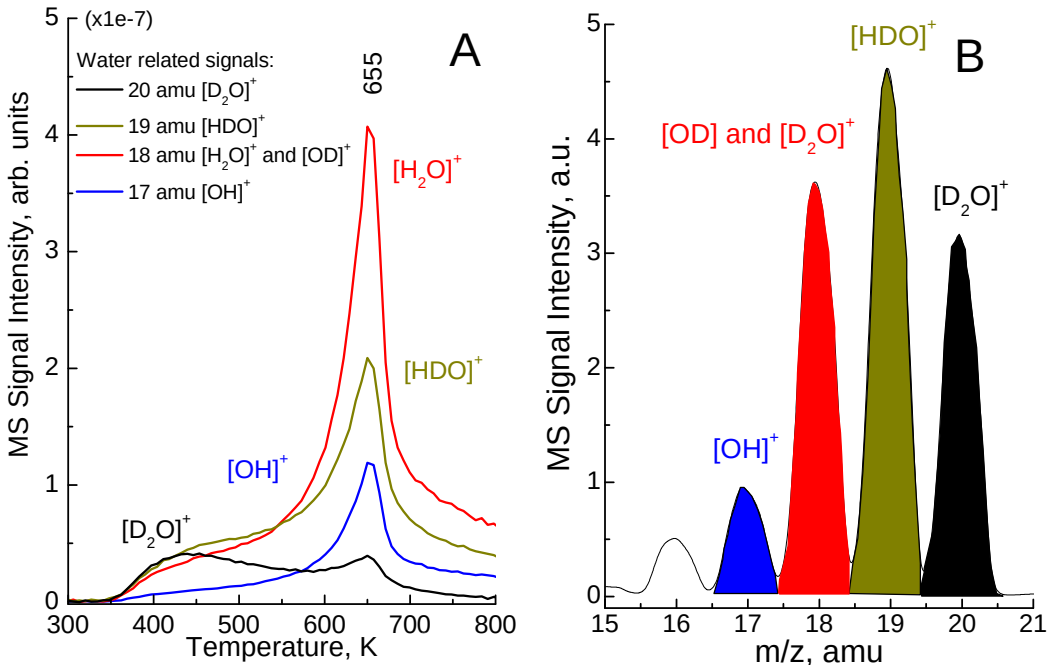

Figure 9: TPD following H-D exchange on the purified SWCNTs with molecules dosed from the gas phase. In the case of a complete H-D exchange and "surface-gas phase" equilibration, the ratio between different water fragments observed during TPD experiment (A) should be the same as ratio between different water fragments in the background gases (B).

4.3.3 FTIR results

The results of FTIR experiments for the as-produced and purified SWCNTs are shown in Figure 10. Heating of the as-produce SWCNTs to successively higher temperatures leads to intensity decrease of bands at 3600-3100 cm^{-1} (with a sharp peak at 3500 cm^{-1}) and at 2950-2850 cm^{-1} - C-H stretching (Figure 10A). Similar bands were observed for the air/HCl purified SWCNTs (Figure 10B). Those bands could be assigned to OH stretching modes[71, 103] and C-H stretching[90], respectively (Table 1).

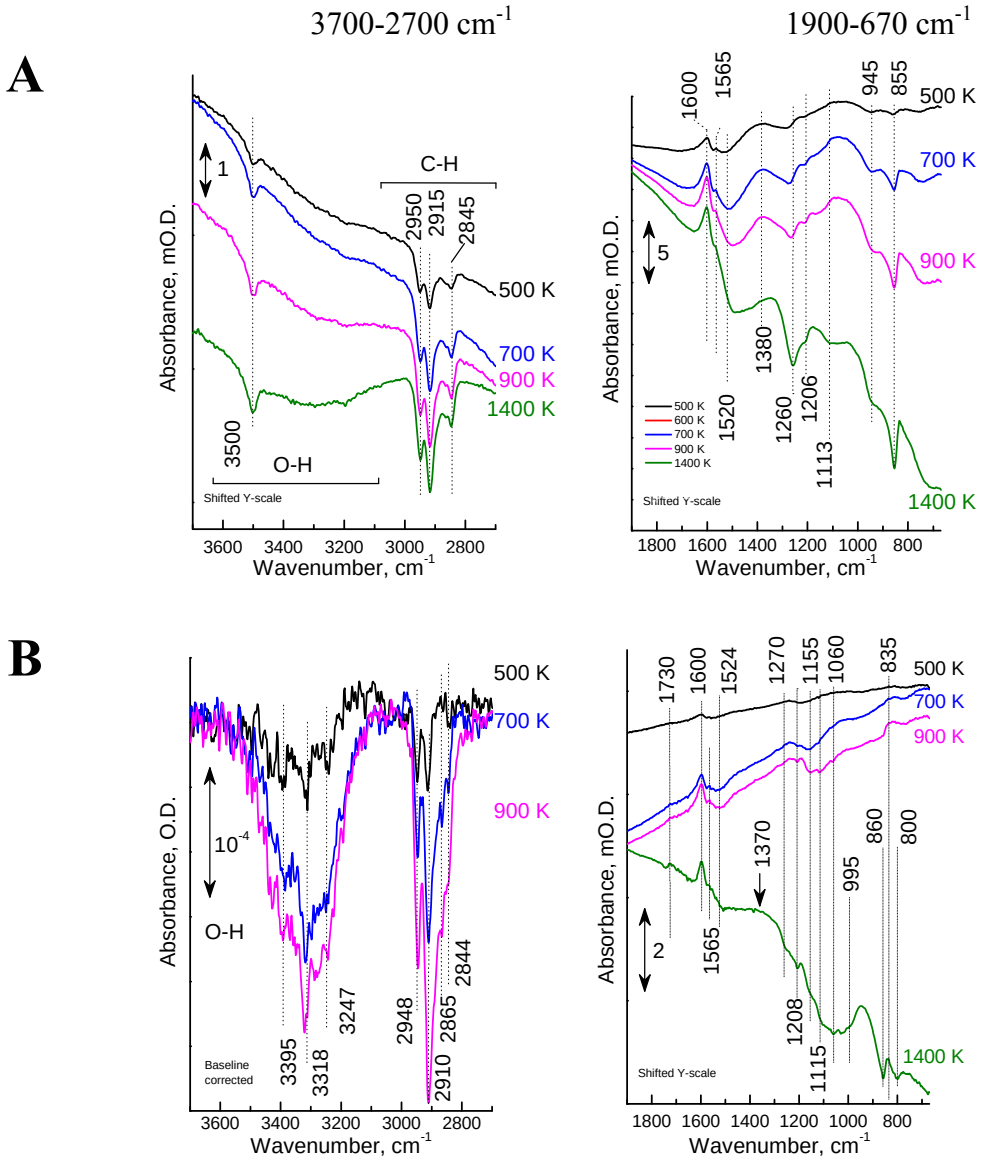

Figure 10: FTIR spectra of the as-produced (A) and air/HCl purified SWCNTs (B) annealed to 500, 700, 900, and 1400 K. The spectral changes are shown in regions of 3700-2700 and 1900-670 cm^{-1}. Negative peaks mean that species leave the surface as the temperature increases.

While heating the as-produced SWCNTs to high temperatures, gradual decrease of intensities of bands at 1510, 1260, 1206, 1113, 945, and 855 cm^{-1} was observed (Figure 10A). At the same time bands at 1600 (shoulder 1560) cm^{-1}, and broad bands ~1380, ~1100, and ~830 cm^{-1} were increasing in intensity. Heating of the air/HCl purified SWCNTs sample resulted in decrease of intensity of bands at 1750, 1507, 1160-950, 860, and 800 cm^{-1} (Figure 10B). The intensity

increase for the air/HCl purified SWCNTs was observed also at 1730, 1600, 1565, 1370 (after 1400 K), 1060, and 830 cm^{-1}. Proposed assignment of bands is given in **Table 1**.

Table 1: Proposed assignment of IR bands observed in the spectra of SWCNTs.

IR active mode	Observed Frequencies* [cm^{-1}]	Additional References
		SWCNTs and graphite intrinsic modes
A_{2u} of graphite or radial[95] mode in SWCNTs	835	805 - Theory of SWCNTs (z-directed mode in C_{120})[96] 806, 854 - first order modes (IR and theory)[93] ~830 (NA**), ~870 – IR of graphite and SWCNTs[104] 860 - IR of SWCNTs, graphite, amorphous carbon[95] 868 - IR of SWCNTs and graphite[105] 820-840 - IR of SWCNTs[106]
"D-band"	1380	1190 - IR of SWCNTs (D-band)[95] 1358 - Theory of SWCNTs (z-directed mode in C_{120})[96] 1369 - first order modes (IR and theory)[93] 1380 - unassigned (SWCNTs)[107] 1430 - IR of SWCNTs[106]
E_{1u} of graphite or tangential[95] mode in SWCNTs	1600	1580 - Theory of SWCNTs (circumference mode in C_{120})[96] 1597, 1590, and 1587 - IR of SWCNTs, graphite (E_{1u}), amorphous carbon, respect.[95] 1587 - IR of SWCNTs and graphite[105] 1540 - IR of SWCNTs[106]
Second order	1730	1700 (NA) - IR of SWCNTs[106] 1708, 1730 - second order modes (IR and theory)[93]
		Surface (oxygen) functionalities
C-O	1040-1250	1040 - C-O-C symmetric stretching[107] 1062 - appear along with band 1600 cm^{-1} after oxygen cycloaddition[108] 1100 - C-O in ether, alcohols, and phenols[71] 1200 - C-O-C asymmetric stretching[107] 1250 - C-O[70]
O-H bending	1230	1230 - O-H bending[71]
C=C	1580-1600	1580 - C=C in proximity of oxygenated group[107] 1585-1600 - aromatics[90] ~1579-1600[70]
C=O	1640-1850	~1640 - quinone[90] 1650 - quinone[107] 1710-1730 - stretching in ketones or carboxylic acid groups 1700 - carboxylic acid[70] 1723 - lactone/carboxyl[90] 1850 - anhydrides[70]
C-H	2850-2960	2850-2960 - aliphatic[90]
O↔H	3200-3600	3200-3251 - in COOH 3230 - in coupled carboxylic acid groups and 3400 in alcohols and phenols[71] 3600-3000 - amorphous ice outside of SWCNTs and 3507 ordered ice inside SWCNTs[103] 1500-1660 - conjugation between C=O and C=C bonds or interaction between localized conjugation of C=O and carboxylic acids and ketons[71]

* Observed in current work **NA= not assigned

4.4 DISCUSSION

The air/HCl purification used in the present work effectively removes residual iron catalyst reducing the iron content from ~21 to ~1wt.% (Figure 6) that is well in agreement with early reported values for the analogous air/HCl procedures.[46, 47, 61, 70, 78] The reduction of iron content improves the thermal stability of SWCNTs in air (Figure 6). Nevertheless, the improved thermal stability is just a sign of reduced Fe content and could not serve as an evidence for pure nanotubes with no carbon admixtures; control TGA experiment with carbon black (CB-460, Cabot) showed the carbon black starts to burn at ~800 K (Figure A3) – close to "ignition" temperature of the air/HCl purified SWCNTs. The question on the SWCNTs purity in terms of carbonaceous impurities after the air/HCl is open for further investigations.

The results of TPD investigation unambiguously show that the air/HCl treatment introduces new type of oxygen functionalities to SWCNTs that decompose upon heating at ~670 K (Figure 7). The maximum peak of desorbing species belongs to H_2O, CO, and CO_2, suggesting simultaneous dehydroxylation of SWCNT surface and decomposition of oxygen functionalities. On carbonaceous materials other than CNTs decomposition of carboxylic functionalities occurs at ~550-750 K and carboxylic anhydrides at ~623-1013 K.[89-92, 109] We doubt that the functionalities that decompose at ~670 K are carboxylic or/and anhydride groups. Decomposition of carboxylic functionalities should be accompanied by release of CO_2 mainly and in the case of carboxylic anhydride decomposition the ratio between CO and CO_2 should be ~1, while in our case the CO peak has a maximal intensity (Figure 7). Besides, elimination of carboxylic groups with either formation of carboxylic anhydride groups due to dehydroxylation or decomposition should be accompanied by intensity decrease in the C=O stretching region. For the air/HCl purified SWCNTs slight increase in the intensity of IR peak at 1730 cm^{-1} was

observed after annealing to 700 K (Figure 10B). After annealing to 1400 K there was a decrease in intensity of the peak at ~1750 cm^{-1} that can be assigned to C=O stretching in carbonyls (Table 1). Peak at 1730 cm^{-1} increased in intensity along with peaks at 1600 and 835 cm^{-1}, and did not change in intensity even after annealing to 1400 K when most of the oxygen containing functionalities decompose. The IR peak at 1730 cm^{-1} was not pronounced for the as-produced SWCNTs. Recently, the peak at ~1730 cm^{-1} was assigned to the second order IR active modes intrinsic to SWCNTs.[93] Feng et al. also observed a broad band ~1680-1700 cm^{-1} for HiPco nanotubes[43] and for Rice Tubes[51] that were annealed to >1300 K, suggesting that this band can be intrinsic to CNTs.

FTIR results suggest that there is no C=O (~1700-1800 cm^{-1}) containing functionalities decompose upon heating of SWCNTs to 900 K. The inability to observe changes in 1750-1700 cm^{-1} region with FTIR can not be explained by limited sensitivity of FTIR. For the air/HCl purified SWCNTs FTIR can detect the changes in O-H stretching region while heating from 500 to 700 K (Figure 10B), though an extinction coefficient of O-H stretching is much lower than an extinction of C=O stretching suggesting that if the change in OH stretching region was observed with FTIR and this change is due to decomposition of carboxylic groups then the change of C=O stretching intensity should be even more pronounced. The TPD peak observed at 670 K can not be assigned to the decomposition of oxygen functionalities containing carbonyl group.

The TPD peak at 670 K might originate from decomposition of OH functionalities. The peak at 670 K is absent for the as-produced SWCNTs and on the as-produced SWCNTs sonicated in water (Figure 7). A control experiment on sonication of the as-produced SWCNTs in HCl without air oxidation step showed TPD desorption profiles of CO and CO_2 similar to profiles of CO and CO_2 developing from the as-produced SWCNTs (Figure A4). The air

oxidation of the as-produced sample sonicated in HCl also revealed no generation of the oxygen functionalities (Figure A4) observed for the air/HCl purified SWCNTs. However, SWCNTs sonicated in HCl and then oxidized in the moist air showed increase in intensity of CO_2 desorbing in 600-900 K range (Figure A4).

The most distinct change in the FTIR spectra of the purified SWCNTs that occurs from 500 to 700 K is a decrease of intensity of bands at ~1155-1200, ~1524 and ~3200-3400 cm^{-1} (Figure 10B) suggesting thermal decomposition of surface functionalities. The band at ~1050-1200 cm^{-1} can be assigned to C-O stretching and/or O-H bending vibrations (Table 1), while the band at 3200-3400 cm^{-1} can be assigned to OH stretching vibrations. The band at ~1507 cm^{-1} was observed for the as-produced SWCNTs suggesting that it can not contribute to the 670 K TPD peak intensity. The FTIR results imply that the TPD peak that we observe at ~670 K correlate with decrease of intensity of bands at ~1050-1200 cm^{-1} (C-O stretching and/or O-H bending) and band at ~3200-3400 cm^{-1} (OH stretching).

The increase of intensity of some adsorption bands in the IR spectra of SWCNTs can be associated with formation of new IR active bonds. Another possibility is a change of molecular symmetry due to reorganization of bonds. Chemical and physical transformations of SWCNTs that reduce the symmetry of C=C bonds will result in observed increase in intensity of the ~1600 cm^{-1} band. For example, increase of intensity for the band 1600 cm^{-1} band can be explained by the deformation of SWCNTs. It should be pointed out that in our FTIR experiments we detect the changes in the optical properties of our sample initiated by heating; background is the sample before heating. The heating of SWCNTs can lead to desorption of chemical species from endohedral and interstitial channels of CNTs, to the decomposition of surface functionalities, and, possibly, to ordering/disordering of carbon nanotubes within CNT bundles. These events

can results in "deformation" (change of symmetry) of carbon nanotubes. Particularly, ordering of carbon nanotubes within the bundle can result in more strong interaction between carbon nanotubes that will lead to radial deformation of nanotubes (Figure 24). The radial deformation should be more pronounced for the nanotubes that are close to the sides of the bundle, because carbon nanotube that are in the middle of the bundle will feel the same forces from all sides (in case of bundle formed of CNTs of the same diameter and having ordered structure). Additional study combined with other methods (such as Raman, Electron Microscopy, and other techniques) is required to identify the mechanisms responsible for increase of IR intensity of certain bands.

According to the results of H-D exchange the introduced oxygen functionalities that decompose at ~670 K contain a mobile proton (Figure 9). However, those functionalities are not easily accessible for proton of water molecules in the gas phase (Figure 9) suggesting that there are either kinetic or physical limitations preventing complete exchange. Based on the results of the present paper we believe that the air/HCl purification introduces hydroxylic groups (-OH) to the sidewalls of carbon nanotubes. The limited accessibility of the sidewall hydroxylic groups (-OH) can be explained by formation of the CNT bundles with OH groups located in the interstitial channels of SWCNTs. In general interstitial channels have limited accessibility for molecules,[110] but for bundles formed of carbon nanotubes of different diameters, some interstitial sites can be accessible.[111, 112]

4.5 SUMMARY AND CONCLUSIONS

It was shown that the air/HCl purification introduces oxygen functionalities absent for the as-produced SWCNTs. The introduced oxygen functionalities decompose by heating under high

vacuum with a maximum decomposition rate at ~670 K. Results of FTIR experiments suggest that there are no carbonyls disappearing after thermal treatment, excluding the possibility that decomposing groups are carboxyls. According to the results of H-D proton exchange, introduced oxygen containing functionalities contain a mobile proton that can partially exchange with the gas phase water molecules. We suggest that the air/HCl procedure utilized here resulted in the formation of hydroxylic groups (OH) on the side walls of SWCNTs.

5.0 INTRODUCTION INTERACTION OF ACETONE WITH SINGLE WALL CARBON NANOTUBES AT CRYOGENIC TEMPERATURES: A COMBINED TEMPERATURE PROGRAMMED DESORPTION AND THEORETICAL STUDY

This part of the thesis was published in Langmuir journal (v. 24 p. 7848, 2008). Theoretical calculations for this part of the work were provided by Professor Irle and PhD student Yoshifumi Nishimura (Institute for Advanced Research and Department of Chemistry, Nagoya University, Japan) and Keiji Morokuma (Department of Chemistry, Emory University, Atlanta, GA).

Abstract

The interaction of acetone with single wall carbon nanotubes (SWCNTs) at low temperatures was studied by a combination of temperature programmed desorption (TPD) and dispersion-augmented density-functional-based tight binding (DFTB-D) theoretical simulations. On the basis of the results of the TPD study and theoretical simulations, the desorption peaks of acetone can be assigned to the following adsorption sites: (i) sites with energy of ~75 kJ mol^{-1} (T_{des} ~300 K) ─ endohedral sites of small diameter nanotubes (~7.7 Å); (ii) sites with energy 40–68 kJ mol^{-1} (T_{des}~240 K) ─ acetone adsorption on accessible interstitial, groove sites, and endohedral sites of large nanotubes (~14Å); (iii) sites with energy 25–42 kJ mol^{-1} (T_{des} ~140 K) ─ acetone adsorption on external walls of SWCNTs and multilayer adsorption. Oxidatively purified SWCNTs have limited access to endohedral sites due to the presence of oxygen functionalities.

Oxygen functionalities can be removed by annealing to elevated temperature (900 K) opening access to endohedral sites of nanotubes. Nonpurified, as-received SWCNTs are characterized by limited access for acetone to endohedral sites even after annealing to elevated temperatures (900 K). Annealing of both purified and as-produced SWCNTs to high temperatures (1400 K) leads to reduction of access for acetone molecules to endohedral sites of small nanotubes, probably due to defects in self-healing and cap formation at the ends of SWCNTs. No chemical interaction between acetone and SWCNTs was detected for low temperature adsorption experiments. Theoretical simulations of acetone adsorption on finite pristine SWCNTs of different diameters suggest a clear relationship of the adsorption energy with tube sidewall curvature. Adsorption of acetone is due to dispersion forces with its C─O bond either parallel to the surface or O pointing away from it. No significant charge transfer or polarization was found. Carbon black was used to model amorphous carbonaceous impurities present in as-produced SWCNTs. Desorption of acetone from carbon black revealed two peaks at ~140 and ~180-230 K, similar to two acetone desorption peaks from SWCNTs. The characteristic feature of acetone desorption from SWCNTs was peak at ~300 K that was not observed for carbon black. Care should be taken when assigning TPD peaks for molecules desorbing from carbon nanotubes as amorphous carbon can interfere.

5.1 INTRODUCTION

Carbon materials are of interest for fundamental science and technological applications.[4] Discovered more then 50 years ago,[2] the importance of carbon nanotubes (CNTs) for technological applications was not initially recognized and became clear only recently.[3, 50] The dimensions and properties of CNTs make their application as nanosensors attractive.[11, 14-16]

Acetone is a simple polar organic solvent, and a major chemical commodity.[113] Acetone is reported to be the dominant non-methane organic atmospheric pollutant.[114] Moreover, acetone forms in the body during ketogenesis.[115] Thus, there is ongoing interest to study the interaction of acetone molecules with CNTs for the development of sensors[11-13, 116, 117] to control the environmental release of acetone from industrial sites and to monitor the acetone level in the human body to prevent ketoacidosis, an issue for people with diabetes[118].

There have been several experimental studies on the interaction of acetone with carbon materials (highly oriented pyrolitic graphite (HOPG) and CNTs) and the application of CNTs to acetone vapor detection.[11-13, 116, 117, 119-122] Recent publications suggest a chemical interaction of acetone with SWCNTs[121] and multiwall carbon nanotubes (MWCNTs)[122] with a maximum desorption energy of ~100 kJ mol^{-1} and ~68 kJ mol^{-1}, respectively. Chakrapani et al. suggested that the curvature of the CNT surface and topological defects play an important role in the strong binding of acetone to the CNT surface.[121] Shih and Li proposed that strong chemical interactions of acetone with MWCNTs is due to topological defects and disorder in MWCNTs.[122] Snow and Perkins used SWCNTs based sensors for acetone detection and proposed that acetone vapors

produce a rapid response in the conductance and capacitance of SWCNTs due to charge transfer and polarizability, but did not discuss the adsorption energetics.[116] Later, Robinson et al. reported that defects play an important role in acetone binding to CNTs and the acetone adsorption energy was estimated from conductance curves as a function of acetone pressure to be 41 kJ mol^{-1}, while theoretical calculations for acetone bound to carboxylic group in proximity of side wall defects gave a binding energy of 34 kJ mol^{-1}.[11] The results of a TPD study on acetone interaction with HOPG suggested that acetone adsorbs in three states: monolayer ($T_{d,max}$~165 K), bilayer ($T_{d,max}$ ~155 K), and multilayer ($T_{d,max}$ ~145 K).[119, 120] Furthermore, the presence of oxygen functionalities have been shown to influence the interaction of acetone with HOPG.[120] Here we present the results of a temperature programmed desorption (TPD) investigation and theoretical simulations of acetone adsorption on SWCNTs at cryogenic temperatures, and explore the influence of oxygen functionalities and anneal temperature on acetone adsorption on SWCNTs. We discuss the implications of these results on SWCNTs based sensor operation and SWCNTs thermal processing.

5.2 EXPERIMENTAL AND THEORETICAL APPROACH

5.2.1 Materials

As-produced (non-purified) SWCNTs, synthesized by the HiPco[43] method, were purchased from CNI (Houston, TX). A detailed purification procedure was described in Section 4.2.1. The only

difference introduced here was oxidation step: SWCNTs were oxidized at 523 K for 5 hours in air saturated with water vapors.

The purity of SWCNTs after air/HCl treatment was checked with X-ray photoelectron spectroscopy (Figure A1) and thermo-gravimetric analysis (TGA) (Figure 6 and Figure B1). No XPS signal, above the noise level, from Fe was detected in the purified SWCNTs, suggesting an iron content of less than 5 wt.% (detection limit for conditions used) whereas the as-produced sample gave a distinct doublet from Fe (Figure B1). According to literature data air/HCl purification reduces residual iron content from initial 20-30 wt.% to 1-5 wt.% according to TGA.[61, 70]

Before introduction into the UHV chamber the samples were sonicated in acetone (Fisher, ACS grade) for 1 hour and then deposited by drop-and-dry method on a W-grid (Alfa Aesar, 100 mesh, 0.002" wire diameter) in a flow of preheated air (~330 K).

5.2.2 Experimental setup

Temperature programmed desorption experiments with mass spectroscopy monitoring (TPD-MS) were performed in a stainless steel ultrahigh vacuum chamber, described in detail earlier (Figure 2),[99] with a base pressure of less than $<5*10^{-9}$ Torr. Before sample deposition, the W-grid was attached by nickel clamps to the sample holder copper wires of a vacuum electrical feedthrough attached to the bottom of a dewar. A K-type thermocouple (Omega) with a short time response was spot-welded to the W-grid. The design of the sample holder allows cooling of the sample to cryogenic temperatures (<100 K) and resistive heating to 1400 K.

Acetone vapor (~10^{-7}-10^{-6} Torr) was dosed through a leak valve (Varian) into the vacuum chamber to a fixed pressure for the time required to achieve the desired dose.[3] Uncorrected pressure was monitored with a nude ion gauge (Varian). To heat the sample, direct current from a power supply (Kepco) was driven through the W-grid and the temperature was monitored via the thermocouple. A shielded residual gas analyzer (RGA 300, Stanford Research Systems) was used to monitor the desorbing species. Custom programs written in Labview were used to control the temperature, monitor the dosing, and to record TPD-MS spectra.

5.2.3 Sample pretreatment and gas exposure procedures

The SWCNTs sample was placed in a vacuum chamber and evacuated to <5*10^{-9} Torr. When the sample was cooled to 90-100 K, the resulting base pressure was <1*10^{-9} Torr. Then the sample was heated at 2 K sec^{-1} to 500 K, held at 500 K for 2 h under vacuum to remove residual solvent and adsorbed gases (this sample will be referred to as SWCNTs-500). After 2 h at 500 K temperature was quenched back to 90-100 K. The SWCNTs-500 was cooled to 100 K and desired amount of acetone was dosed to the sample. After dosing, the pressure was allowed to reach approximately the same level as before dosing and allowed to stabilize for 2-5 min. Only after that were TPD-MS spectra collected. The following doses of acetone were used: 1, 5, 10, 25, 50, 100, 500, and 1000 L. After the last dose of acetone was injected and TPD-MS was collected, the sample was allowed to warm up to ambient temperature.

On the next day the sample was annealed to a higher temperature. The anneal temperatures (and times) used were 700 K (1 h), 900 K (0.5 h), and 1400 K (5 min). To indicate

[3] Exposures are given in Langmuir units, 1 L = 10^{-6} Torr sec

the anneal temperature of the sample used before acetone adsorption we abbreviate the corresponding samples as SWCNTs-500, SWCNTs-700, SWCNTs-900, and SWCNTs-1400. The adsorption energies that were evaluated from TPD profiles were calculated based on Redhead analysis with the assumption of a pre-exponential factor of 10^{13} sec^{-1}.[123]

5.2.4 Theoretical Studies - Computational Methodology[4]

Similar to our approach in a previous study,[10] we have first compared the performance of the dispersion-augmented self-consistent-charge density functional tight binding[124, 125] (SCC-DFTB-D, denoted in the following DFTB-D for brevity) method for the prediction of Cπ-acetone interaction energies ΔE to the corresponding *ab initio* large-basis-set MP2 energetics for a coronene ($C_{24}H_{12}$)-acetone model system. Here, we employed the resolution-of-identity (RI-) approach for the MP2 calculations as implemented in the program system TURBOMOLE,[126] using the supplied Ahlrichs basis sets SVP (split-valence polarized, containing up to d/p basis functions for 2nd and 1st row elements),[127] TZVPP (triplet-zeta valence polarized, containing up to f/d basis functions for 2nd and 1st row elements),[128] and QZVPP (quadruple zeta polarized, containing up to g/d basis functions for 2nd and 1st row elements)[129] and their corresponding auxiliary basis sets for the RI approximation.[126] Full geometry optimizations for various molecular adsorption configurations of the acetone molecule relative to the coronene plane were performed at the MP2/SVP levels of theory as well as at the SCC-DFTB-D level for comparison, making use of molecular symmetry where possible for MP2 calculations. MP2/TZVPP and

[4] This chapter was written by Professor Irle and PhD student Yoshifumi Nishimura (Institute for Advanced Research and Department of Chemistry, Nagoya University, Japan) and Keiji Morokuma (Department of Chemistry, Emory University, Atlanta, GA).

MP2/QZVPP single point energies were computed for the MP2/SVP geometries. The influence of the basis set superposition error (BSSE) on ΔE was evaluated by performing standard Boys-Bernardi counterpoise correction.[130] In all calculations, default convergence criteria were adapted for wavefunctions and geometries. The DFTB-D method includes the dispersion energy E_{dis} by adding the sum of two-center London dispersion term between nuclei α and β separated from each other by a distance $R_{\alpha\beta}$:

$$E_{dis} = -\sum_{\alpha\beta} f(R_{\alpha\beta}) C_6^{\alpha\beta} (R_{\alpha\beta})^{-6}, \qquad (1)$$
$$f(R_{\alpha,\beta}) = [1 - \exp(-3 * (R_{\alpha,\beta} / R_0)^7)]^4$$

where $f(R_{\alpha\beta})$ is a damping function to suppress contributions of E_{dis} for small interatomic distances where the London dispersion term is not valid. We follow Elstner *et al.* who assume R_0 to be 3.8 Å for all elements of the first row of the periodic table.[124] The derivation of the C_6 parameters was described in detail elsewhere.[124] Recent, very favorable performance benchmarks were described for instance for carbon nanosystems[131-133] and biosystems[134].

5.3 EXPERIMENTAL RESULTS

The desorption of acetone was followed by monitoring the 43 amu (CH_3CO) and 58 amu ($CH_3(CO)CH_3$) signals. Our data will be presented in terms of 43 amu profile as it was the dominant fragment in the mass spectrum of pure acetone: the signal for the parent fragment 58 amu was 4.2 times less intense than the 43 amu signal. In addition, TPD-MS for masses 44 and 18 amu were collected.

Acetone desorption from purified SWCNTs was characterized by three desorption peaks in the 1-100 L exposure range (Figure 11A). For SWCNTs-500, two dominant peaks were present at ~240 (~50 kJ mol^{-1}) and ~300 K (~75 kJ mol^{-1}), and a smaller peak at 140 K (~35 kJ mol^{-1}). The peak at 300 K grew faster than the other peaks for exposures of 1-50 L (Figure 11A), while for higher exposures (>50 L) the peak at 240 K for SWCNTs-500 increased faster than the peak at 300 K. For samples annealed to higher temperatures the ratio between 240 and 300 K peaks changed: for the SWCNTs-700 and SWCNTs-900 samples the peak at 300 K was dominant for exposures up to 100 L (Figure 11A), suggesting limited access to sites with the highest adsorption energy for SWCNTs-500. The annealing to 1400 K decreased the 300 K peak intensity at the expense of the 140 and 240 K peaks reversing the tendency observed for 500-700-900 K annealing temperatures, i.e., the increase of intensity for the 300 K peak. The comparison of acetone desorption profiles for SWCNTs-900 and SWCNTs-1400 suggests the loss of the sites responsible for the peak at 300 K for SWCNTs-1400 in comparison with SWCNTs-900 (Figure 11A) at the expense of sites responsible for the peaks at 140 and 240 K. Qualitatively, the acetone desorption profile for SWCNTs-1400 looked similar to the profile for SWCNTs-700, except for the absence of the high temperature tail that lasts up to 450 K for SWCNTs-700 sample. The SWCNT anneal temperature had a strong impact on the acetone adsorption behavior. It appears that annealing to consecutively higher temperatures (500-700-900 K) opened access to energetically more favorable adsorption sites (i.e., peak at 300 K and extended up to 450 K desorption tail), while annealing to 1400 K led to partial re-blocking of these sites.

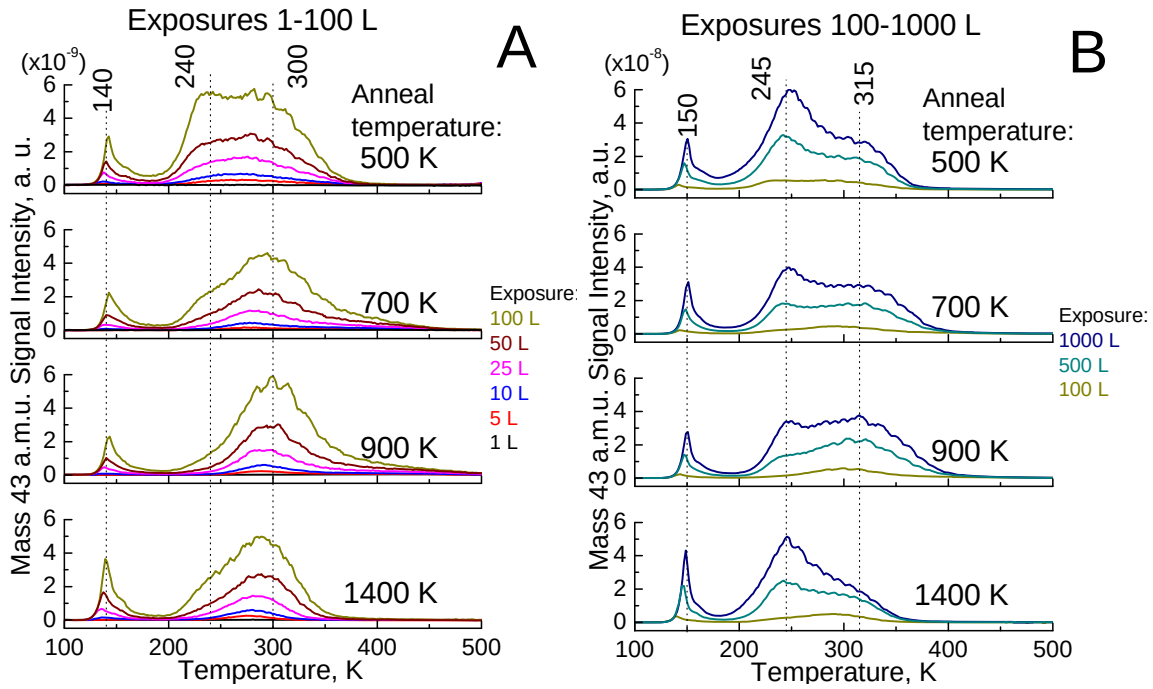

Figure 11: Desorption of acetone (mass 43 amu (e.g., CH_3CO)) from purified SWCNTs annealed to 500, 700, 900, and 1400 K. (A) Acetone exposure 1-100 L. (B) Acetone exposure 100-1000 L. Sites with three different adsorption energies ~35, 50, and 75 kJ/mol appear to be present on SWCNTs. The acetone uptake by each site depends on the SWCNT anneal temperature.

To understand whether acetone undergoes irreversible chemical transformation during interaction with SWCNTs,[121, 122] several acetone fragments were traced simultaneously during TPD: 43 amu (CH_3CO), 15 amu (CH_3), 58 amu ($CH_3C(O)CH_3$), and 28 amu (CO). The desorption of all acetone fragments have similar profiles (Figure A3). Moreover, the relative intensities of the different mass fragments were the same as for gas phase acetone[5]. Those findings imply that acetone cryogenically adsorbed on SWCNTs desorbs as an intact molecule.

Several control experiments were performed to verify the assignment of TPD-MS peaks. First, the interaction of acetone with the W-grid, used as a sample support, was studied as a

[5] The relative intensities of the different mass fragments for gas phase acetone were obtained by introducing a constant pressure of acetone (10^{-7} Torr) into the TPD chamber while monitoring the mass spectrum (1-100 amu).

function of the anneal temperature: independent of anneal temperature acetone desorbs from the W-grid with a maximum at 136-153 K depending on acetone exposure (5-1000 L) (Figure B2).

A second control experiment was the adsorption of acetone on as-produced SWCNTs without any chemical purification treatment (Figure 12A). The as-produced SWCNTs are characterized by admixtures of amorphous carbon and iron catalyst particles[43] that might influence the adsorption behavior of the purified SWCNTs as well. Control experiments identified three peaks for acetone desorption from the as-produced SWCNTs: 140-150, 180-240, and 280 K. The peak at 280 K had a small intensity and was observed as a shoulder of the more intense peak at 220-240 K at moderate exposures (<100 L). Only after anneal at 900 K did the peak at 280 K became comparable in intensity to the peak at 220-240 K ($\leq$50 L). Annealing of the as-produced SWCNTs to 1400 K resulted in a compete cancellation of the 280 K peak. High acetone exposures (1000 L) to the as-produced SWCNTs resulted in a broad peak with desorption maximum at 185-200 K depending on anneal temperature (Figure 12A). To summarize, as-produced SWCNTs had peaks similar to purified SWCNTs except that the ratio between peaks was different. The peak at 180-240 K was the dominant feature in desorption spectra of acetone for the as-produced SWCNTs, while the peak at 280 K was pronounced only for low exposures (<50 L), and much smaller for purified SWCNTs.

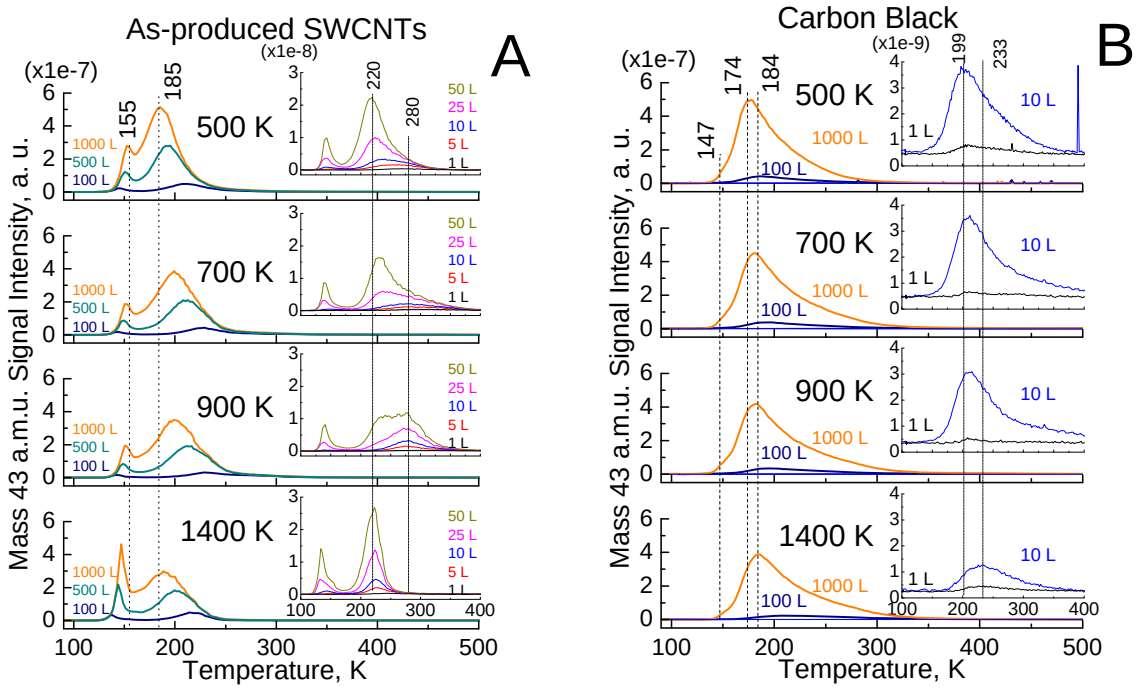

Figure 12: Comparison of acetone adsorption on as-produced SWCNTs (**A**) and carbon black (**B**) annealed to different temperatures. As-produced SWCNTs contain amorphous carbon, iron catalyst, and are characterized by low access to the endohedral sites due to caps present at the ends of SWCNTs.[6, 135] Three desorption peaks of acetone for as-produced SWCNTs can be detected: 140-150, 180-240, and 280 K. As-received carbon black has a limited porous structure that favors stronger acetone adsorption than HOPG.[17, 19] Two desorption peaks can be detected for carbon black: small shoulder at 140-150 K, and intense peak at 180-240 K.

In order to isolate features characteristic of acetone interaction with SWCNTs, acetone adsorption was performed on a carbon black sample (CB-460, Cabot) characterized by a limited porous structure (S_{BET}~76 m^2/g, Figure C1). Carbon black sample was used as a model material for amorphous carbon present in as-produced SWCNTs. Carbon black was degassed at the same temperatures as SWCNTs before acetone dosing (Figure 12B). For the carbon black sample annealed to 500 K, a peak with desorption maximum at 200 K was observed for low exposures (10 L) that shifted to lower temperatures with exposure increase: for the 1000 L peak shifted to 174 K (Figure 12B). The small shoulder at 150 K was noticeable only for high acetone exposures. Annealing to consecutively higher temperatures resulted in a small shift of the acetone (10 L) desorption peak maxima from 199 K (anneal 500 K) to 233 K (anneal 1400 K).

Overall, acetone adsorption on carbon black was characterized by two peaks: the peak at 150 K noticeable only for high exposures and the peak at 180-240 K. The position of 180-240 K peak was a function of exposure (the higher exposure – the lower $T_{des.}$) and anneal temperature (the higher anneal temperature – the higher $T_{des.}$) (Figure 12B). Acetone adsorption behavior on the carbon black at high exposures (1000 L) annealed at 500-700-900 K was similar to the behavior of acetone adsorption on as-produced SWCNTs annealed to the same temperatures suggesting that the acetone adsorption behavior of as-produced SWCNTs was, in some extent, determined by the presence of carbonaceous impurities. The acetone desorption peak at 280-300 K, specific for as-produced and purified SWCNTs, was absent for the carbon black.

5.4 DISCUSSION OF EXPERIMENTAL RESULTS

Previous experiments suggest that CNT purification by oxidative methods leads to the introduction of oxygen functionalities[10, 45, 70, 75] and defects[74, 76] to SWCNTs. Typically, nanotubes assemble into bundles[51] due to van der Waals forces.[136] The bundle structure favors multiple adsorption sites such as endohedral, interstitial, grooves, and external walls. It is reasonable to expect different interaction energies for molecules adsorbed on different sites.

The observation of all four adsorption sites is possible if all the sites are accessible. The interstitial sites of nanotube (with d ~ 10 Å) bundles are ~0.26 nm[137] wide and cannot be filled even by small molecules, e.g., Xe, CH_4, Ne,[138] and Ar[139]. On the other hand, interstitial sites of heterogeneous bundles, formed by nanotubes of different diameters, are accessible as was shown by Monte Carlo simulations.[111] A narrow distribution of nanotube diameters is also important

for the observation of distinct desorption peaks as the adsorption of acetone on endohedral sites becomes stronger with increasing SWCNT walls curvature (see Figure 15).

Adsorption energies depend also on intermolecular interactions. For alkanes adsorbed on bundled SWCNTs the existence of three adsorption sites has been suggested, endohedral, grooves, and external wall, while the fourth observed TPD peak was assigned to multilayer adsorption.[110] In contrast to the well-resolved desorption peaks of paraffins,[110] methanol (CH_3OH) adsorption on SWCNTs was characterized by a single peak with a weak high temperature shoulder that was noticeable only for small exposures.[140] The absence of distinct peaks corresponding to different adsorption sites for methanol suggests that intermolecular interactions (e.g., hydrogen bonding) might be important for methanol.[140] There is no evidence that acetone─acetone interactions are responsible for the observed desorption behavior (Figure 11). The desorption of acetone multilayers, reflecting intermolecular interactions, from the surface of HOPG occurs at ~145 K.[119]

In order to assign the desorption peaks of acetone from SWCNTs observed in the TPD spectra, we considered four adsorption sites: endohedral, interstitial (including large interstitial channels[111]), grooves, and external walls. The TPD spectra, however, show only three desorption peaks (Figure 11). For as-produced SWCNTs, characterized by capped ends,[6, 135] the intensity of the desorption peak at 300 K was suppressed, while peaks at 140 and 240 K were well-developed (Figure 12A). Finally, peaks with desorption temperatures higher than 180 K, observed for acetone adsorption on SWCNTs, were not observed for acetone adsorption on HOPG.[119, 120]

On the basis of the preceding discussion and the results of theoretical simulations (section 5), the following assignments were made: the peak at ~300 K (with estimated adsorption energy

of ~75 kJ mol^{-1}) was assigned to the adsorption of acetone on endohedral sites of small SWCNTs (~7.7 Å). The peak at ~300 K had a limited intensity for oxidatively purified SWCNTs-500 (Figure 11) and for the as-produced SWCNTs (Figure 12A), both known to have limited access to the endohedral sites.[6, 101, 135] The peak at ~240 K (~50 kJ mol^{-1}) was assigned to adsorption of acetone on grooves, in accessible interstitial channels, and in endohedral sites of large SWCNTs (~14 Å). The peak at 240 K could arise from acetone interaction with amorphous carbon, as it has been shown to be present for carbon black (Figure 12B). Finally, the peak at 140 K (~30 kJ mol^{-1}) was assigned to acetone adsorption on external walls and multilayer adsorption.[119, 120] Desorption of acetone from the W-grid can also contribute to the 140 K peak signal intensity (Supporting Information Figure B2).

Accessibility of endohedral sites appears to be strongly affected by the pretreatment procedure. Endohedral sites of small diameter (~7.7 Å) oxidatively purified SWCNTs are presumably blocked by oxygen functionalities (Figure 13A).[70] These are probably not removed until annealing to $\geq$600 K, when some surface functional groups decompose,[70] allowing more access to endohedral sites (Figure 7C). Annealing of SWCNTs to 900 K results in some additional decomposition of oxygen functionalities in agreement with the TPD profile of CO_2 release (Figure 7C and Figure B4), further increasing access to endohedral sites (Figure 13B).[70, 101] The acetone TPD profiles of the SWCNTs samples annealed to 700 and 900 K are characterized by temperature tails that extend up to 450 K, associated with an apparent acetone desorption energies ~110 kJ mol^{-1}. We believe that nanotubes of small diameter (<0.9 nm) might contribute to such an extended desorption profile due to high binding potential or/and diffusion limitations. To summarize, the presence of oxygen functionalities, which form on

SWCNTs during the oxidative purification process, limits acetone access to endohedral sites, until removal by annealing to high temperatures (700-900 K) in agreement with the literature.[101]

(**A**) SWCNT showing presence of oxygen functionalities after oxidative purification step. Oxygen functionalities block the access to endohedral sites of nanotubes.[101]

(**B**) Upon annealing decomposition of oxygen functionalities results in structural defects on SWCNT opening access from the ends and through side wall defects to endohedral sites.[101]

(**C**) Structural defects may recombine with formation of Stone-Wales defects[141] and caps[142].

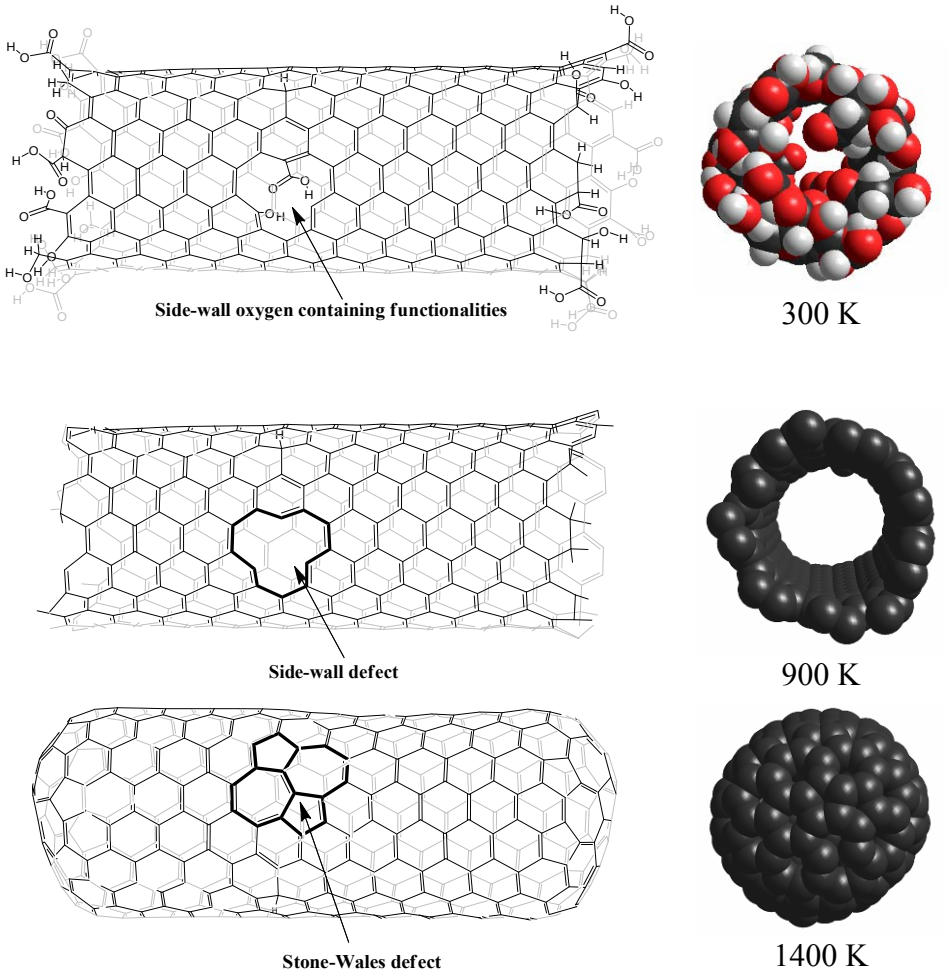

Figure 13: Proposed evolution of endohedral sites accessibility based on SWCNT (8,8) model. Color code: black, carbon; red, oxygen; white, hydrogen.

We think that, after anneal of SWCNTs to 1400 K, the nanotubes become partially closed and less defective due self-healing that reduces access to endohedral sites: the desorption peak at~300 K was reduced in intensity for SWCNTs after anneal at 1400 K (Figure 11). It was shown by molecular dynamics simulations that CNT defects may disappear by recombination with carbon adatoms and by Stone-Wales defects formation.[141] Moreover, according to results

of theoretical calculations, pristine nanotubes can cap themselves at elevated temperatures.[142] It was established by HR-TEM that anneal of SWCNTs even to 1073 K leads to partial closing of SWCNTs.[143] Reduction of sidewall defects and closing of nanotubes limit the accessibility of endohedral sites (Figure 13C). Another possible explanation for the disappearance of the acetone peak at 300 K is a temperature-induced coalescence of SWCNTs with formation of nanotubes of larger diameter.[144, 145] We believe that coalescence of nanotubes is not likely in our work, because the conditions used (1400 K) are milder than conditions ($\geq$1773 K) where coalescence of SWCNTs was reported.[144, 145] Moreover, Raman data suggest that SWCNTs preserve their tubular structure even after annealing to 1300/1400 K.[70]

The results on cryogenic adsorption of acetone on SWCNTs suggest the presence of adsorption sites that are not characteristic for acetone adsorption on a simple planar carbon surface, e.g., HOPG.[119, 120] Moreover, the C-black sample studied for control purposes showed two desorption peaks at 140-150 K and at 200-230 K (Figure 12B). It appears that the acetone binding energy correlates with available porous structure: adsorption in pores is defined by dispersion forces and ultimately the ratio of the molecule size to the pore diameter defines the overall potential.[146, 147] For pores with a large diameter, i.e., significantly exceeding the effective size of an adsorbate, the interaction potential would be close to the potential of a flat surface (e.g., HOPG). As the diameter of the pore reduces, the adsorbate will interact more strongly with the internal walls (Figure 15). The differences in adsorption behavior between HOPG, carbon black, and SWCNTs are likely associated with morphology of each material. HOPG is known to have no porous structure,[7] while carbon black has limited porous structure. SWCNTs have unique adsorption properties due to self-organization in bundles that provides a variety of adsorption sites, whose availability depends on pretreatment conditions. The increased capacity

for acetone strongly bound to the SWCNTs after purification correlates well with an increase of microporous structure.[46, 69]

We detected no irreversible chemical interaction upon low temperature adsorption of acetone on SWCNTs (Supporting Information Figure A3). It has been suggested that acetone adsorbs chemically on as-produced SWCNTs[121] and MWCNTs.[122] The conditions under which acetone was introduced to SWCNTs in the present work (100 K, $\leq 10^{-6}$ Torr) are different from the conditions used by others.[121, 122] Chakrapani et al. used sonication to interact SWCNTs with acetone.[121] It is possible that sonication-induced changes in temperature and pressure[32] might result in chemical interaction of acetone with SWCNTs.[121] Shih and Li, who dosed acetone to MWCNTs at temperatures of $\geq$303 K, proposed chemical interaction between MWCNTs and acetone based on high adsorption enthalpies (−68.3 kJ mol^{-1}), but provided no further evidence.[122] The highest estimated adsorption energy for acetone adsorbed on SWCNTs-700 and 900 was ~110 kJ mol^{-1} (450 K tail). However, our results suggest that acetone dosed from the gas phase desorbs as an intact molecule, suggesting that the interaction of acetone with SWCNTs upon low temperature adsorption is chemically reversible.

The results of the current work do not provide insight into why SWCNT-based sensors respond to acetone vapors.[11, 116] Acetone adsorbed at low temperature interacts reversibly with SWCNTs due to dispersion forces with essentially no electron transfer or polarization (section 5). Charge transfer might occur for acetone adsorption on oxygen functionalities, as it was established that sensor response improved with increasing degree of SWCNT oxidation.[11] It should be noted that the interaction of acetone with carboxylic groups on the surface of SWCNTs could not explain the small irreversible shift of sensor baseline after the first pulse of

acetone as reported by Snow and Robinson.[116] The baseline shift might be due to irreversible chemical interaction of acetone with defect sites.[121, 122]

Our experiments suggest that annealing of carbon nanotubes to high temperatures (> 900 K) leads to defect self-healing and closing of SWCNT ends. Annealing leads to decomposition of the surface oxygen functionalities that presumably stabilize the defects. This phenomenon is important for processing of carbon nanotubes for technological applications. In some cases, this nanotube closing should be avoided if availability of endohedral sites is a target factor, e.g., for hydrogen storage applications. In other cases, capped nanotubes might be useful, e.g., for fabrication of field emitters.[148, 149]

5.5 THEORETICAL RESULTS AND DISCUSSION[6]

5.5.1 Comparison of DFTB-D with MP2 Energetics: Benchmark Results

The model systems employed in this benchmark study are classified as planar parallel 1 (**PP1**) and 2 (**PP2**), up-perpendicular 1 (**UP1**) and 2 (**UP2**), and down-perpendicular 1 (**DP1**) and 2 (**DP1**), where up and down refer to the position of the oxygen relative to the coronene plane assumed "underneath" the acetone molecule; "1" and "2" labels distinguish the two possible

[6] This chapter was written by Professor Irle and PhD student Yoshifumi Nishimura (Institute for Advanced Research and Department of Chemistry, Nagoya University, Japan), and Professor Keiji Morokuma (Department of Chemistry, Emory University, Atlanta, GA).

orientations of the acetone molecule relative to the hexagons two symmetry-unique C_2 axes parallel to the plane of the carbon hexagon (Figure 14).

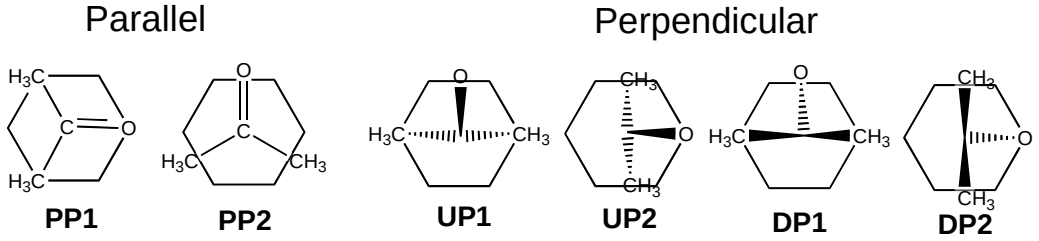

Figure 14: Relative orientations of the acetone molecule on the central hexagon ring of coronene. Only the central coronene ring is shown, and is positioned underneath the acetone molecule. From left to right: planar parallel 1 (**PP1**) and 2 (**PP2**), up-perpendicular 1 (**UP1**) and 2 (**UP2**), and down-perpendicular 1 (**DP1**) and 2 (**DP2**).

Table 2: Counterpoise corrected interaction energies ΔE (MP2 BSSE counterpoise corrections in parentheses) [kJ mol^{-1}] and for acetone-coronene complexes shown in Figure 14 MP2 energies were obtained at MP2/SVP geometries.

ΔE [kJ/mol]	MP2/SVP	MP2/TZVPP[a]	MP2/QZVPP[a]	DFTB-D[b]
PP1 [c]	-23.92 (29.91)	-36.15 (12.93)	-39.38 (6.21)	-28.78
PP2 [c]	-15.20 (28.36)	-31.02 (12.41)	-34.30 (5.74)	-41.90
UP1	-18.47 (16.36)	-29.65 (7.01)	-29.64 (3.24)	-27.84
UP2	-16.66 (16.51)	-27.88 (7.00)	-29.59 (3.29)	-28.56
DP1	-4.35 (15.23)	-8.91 (7.76)	-10.72 (3.84)	-9.85
DP2	-5.13 (14.31)	-8.91 (7.22)	-10.36 (3.69)	-9.86

[a] Geometry from MP2/SVP optimization. [b] Geometry optimized at DFTB-D level of theory. [c] Due to geometrical edge effects these energies are remarkably different, see text.

Table 2 lists the interaction energies ΔE between acetone and coronene for the counterpoise-corrected various MP2 and DFTB-D levels of theory, as well as MP2 counterpoise correction (CP) in parentheses. CP is largest for **PP** compounds and is almost halved in **UP** and **DP** compounds, likely because of the reduced amount of orbital overlap due to geometrical

reasons. As expected, CP is largest for the smallest basis set (SVP) and is reduced by about a factor of 2 going from one size of basis set to the next larger one. The most accurate CP-corrected MP2/QZVPP//MP2/SVP results are reproduced by DFTB-D within 2 kJ mol^{-1} accuracy when **UP** and **DP** geometries are reoptimized by the latter method. In case of **PP** geometries, the computed interaction energy very much depends on the position of the center of the acetone molecule relative to the coronene center. The center of mass of acetone in the case of the **PP1** complex is offset from the center of the acetone─coronene complex by 0.01 Å (MP2/SVP) and 0.77 Å (DFTB-D), while in the case of the **PP2** complex, the offsets are smaller and amount to 0.01 Å (MP2/SVP) and 0.32 Å (DFTB-D). If one additional hexagon ring is added around coronene (circumcoronene $C_{54}H_{18}$), DFTB-D interaction energies for corresponding **PP1** and **PP2** complexes are smaller and more similar with ─24.9 and ─24.4 kJ mol^{-1}, respectively, indicating that the influence of coronene edge hydrogen atoms provides an undesirable but unavoidable contribution to the DFTB-D stabilization energies. If averages are taken between the **PP1** and **PP2** structures, the DFTB-D average (─35.3 kJ mol^{-1}) is very close to the CP-corrected MP2/QZVPP average (─36.8 kJ mol^{-1}) with a difference less than 2 kJ mol^{-1}. However, we must stress that the best MP2 energies are probably still too high by a few kJ mol^{-1} compared to the basis set limit. Nevertheless, at all levels of theory the planar parallel structures are energetically more favorable than perpendicular complexes, of which the ones with oxygen pointing toward coronene are decidedly the least favorable. We presume that the multicenter contact favors the **PP** structures in dispersion energy more than the perpendicular structures. DFTB-D optimized structures give generally reduced intramolecular distances by about 0.1 to 0.2 Å relative to MP2/SVP, which, however, does not result in a large difference in energy, because the intermolecular potential energy surface is rather flat with respect to interatomic

distances. Therefore, we conclude that the overall agreement between the computationally inexpensive DFTB-D interaction energies and the much more expensive CP-corrected MP2/QZVPP energetics is excellent, in agreement with other benchmark studies that focused on molecule adsorption on graphitic walls.[131-133] This finding makes us confident to use DFTB-D for the estimation of interaction energies in much larger SWCNT─acetone complexes.

Regarding the physical nature of the interaction between acetone and coronene, we note that the adiabatic ionization potentials of coronene and acetone are very high, 7.29 and 9.70 eV, respectively, and the corresponding adiabatic electron affinities (EAs) are only 0.470 and 0.001 eV, respectively. No substantial charge transfer is therefore expected, and Mulliken population analysis[150, 151] and Heinzmann-Ahlrichs modified atomic orbital (MAO) partial charges[152] derived from Hartree─Fock/SVP wave functions confirm essentially zero electron transfer. Charge polarization on the coronene surface amounts to at most a few hundredths of an electron per carbon atom by MAO and even less with Mulliken charge, and therefore we do not find that mirror charges are created on the graphitic surface due to the presence of the polar acetone molecule. This is equally true for the DFTB-D Mulliken charge analysis. Hence, we conclude that the interaction is almost entirely dominated by dispersion energies and can be treated reasonably well with the empirically damped $1/R^6$ London dispersion term. In **PP** compounds, CO/coronene π─π interactions are possible, which are considered a special case of dispersion interactions. The CO bond is slightly tilted with oxygen pointing toward the coronene surface, with the shortest OC(coronene) distances around 2.9 Å and the shortest C(central acetone carbon)C(coronene) distances around 3.2 Å at the MP2/SVP level of theory. In case of corresponding DFTB-D geometries, the distances are slightly longer at 3.0 Å (OC(coronene)) and 3.3 Å (CC(coronene)). The exact values depend on the orientation of the acetone with

respect to the coronene molecule. These distances are shorter than the sum of van der Waals radii and are therefore consistent with π–overlap between the C=O double bond of acetone and the π–orbitals of coronene.

5.5.2 DFTB-D Interaction Energies for Acetone-SWCNT Complexes

We have used the DFTB-D method to study the physisorption sites and interaction energies, ΔE, of acetone at various sites of SWCNTs, using a hydrogen-terminated, 10 Å long (11,9) SWCNT model tube as well as a hydrogen-terminated 10 Å (6,5) SWCNT model tube. The diameters for these species were found after geometry optimization to be 14.0 Å and 7.7 Å, respectively.

Table 3 lists all computed DFTB-D interaction energies ΔE for optimized structures obtained in the respective endohedral and exohedral complexes for the (11,9) and (6,5) tubes.

Table 3. DFTB-D interaction energy ΔE and its components [kJ mol^{-1}] for acetone-SWCNT complexes. N/A means that optimization from this conformation resulted in a different confirmation (see text)

	DFTB-D		DFTB only		D only	
ΔE [kJ/mol]	endo	exo	endo	exo	endo	exo
(11,9) perpendicular to tube axis						
PP1	-44.38	-26.32	2.93	3.03	-47.32	-29.35
PP2	-44.95	-24.91	4.17	4.57	-49.11	-29.48
UP1	-39.45	-22.73	2.95	1.05	-42.40	-23.78
UP2	-39.86	-23.85	2.19	0.22	-42.05	-24.07
DP1	N/A	-7.67		6.76		-14.43
DP2	N/A	-8.41		6.34		-14.76
(11,9) parallel to tube axis						
PP	-45.28	-26.04	0.93	4.17	-46.21	-30.21
UP	-38.82	-23.24	1.47	0.70	-40.29	-23.95
DP	-23.69	-9.31	6.64	5.29	-30.33	-14.61
(6,5) parallel to tube axis						
PP	-74.35	N/A	23.80		-98.15	
UP	N/A	-24.56		-1.99		-22.57

Following our previous systematic scheme of placing acetone on coronene, we attempted to optimize, for each endohedral and exohedral acetone complex with the (11,9) SWCNT model tube, the two planar parallel as well as the four perpendicular adsorption arrangements of acetone on the central hexagon rings of the sidewall. In addition, in a nanotube, the tube axis breaks the centrosymmetry that existed in a coronene, and the alignments of acetone parallel or perpendicular to the tube directions are not equivalent. Therefore, we should formally consider 12 possible conformations. However, for the endohedral complexes with parallel axis alignment, we found that no local stable minimum of **DP** type exists with oxygen pointing toward the sidewall; optimization for these structures always resulted in parallel planar **PP** type complexes. For each acetone orientation of parallel alignment structures, only one minimum was found where the C─C─C axis of acetone was aligned closely to the tube direction, namely, in "armchair direction"; the alternative zigzag conformation does not correspond to a minimum

structure in the case of parallel alignment. In the case of the much smaller (6,5) tube, we only found a single minimum associated with the endohedral complex, namely, the acetone aligned parallel to the tube direction, the **PP** structure. Similarly, we found only a single minimum with the exohedral structure, the **UP** structure.

The resulting interaction energies for the (11,9) model tube can be compared with the values obtained for coronene at the DFTB-D level. In general, endohedral complexes between acetone and SWCNTs are more strongly bound than acetone─coronene, while exohedral complexes are slightly more weakly bound than acetone─coronene. The energy differences of similar structures between perpendicular or parallel alignments (such as perpendicular **PP1** and **PP2** and parallel **PP**) are small and on the order of a few kJ mol^{-1}. The order of the binding energy $|\Delta E|$ with respect to the position of oxygen decreases in the order: **PP** > **UP** > **DP**, with differences more pronounced for the more strongly bound endohedral complexes (46 > 39 > 24 kJ mol^{-1}) compared to the exohedral complexes (26 > 23 > 8 kJ mol^{-1}). This order is the same as found for the acetone─coronene complexes. Interestingly, the energy difference between **UP** and **DP** complexes is independent from endo- or exohedral adsorption, and is roughly 15 kJ mol^{-1} in favor of the minimum with O pointing away the carbon wall. This difference is almost the same as for coronene, where the **UP-DP** interaction energy gap is 18 kJ mol^{-1}.

By far the strongest interaction was found for the endohedral acetone complex with the small-diameter (6,5) tube with ΔE=─74.4 kJ mol^{-1}. From the present results, we can roughly estimate the range of interaction energies; the strongest adsorption is inside small-diameter tubes with $\Delta E \sim$ ─74 kJ mol^{-1} for the (6,5) tube, which will reduce to $\Delta E \sim$ ─45 kJ mol^{-1} for the (11,9) tube and becoming slightly smaller as the tube diameter further increases. Exohedral adsorption with $\Delta E \sim$ ─24 kJ mol^{-1} is weaker regardless of the size of the tube.

Table 3 also shows DFTB electronic energy ("DFTB-only") and dispersion energy E_{dis} ("-D-only", eq 1) contributions to the DFTB-D energy separately. This partitioning shows that the nature of the interaction is entirely due to dispersion. DFTB-D Mulliken population analysis reveals, as in the case of coronene, virtually zero intermolecular charge transfer and zero intramolecular charge polarization. The role of a strong dispersion field inside a small nanotube becomes clear in the case of the endohedral complex for the (6,5) tube, where the DFTB interaction without dispersion term is repulsive by 23.8 kJ mol^{-1}, while the attraction by dispersion interaction ~100 kJ mol^{-1}. Preliminary results for acetone adsorption in groove sites suggest that $|\Delta E|$ may indeed follow an estimate of 1.5-1.7 times the interaction energy of exohedral sites proposed recently by Ellison et al.,[153] and suggest adsorption energies to be about 30-50 kJ mol^{-1}.

In Figure 15 we have plotted the averaged interaction energies ΔE for **PP** and **UP** structures as a function of sidewall curvature, measured continuously by the inverse of the tube diameter $1/d$, as we have done before in the case of covalent X-SWCNT bonding.[154] In the case of the small-diameter tube, we used the same ΔE for **PP** and **UP**, since in the endohedral compound, no such distinction can be made (Figure 15). Endohedral complexes exhibit acetone interaction with negative curvature and are therefore associated with negative values of $1/d$, while the situation in exohedral complexes corresponds to positive curvature/positive values of $1/d$. For zero curvature (infinite diameter), we tentatively used the averaged interaction energies for the coronene model system. Figure 15 clearly shows a trend in that the interaction strength of the acetone with the tube sidewall strongly depends on the sidewall curvature, and that endohedral complexes are only substantially stabilized over the normal graphite─acetone interaction when the sidewall curvature becomes very large.

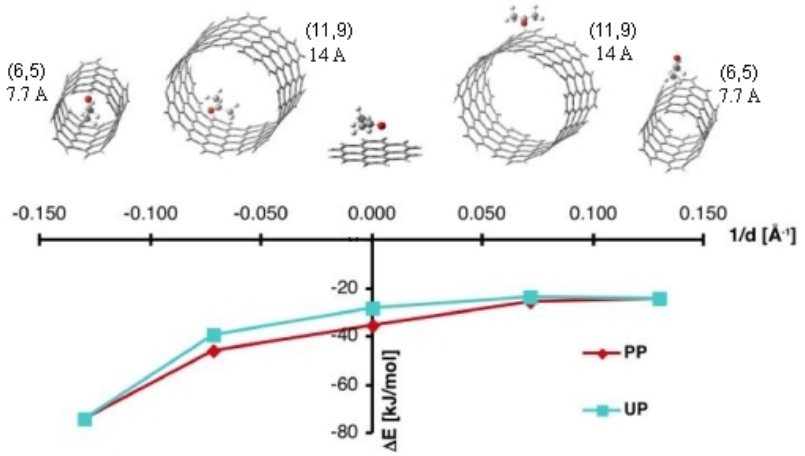

Figure 15: DFTB-D interaction energy ΔE plotted versus sidewall curvature for averaged series of **PP** and **UP** complexes. For details of the plot see text

5.6 CONCLUSIONS

In the course of acetone adsorption on SWCNTs studies at low temperature by TPD-MS and theoretical simulations, several important findings were made.

I. Acetone desorbs from SWCNTs giving three distinct desorption peaks:

   a. A strongly bound adsorption form with a peak desorption maximum at 300 K (~75 kJ mol^{-1}), assigned to adsorption in endohedral sites of small nanotubes (~7.7 Å).

   b. A second form of acetone adsorption with a desorption maximum at 240 K (~50 kJ mol^{-1}), assigned to adsorption on endohedral sites of large nanotubes (~14 Å). In the case of bundled SWCNT systems this TPD peak can be assigned to acetone adsorption on grooves and possibly accessible interstitial channels. For SWCNT samples

with a high fraction of amorphous carbon content, this peak might originate from interaction with amorphous carbon as well.

c. A third form with a desorption maximum at ~140 K (~30 kJ mol^{-1}) was assigned to acetone adsorption on external walls and multilayer formation. This peak was more pronounced for SWCNTs (systems with more graphitic-like structure), rather than for carbon black (disordered carbon).

II. Oxygen functionalities present on the surface of SWCNTs can block access to endohedral sites of small SWCNTs (~7.7 Å). Oxygen functionalities decompose at high temperatures (>500 K) allowing access to endohedral sites.[101]

III. Acetone adsorbed at cryogenic temperatures desorbs as an intact molecule (Supporting Information Figure B3).

IV. Annealing to 1400 K leads to partial re-blocking of endohedral sites for acetone. We assign this observation to the thermal closing of SWCNTs.[142, 143]

V. Theoretical results indicate the following:

a. The nature of acetone interaction with SWCNTs is entirely due to the dispersion forces. No significant charge transfer or polarization was found.

b. Acetone orientation with oxygen pointing toward graphitic surfaces is energetically the least favorable orientation. Energetically most preferable is adsorption where the CCCO plane of acetone is parallel to the sidewall, followed by conformations where oxygen is pointing away from the sidewall.

c. A strong correlation between physisorption energy and sidewall curvature was found. Exohedral sites are slightly less favorable than acetone─graphite interactions (ΔE between 24 to 26 kJ mol^{-1}), while large-diameter nanotubes with endohedrally

encapsulated acetone are somewhat more favorable with ΔE around 45 kJ mol^{-1}. The strongest interaction was obtained when placing acetone inside a small-diameter (6,5) nanotube, where we obtained a ΔE of 74 kJ mol^{-1}.

Acknowledgment

Author acknowledges the help of Professor Strongin and Doug Hausner (Temple University) for XPS analysis and Professor Baran and Dr. Quan Wan (Temple University) for TGA analysis.

Supplemental Information (Appendix B)

Figure B1 shows results of XPS and TGA analysis that highlights the effect of air-HCl purification. The results of acetone desorption from a W-grid are shown in Figure B2: acetone physisorbs on tungsten with a desorption temperature of 140-150 K. In Figure B3: the same desorption profiles for different acetone fragments suggests that acetone desorbs as an intact molecule. Figure B4: profile of CO_2 extracted from full TPD spectra of a SWCNT sample in a range of 220-1400 K.

6.0 TEMPERATURE AND PRESSURE DEPENDENCE OF SOLVENT MOLECULE ADSORPTION ON SINGLE WALL CARBON NANOTUBES AND THE EXISTENCE OF A "PRESSURE GAP".

This chapter was submitted for publication. Theoretical calculation for this part of the work were provided by Professor Irle and PhD student Yoshifumi Nishimura (Institute for Advanced Research and Department of Chemistry, Nagoya University, Japan)

Abstract

The use of solvents for the dispersion of single wall carbon nanotubes (SWCNTs) is important for multiple applications. In the present paper, the interaction of acetone and ethanol with purified SWCNTs was studied by temperature programmed desorption with mass spectrometric analysis (TPD-MS), after reflux, sonication, or exposure to ambient pressures of solvent vapors. It was found that after reflux, sonication, or exposure to solvent vapors, solvent molecules bind tightly to SWCNTs. Upon heating the bound acetone desorbs in ~400-900 K range, corresponding to binding energies of ~100-225 kJ mol^{-1}. Simultaneous tracking of multiple acetone fragments suggests that acetone (T_{des}~400-900 K) desorbs as an intact molecule. Upon heating ethanol desorbs as an intact molecule from SWCNTs in ~400-800 K region, suggesting binding energies of ~100-200 kJ mol^{-1}. Carbon black also showed the ability to bind strongly simple organic molecules. The uptake capacity of carbon black with respect to simple organic

molecules was significantly less than the uptake capacity of SWCNTs. The binding energies reported here are in stark contrast to the energies reported early for SWCNTs interacting with solvent vapors under high vacuum conditions and cryogenic temperatures, revealing a "pressure gap" with implications for a number of areas including CNT based sensor and gas storage devices. Quantum chemical calculations show that physisorption energies of acetone on pristine or defective SWCNT sidewalls or inside grooves formed by SWCNT dimers do not exceed 80 kJ mol^{-1}. On the other hand, interstitial adsorption in large-diameter SWCNT bundles is possible, and can account for very high barriers towards desorption due to strong dispersion interactions between the SWCNTs.

6.1 INTRODUCTION

The interaction of carbon nanotubes (CNTs) with solvents is important for applications of CNTs in nanofluidic devices,[155, 156] the development of CNT based sensor,[11, 12, 116, 117] and the technological processing of CNTs.[28, 30] The interaction of SWCNTs with acetone and ethanol, solvents often used for CNT processing,[10, 113, 157-159] upon refluxing, sonication, and contact with ambient pressures of solvent vapors will be considered in the present paper. The dispersion of SWCNTs in solvents often involves sonication, a process that is accompanied by changes in temperature and pressure that can favor chemical reactions that would not proceed under normal conditions.[32] As a result, sonication can induce chemical interaction of CNTs with solute molecules.[30, 31]

There is ongoing interest in acetone interaction with CNTs for sensor applications.[11-13, 116, 117] Acetone is used as a solvent to prepare CNTs-polymer composites.[28] Recently, Chakrapani et al. reported chemical interaction of acetone with as-produced SWCNTs.[121] Shih and Li also suggested that acetone interacts chemically with multiwall carbon nanotubes (MWCNTs).[122] Kazachkin et al., studying cryogenic acetone adsorption on SWCNTs, concluded that acetone binds reversibly to SWCNTs.[159] The conditions used by Chakrapani et al.[121], Shih and Li[122], and Kazachkin et al.[159] are different. Chakrapani et al.[121] used sonication to disperse SWCNTs in acetone, Shih and Li exposed MWCNTs to acetone vapors at 303-363 K,[122] while Kazachkin et al.[159] dosed acetone to SWCNTs at 100 K under high vacuum ($\leq 10^{-6}$ Torr). The conditions used by the first two research groups[121, 122] are more aggressive in comparison with the conditions used by Kazachkin et al.[159], and can favor the chemical interaction of acetone with CNTs.[121, 122]

The interaction of alcohols with CNTs is critical for the development of fuel cells and molecular sieves[160-162], and for CNT based sensor development[17]. Theoretical consideration of gas phase esterification of SWCNT-COOH with alcohols suggests different reactivity of zigzag and armchair tubes.[163, 164] Fu et al. showed experimentally that mild treatment of CNTs in deuterated ethanol (48 h stirring at 343 K) results in deuterium attachment to CNTs: the deuterium in OD groups of ethanol was suggested to be responsible for deuteration.[165] Deuterium attachment was also observed for interaction of D_2O with carbon nanotubes.[166]

The present paper reports study of interaction of acetone and ethanol with SWCNTs upon reflux, sonication, and exposure to solvent vapors. Results suggest that after reflux, mild sonication, or adsorption from the gas phase acetone and ethanol can strongly bind to the SWCNTs and desorb as intact molecules at >400 K that correspond to desorption energies >100 kJ/mol. These findings are in stark contrast to the behavior observed after dosing the SWCNTs

with vapors under high vacuum conditions at cryogenic temperatures[159, 167] and suggest a "pressure gap" with implications for a number of CNT applications. Theoretical calculations are presented for binding energies of physisorbed acetone on pristine and defective SWCNT sidewalls, inside grooves formed by SWCNT dimers, and inside the hollows of interstitial sites of various SWCNT bundles. From the SWCNT dimer binding energies we estimate barriers for desorption from these interstitial sites.

6.2 EXPERIMENTAL

6.2.1 Materials purification

As-produced SWCNTs, synthesized by the HiPco[43] method, were purified according to the air/HCl procedure as described in detail elsewhere.[159] The residual iron content was ~20 wt.% for as-produced SWCNTs and ~1 wt.% after air/HCl purification (Supporting Information in [159]).

Carbon black (CB-460, Cabot) was used as a model compound to mimic possible carbonaceous impurities present in as-produced CNTs. Carbon black is produced by incomplete combustion of organics[168] and characterized by limited microporous structure.[169] According to analysis based on results of volumetric adsorption measurements, carbon black has a specific surface area of ~76 m/g^2 and 95% of the pores are larger than 10 nm (Figure C1).

6.2.2 Sample preparation

Treatment in solvents. The air/HCl purified SWCNTs were either refluxed or sonicated in solvents before loading them into vacuum chamber. For sonication, ~0.5-1 mg of the SWCNTs was treated in ~3 ml of solvent for 3 h using laboratory ultrasonic cleaner (Branson, 2510R). For reflux, ~0.5-1 mg of SWCNTs were boiled in ~3 ml of solvent for 3 h in a vial covered on top with aluminum foil which served as a condenser for solvent vapors. Right after sonication the sample was deposited by drop-and-dry method onto a W-grid (AlfaAesar, 0.002") at ambient temperature. Before sample deposition, the W-grid was connected to the sample holder by copper clamps, and a K-type thermocouple (Omega) was spot-welded to the grid. The design of the sample holder allows sample cooling to ~100 K and controlled heating to 1400 K.[99] After deposition onto the W-grid, samples were placed in a TPD vacuum chamber and pumped down overnight to $<10^{-8}$ Torr. Before TPD-MS experiments, the sample was cooled to ~100 K.

Solvents, ethanol (Pharmco-Aaper, ACS grade) and acetone-d6 ($(CD_3)_2CO$, Acros, 99.5% D), were used as received. Ultra pure water was produced by a water purification system (Easypure II UV, Barnstead). Samples sonicated in water did not have any contact with either acetone or ethanol and TPD-MS results obtained from those samples were used for reference purposes. For experiments where solvents were dosed in vacuum chamber, the liquids were degassed by several freeze-pump-thaw cycles. Before experiments the purity of the solvents was verified with MS.

6.2.3 TPD-MS measurements

The TPD-MS studies were performed in a stainless steel ultrahigh vacuum chamber equipped with residual gas analyzer RGA 300 (SRS, CA).[99] The base pressure in the TPD vacuum chamber before experiments was $\leq 10^{-8}$ Torr.

For the full TPD-MS study SWCNT sample sonicated or refluxed in a given solvent was cooled to ~100 K and then heated at 2 K sec^{-1} to the desired temperature ($\geq$900 K) with simultaneous monitoring of all the mass fragments desorbing in the 1-70 amu range (e.g., see Figure 17A). Typical resolution for the full TPD spectrum was 1 data point for a given mass per ~8 K. The data in 100-300 K range were collected for control purposes: upon cooling of a sample, water (naturally present in the background gases of the TPD chamber) physically adsorbs on the sample, and later it desorbs in the 160-170 K range in the case of proper thermocouple connection to the W-grid and thermal contact of the W-grid to the sample.

The interaction of acetone and ethanol vapors with SWCNTs was also investigated. For that purpose SWCNTs annealed at 900 K were exposed to solvent vapors (7.6 Torr) at ambient temperature (~300 K) for 10 min. The exposure was performed inside the TPD chamber. After exposure the TPD chamber was evacuated for ~20 h at ambient temperature (~300 K) to $<10^{-8}$ Torr. Then the sample was cooled to ~100 K and the full TPD spectrum was collected. The objective of this experiment was to compare the interaction of solvents with SWCNTs under different conditions: sonication, reflux, and exposure to solvent vapors in Torr range at ambient temperature.

Acetone and ethanol adsorption experiments at cryogenic temperatures were performed according to the procedure described elsewhere.[159] For that purpose, solvent vapors were dosed to the sample cooled to 100 K and then a full TPD-MS spectrum (1-70 amu) was recorded (100-

900 K, 2 K sec^{-1}). Samples before cryogenic adsorption of solvent vapors were annealed at 900 K for 0.5 h under vacuum. The objective of the low temperature acetone adsorption experiment was to find out how much solvent (in Langmuir equivalent) binds to the SWCNTs after sonication, reflux, and exposure to solvent vapors (300 K).

6.3 RESULTS

6.3.1 Interaction of acetone with SWCNTs

Acetone-d6 was selected to study the interaction with SWCNTs to simplify the MS analysis. Upon heating both the as-produced or air/HCl purified SWCNTs release multiple MS-fragments that can be misinterpreted as fragments of acetone-h6 and/or acetone-d6 (Figure A1 and C3). However, the relative intensity of fragments intrinsic to the SWCNTs that can be assigned to acetone-d6 was approximately 10 times less than the intensity of fragments that can be assigned to acetone-h6 (Figure C3). The most abundant fragments in the spectra of acetone-d6 vapors were CD_3 (18 amu), CO (28 amu), CD_3CO (46 amu), and $CD_3C(O)CD_3$ (64 amu). The CD_3 and CO fragments overlap with masses of H_2O (18 amu) and CO (28 amu) that originate from the thermal decomposition of oxygen containing functionalities on SWCNTs and possible desorption of molecules (H_2O, CO, N_2) trapped inside SWCNT pores (Figure A1). The fragments CD_3CO (46 amu) and $CD_3C(O)CD_3$ (64 amu) were chosen to characterize acetone-d6 desorption.

Purified SWCNTs sonicated or refluxed in acetone-d6 showed ~50-100 times more intense TPD-MS signals of acetone-d6 related fragments than purified SWCNTs that had no contact with acetone (Figure 16). The difference in intensity of acetone-d6 fragments from SWCNTs

refluxed or sonicated in acetone-d6 (Figure 16A and B) is within the reproducibility of the measurements: the signal intensity depends on the amount of sample deposited on W-grid, sample heterogeneity, and distance of the RGA cone (~0.5-1 mm) from the sample.

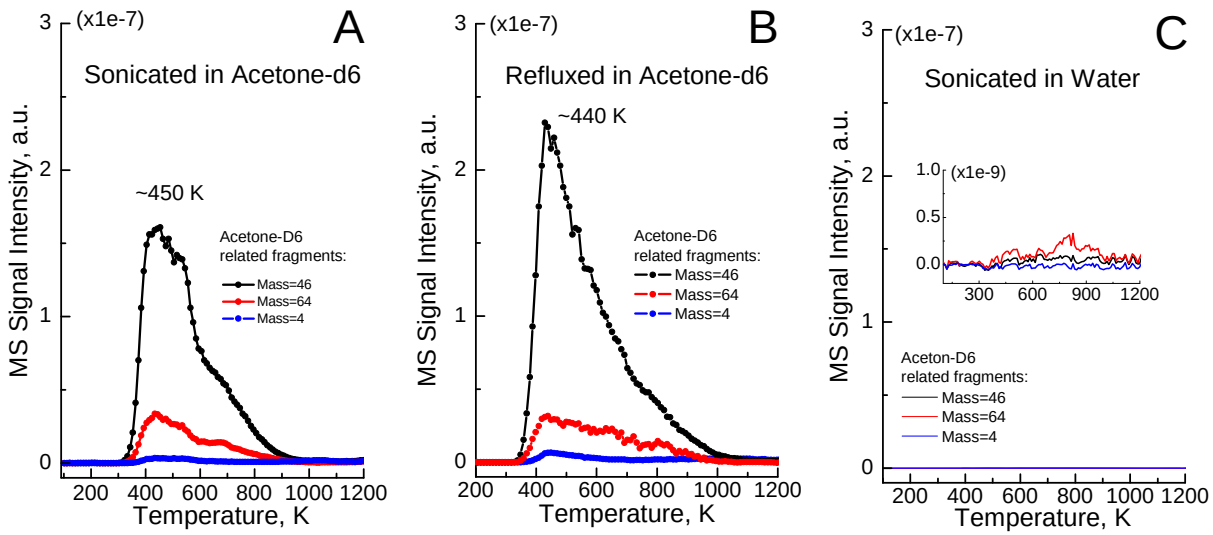

Figure 16: TPD profiles of acetone-d6 related fragments evolving from the air/HCl purified SWCNTs (**A.**) sonicated in acetone-d6; (**B.**) refluxed in acetone-d6; (**C.**) sonicated in ultra-pure water (note difference in the scale of inset on C). The TPD results suggest that SWCNTs treated in acetone-d6 release ~50-100 times more acetone-d6 related fragments in comparison with SWCNTs sonicated in water. Contact of the purified SWCNTs with liquid acetone results in retention of acetone molecules by SWCNTs up to high temperatures.

During sonication, temperature oscillations can hypothetically lead to decomposition and or formation of oxygen functionalities.[32] Oxygen functionalities can block the access for molecules to/from endohedral sites of the SWCNTs.[101, 170] Decomposition of oxygen functionalities upon temperature increase can lead to enhancement of solvent uptake inside nanotubes. In turn, formation of oxygen functionalities during the temperature oscillations can result in encapsulation (trapping) of molecules inside CNTs. By matching the profiles for acetone-d6 related fragments (Figure 16) and fragments desorbing upon decomposition of oxygen

functionalities (CO_2[89, 90, 109, 171]) it became clear that the release of acetone related fragments does not correlate with decomposition of oxygen functionalities (Figure 7C and Figure C4); the maximum of CO_2 release, that typically forms upon decomposition of carboxylic acids groups (COOH),[89, 90, 109] lactone (-C-O-C(=O)-),[89, 171] anhydride (-C(=O)-O-C(=O)-),[89, 109, 171] was observed at 680-740 K (Figure 7C and Figure C4), while the acetone-d6 related fragments show a desorption maximum at ~450 K (Figure 16). To conclude, acetone strongly binds to SWCNTs and thermally induced desorption of acetone does not correlate with the decomposition of oxygen containing functionalities, excluding the possibility of acetone trapping inside SWCNTs due to oxygen functionalities.

An *in situ* control experiment was performed to address the role of reflux and sonication in acetone binding to SWCNTs. The idea of the experiment was to bring solvent vapors into contact with "pristine" SWCNTs to find out whether solvent molecules will bind to SWCNTs. For that purpose, purified SWCNTs were annealed to 900 K (0.5 h) under vacuum (~10^{-8} Torr) to remove volatile compounds adsorbed on SWCNTs from ambient and to decompose most oxygen functionalities.[70] The annealed SWCNTs were exposed to 7.6 Torr of acetone-d6 at ~300 K for 10 min inside the TPD vacuum chamber. After exposure of annealed SWCNTs to acetone-d6 the TPD chamber was evacuated ~20 h at ambient temperature (~300 K) to <10^{-8} Torr, then the sample was cooled to ~100 K and after that full TPD analysis was performed. The results (Figure 17) suggest that acetone-d6 adsorbed from the gas phase at 7.6 Torr and 300 K strongly binds to the SWCNTs desorbing upon heating with a maximum at ~450 K (Figure 17B). The control experiment suggests that neither reflux nor sonication play a crucial role in strong acetone binding to SWCNTs; acetone dosed from the gas phase 7.6 Torr and 300 K can also strongly bind to SWCNTs.

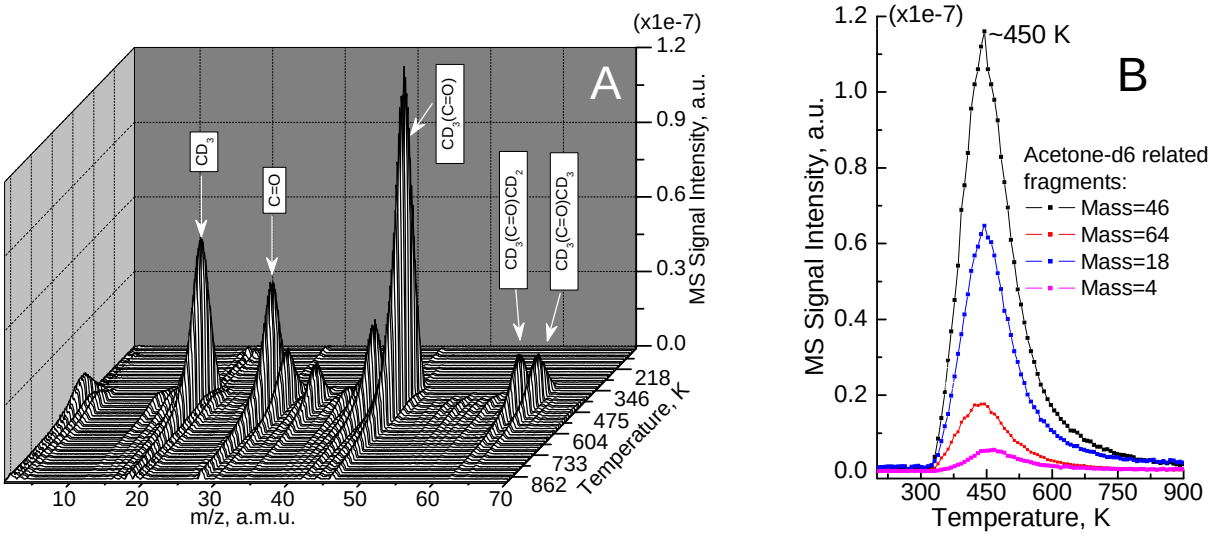

Figure 17: (**A**.) Full TPD spectrum collected from purified SWCNTs annealed to 900 K and exposed to acetone-d6 (7.6 Torr, 300 K, 10 min); (**B**.) Most abundant acetone-d6 related fragments extracted from the full TPD spectrum are plotted as versus temperature. Exposure of SWCNTs to acetone vapors results in acetone binding to SWCNTs.

In order to find out whether acetone related fragments originate from desorbing molecular acetone, a comparison of the temperature profiles for different acetone related fragments was performed. The temperature profiles for different acetone-d6 related fragments coincide (Figure 18). A coefficient of 5.5 was introduced to correct for the relative abundance of the 46 and 64 amu fragments based on the ratio of their MS intensities in the gas phase of acetone-d6. The matching of profiles for different acetone-d6 related fragments (Figure 18) suggests molecular desorption of acetone. Acetone retained by SWCNTs either after sonication, reflux, or dosing from the gas phase leaves the surface of SWCNTs upon heating as intact molecules.

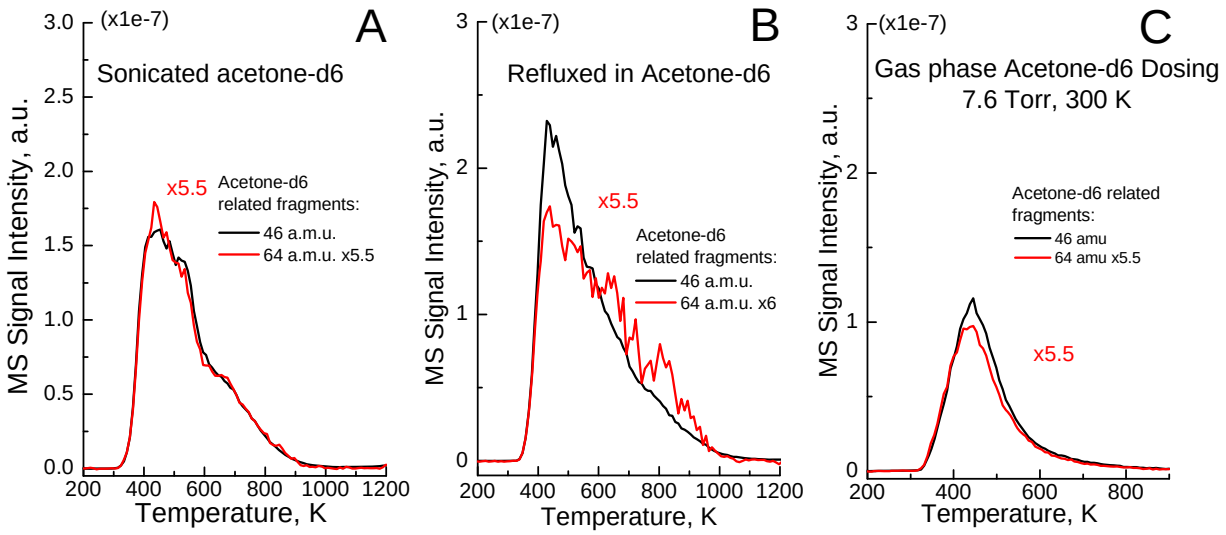

Figure 18: Temperature profiles of acetone-d6 fragments - 46 amu (CD_3CO) and 64 amu ($(CD_3)_2CO$). Profiles for acetonde-d6 related fragments coincide, suggesting that acetone desorbs from SWCNTs as an intact molecule. Acetone interacts reversibly with SWCNTs either after reflux, sonication or dosing from the gas phase at ~300 K.

In order to provide additional evidence of reversible adsorption/desorption for acetone strongly bound to SWCNTs an exchange experiment was performed. The objective of the experiment was to find out if acetone adsorbed on SWCNTs can be replaced with acetone from the gas phase. To start, SWCNTs annealed to 900 K were exposed to 7.6 Torr of acetone-h6 ($(CH_3)_2CO$) inside a TPD chamber for 10 min at ambient temperature and the sample was evacuated overnight at ambient temperature to ~10^{-8} Torr. On the next day, the sample was exposed to 7.6 Torr of acetone-d6 ($(CD_3)_2CO$) for 10 min at ambient temperature. After overnight evacuation to ~10^{-8} Torr the sample was cooled down to 100 K and a full-TPD experiment was performed.

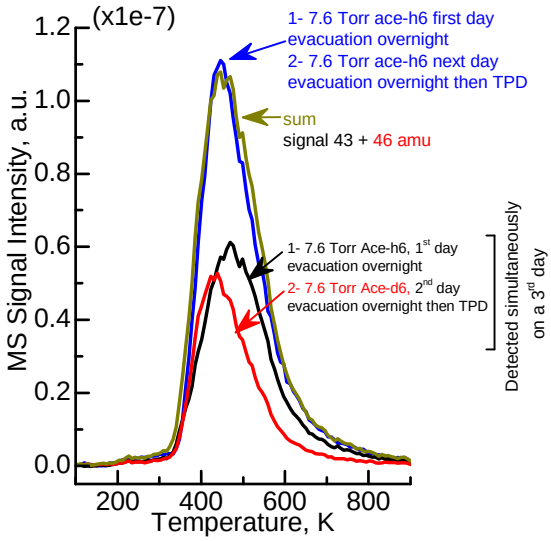

Figure 19: Exchange experiment. SWCNTs with pre-adsorbed acetone-h6 were exposed to acetone-d6 and after evacuation signal from acetone-h6 and acetone-d6 were collected simultaneously with TPD-MS. The results suggest that acetone-h6 that is strongly bound to the surface can be partially replaced with acetone-d6, suggesting limited mobility of strongly bound acetone. Signals from acetone-h6 (black curve), acetone-d6 (red curve), the sum of signals from acetone-h6 and acetone-d6 (dark yellow curve) and the signal from acetone-h6 (blue curve) (two consecutive doses of acetone-h6) are displayed. See text for more details.

The amount of acetone desorbing from SWCNTs after different pretreatments is similar (Figure 18 and Figure 19) and comparable to the amount of acetone dosed from the gas phase (Figure 18C and Figure 19). The total amount of acetone strongly bound to the surface does not change significantly after two consecutive doses of 7.6 Torr acetone (compare the intensities of the blue curve in Figure 19 and the black curve in Figure 17B).

It follows from Figure 19 that acetone strongly bound to the surface of SWCNTs can be partially replaced by acetone from the gas phase. Signals from both acetone-h6 (black curve) and acetone-d6 (red curve) were detected (Figure 19) simultaneously, while the total amount of acetone strongly bound to the surface did not change (dark yellow curve has the same intensity as the blue curve in Figure 19). The maximum peak position of acetone-d6 was at ~425 K while

the peak maximum of acetone-h6 was at ~470 K (Figure 19); acetone-d6 that was dosed to the sample with pre-adsorbed acetone-h6 replaced preferentially acetone-h6 molecules that had lower binding energies. The most important conclusion that follows from this experiment is that acetone strongly bound to carbon nanotubes can exchange with acetone from the gas phase.

Some carbonaceous impurities, present in as-produced SWCNTs, can survive the air/HCl purification and could hypothetically be responsible for the strong binding of acetone. To investigate this, carbon black was used to model acetone interactions with carbonaceous impurities. When acetone is adsorbed at cryogenic temperature on carbon black desorption peaks similar to acetone desorption from SWCNTs are observed.[159] Carbon black samples were annealed to 900 K (for 0.5 h) before adsorption of acetone-d6 at cryogenic temperature (100 K-10^{-6} Torr) or at ambient temperature (7.6 Torr, 300 K, 10 min). The carbon black exposed to 7.6 Torr of acetone revealed desorption of multiple acetone related fragments with similar TPD profiles suggesting molecular acetone desorption. The maximum desorption temperature for all profiles was ~450 K (Figure 20A) similar to SWCNTs (Figure 20B) after 7.6 Torr-300 K acetone exposure. However, the amount of strongly bound acetone retained by the carbon black appears to be at least 50 times less than the amount of acetone retained by purified SWCNTs, for an equivalent dose. This conclusion is reached by comparing the amount of acetone retained by carbon black and SWCNTs after dosing 7.6 Torr-300 K with dosing at 100 K and 10^{-6} Torr. Carbon black appears to retain the equivalent of ~15 L of acetone dosed at 100 K (compare solid blue and doted black curves in Figure 20A), while purified SWCNTs retained the equivalent of ~750 L after 7.6 Torr-300 K exposure (compare solid blue and doted black curves in Figure 20B). Thus, carbonaceous impurities can also strongly bind acetone, similar to SWCNTs. The uptake capacity depends on the nature of carbonaceous material.

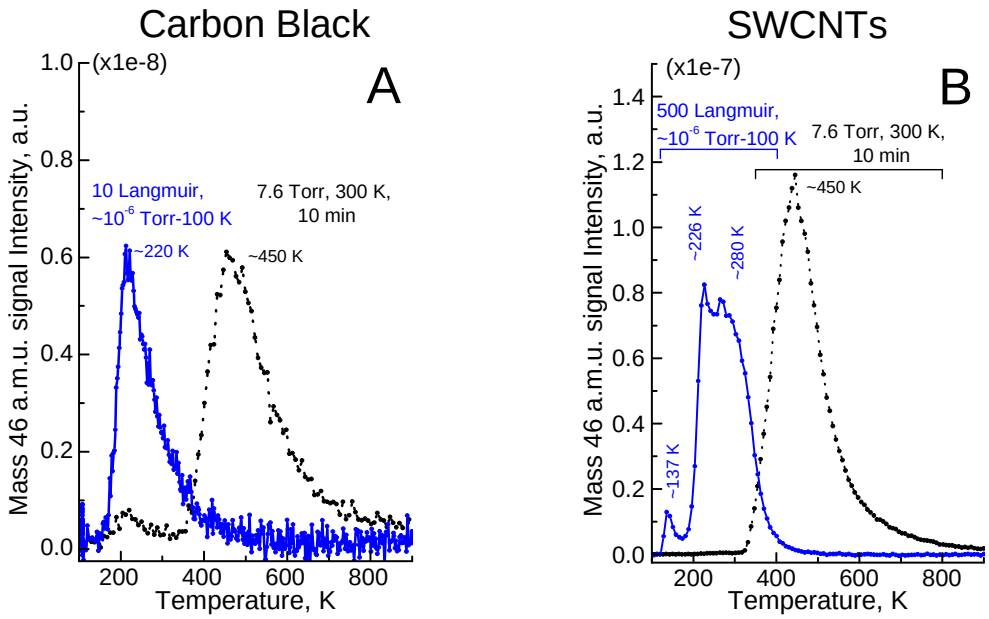

Figure 20: Comparison of TPD profile of acetone-d6 (46 amu – CD_3CO) adsorbed at ~10^{-6} Torr-100 K (blue curve) to profile of acetone adsorbed at 7.6 Torr-300 K (black curve). (**A.**) Adsorption of acetone on carbon black annealed to 900 K (0.5 h); (**B.**) Adsorption of acetone on the purified SWCNTs annealed to 900 K (0.5 h). The TPD analysis was performed immediately after 100 K-10^{-6} Torr dosing, while after 300 K-7.6 Torr dosing the samples were evacuated overnight to reduce background pressure to <10^{-8} Torr.

To summarize, acetone was found to bind strongly to carbonaceous materials (carbon black and SWCNTs) either upon reflux, sonication, or exposure to acetone vapors. Strongly bound acetone desorbs upon heating of carbonaceous materials as an intact molecule. The adsorption capacity with respect to acetone of the air/HCl purified SWCNTs exceeds adsorption capacity of carbon black by at least 50 times.

6.3.2 Interaction of ethanol with SWCNTs

The procedures used to study interaction of ethanol with SWCNTs were analogous to procedures used to study interaction of acetone with SWCNTs (see Section 6.2).

After sonication of purified SWCNTs in ethanol (3 h) ~100 times increase in intensity of desorbing ethanol related fragments was observed (Figure 21A) in comparison with the purified SWCNTs sonicated in water (Figure 21B). After sonication, some ethanol was strongly bound with SWCNTs as evidenced by the 450 K desorption peak.

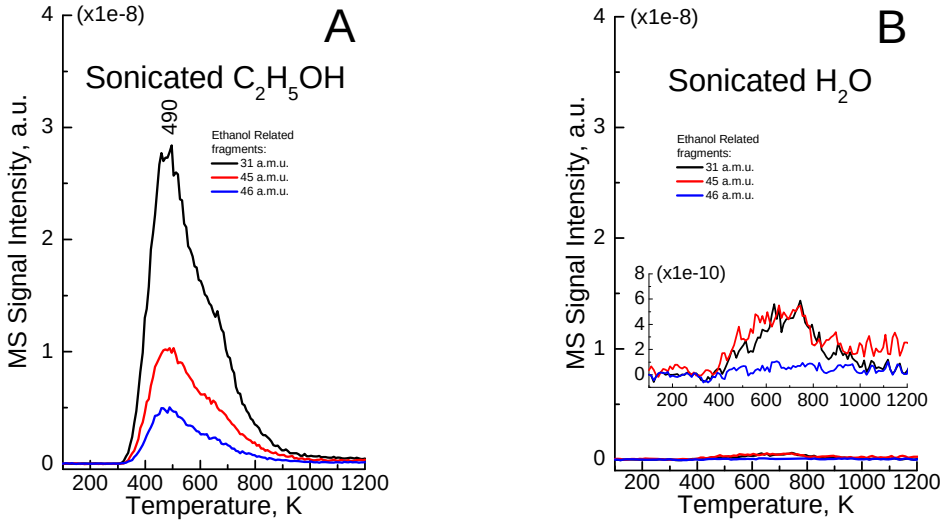

Figure 21: Temperature profiles of ethanol related fragments extracted from full TPD spectra of purified SWCNTs sonicated in (**A**) ethanol, and (**B**) H_2O. The SWCNTs sonicated in ethanol evolve significant amount of fragments that can be assigned to ethanol: [CH_2OH] - 31 amu, [C_2H_5O] - 45 amu, [C_2H_5OH] - 46 amu.

To find out whether ethanol binds to SWCNTs after exposure to ethanol vapors the following experiment was performed. Purified SWCNTs (vacuum annealed at 900 K for 0.5 h) were exposed to 7.6 Torr of ethanol at 300 K for 10 min in the TPD chamber and then evacuated overnight to $<10^{-8}$ Torr. The subsequent TPD analysis of desorption products revealed ethanol related fragments desorbing between 400 and 800 K from SWCNTs (Figure 22A) with a

maximum desorption temperature of ~450 K (Figure 22B), close to ~490 K observed for the sample sonicated in ethanol (Figure 21A).

The temperature profiles of ethanol related fragments evolving from purified SWCNTs either sonicated in ethanol or exposed to 7.6 Torr of ethanol vapors coincide (Figure 22) suggesting that ethanol desorbs as an intact molecule. Ellison et al. recently reported that exposure of SWCNTs to saturated ethanol vapors at room temperature results in binding of ethanol to the SWCNTs and its retention in a molecular form.[153]

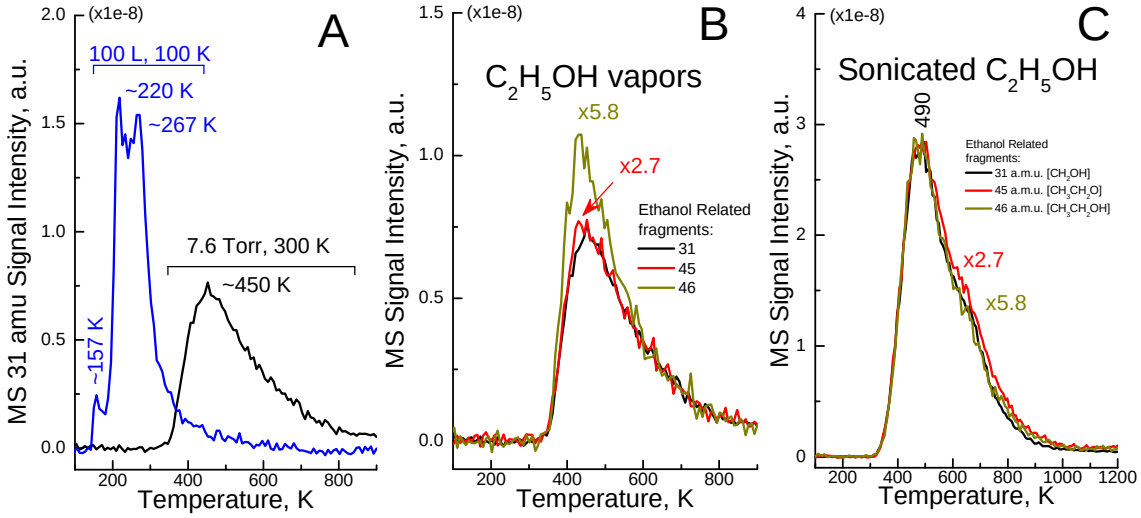

Figure 22: TPD-MS spectra of ethanol desorbing from SWCNTs after adsorption from the gas phase on SWCNTs at 100 K-10^{-6} Torr and 300 K-7.6 Torr (**A.**). Ethanol related fragments have similar desorption profiles either after exposure SWCNTs to ethanol vapors (**B.**) or sonication of SWCNTs (**C.**) in ethanol. Multiplication coefficients 2.7 and 5.8 were determined experimentally by introducing ethanol vapors into the TPD vacuum chamber.

To summarize, the interaction of ethanol with SWCNTs, whether during sonication or exposure SWCNTs to ethanol vapors, can lead to strong binding of ethanol to SWCNTs. The strongly bound ethanol desorbs as an intact molecule.

6.3.3 Quantum chemical modeling of acetone binding to individual SWCNTs and SWCNT bundles[7]

The precise knowledge of the atomistic nature of binding sites, corresponding adsorption binding energies (=negative interaction energies ΔE), barriers for desorption $\Delta E^{\#}$, and the site population in dependence on adsorption gas pressure is at the heart of the present study. However, the large number of possible binding sites and conformations for gas molecules on single and/or multiple SWCNTs exacerbate a systematic atomistic study. Previously, we computed the interaction energies for acetone adsorbed inside and outside small (6,5) and large (11,9) diameter SWCNTs,[159] using dispersion augmented self-consistent-charge density-functional tight-binding[124, 125] (SCC-DFTB-D, denoted DFTB-D for brevity in the remainder of the text) after benchmarking this method against counterpoise-corrected large basis set MP2 calculations for the acetone-coronene model system. It was found that the adsorption energy depends strongly on the sidewall curvature in the case of endohedral absorption, while exohedral adsorption displays a less pronounced dependence.[159] Endohedral adsorption inside small diameter tubes is strongest with ΔE = -74.4 kJ mol^{-1} for the (6,5) tube, and weakest for exohedral adsorption with ΔE = -26.3 kJ mol^{-1} (11,9) and ΔE = -24.6 kJ mol^{-1} (6,5) for the energetically most favorable planar parallel conformation.[159] Recently, Pankewitz *et al.*[132] computed interaction energies for exohedral adsorption of methanol on various tube models using a number of *ab initio* and dispersion-augmented density functional theory (DFT-D) methods,[172] and predicted adsorption

[7] This chapter (3.3) was written by Professor Irle and PhD student Yoshifumi Nishimura (Institute for Advanced Research and Department of Chemistry, Nagoya University, Japan)

interaction energies ΔE on the order of -15 to -20 kJ mol^{-1} for the range of tube diameters from (4,4) to (10,10) SWCNTs. Therefore, the unusually high desorption temperatures reported in this work corresponding to physisorption energies in excess of 100 kJ mol^{-1} call for an alternative explanation.

For exohedrally adsorbed gas species, knowledge of the adsorption interaction energies is obviously sufficient as no barrier will add to the value of ΔE. A question one may ask is whether Stone-Wales or mono-vacancy defect sites may increase the physisorption energies of acetone to SWCNT sidewalls. This possibility is investigated, and from the results reported below one can safely exclude defect site adsorption as explanation for strong binding. On the other hand, for endohedral sites, a more important quantity might be the energy barrier for desorption $\Delta E^{\#}$, originating from the difficulty of the adsorbate molecule to sneak through narrow "exit holes" in the sidewalls, caused for instance by vacancy defects.[173] Below we discuss DFTB-D interaction energies and estimates for desorption barriers of acetone adsorbed in grooves (2 SWCNTs + acetone) and interstitial sites (3 SWCNTs + acetone), and compare the results with acetone adsorbed on the in- and outside of single SWCNTs.

Acetone adsorbed in SWCNT sidewall defect sites. Among sidewall defects, the most likely candidates are Stone-Wales and mono-vacancy defects that frequently are encountered. However, their numbers and concentrations are not expected to be large enough to be responsible for the observation of strong binding. Nevertheless, we computed acetone adsorption to these defects using the same model systems previously employed[159] for the calculation of adsorption to intact honeycomb networks, namely hydrogen-terminated, 10 Å long tube fragments of a large-diameter (11,9) (L) and a small-diameter (6,5) (S) nanotube. Stone-Wales defects increase the magnitude of ΔE of the weaker exohedral adsorption only by 6 kJ mol^{-1}, while endohedral

adsorption is less affected. The lowest ΔE for acetone on a Stone-Wales defect was found for the planar parallel conformation outside the (11,9) tube with -32.4 kJ mol^{-1}. In the case of mono-vacancy defects, we are dealing with 5/9-type defects as described in reference [173]. Here, the carbon atom possessing a dangling bond can electrostatically interact favorably with the methyl H atoms of acetone, and we note energy increase of ~5 kJ mol^{-1} due to this attraction. Thus, the endohedral adsorption inside a mono-vacancy defect containing (6,5) SWCNT bears an interaction energy of -78.4 kJ mol^{-1}. It is obvious that neither Stone-Wales nor mono-vacancy defects can cause increase in interaction energies beyond 100 kJ mol^{-1}.

Acetone adsorbed in groove sites. It has been estimated that physisorption of molecules in groove sites is about 1.5 to 1.7 times stronger than exohedral adsorption on single SWCNTs, due to the added interaction with the neighbor tube.[153] We tested this hypothesis by performing calculations for the adsorption of acetone in grooves formed by the same L and S SWCNT model systems that are described above. The combination of them yields three different groove sites: LL, LS, and SS. Table 4 lists the interaction energies ΔE for these SWCNT fragment dimers, which become larger in magnitude with the diameter of the constituent tubes: ΔE(SS) = -105.4 kJ mol^{-1}, ΔE(LS) = -125.6 kJ mol^{-1}, and ΔE(LL) = -155.9 kJ mol^{-1}, and can be seen as tube-tube interaction energy per nanometer. Szabados *et al.* had given an estimate for the (11,9)-(11,9) dimer as -267.5 kJ mol^{-1} based on tight-binding calculations including a Lennard-Jones potential that was chosen to reproduce MP2/6-31G* binding energies of the naphthalene dimer.[174] In their MP2 calculations, it seems that no correction was made for basis set superposition error, which should account for approximately 50% of the interaction energy according to our experience from acetone-coronene MP2 calculations.[159] Therefore, the DFTB-D result of -155.9 kJ mol^{-1} seems to be a reasonable value for the interaction energy between two 10 Å-long (11,9)

SWCNTs. We note that all of the attractive contribution is due to the dispersion "–D" term, and that the DFTB-only contribution is slightly repulsive, owing to Pauli repulsion between the electron densities of the tubes.

Table 4: Interaction energies ΔE in [kJ mol^{-1}] for dimers of 10 Å-long, hydrogen-terminated (11,9) (L) and (6,5) (S) tube fragments, and for acetone in the groove site relative to the tube dimers, averaged over six optimized geometries. Energy contributions are listed as follows: total ΔE (DFTB-D), which is the sum of ΔE from the pure DFTB contribution and ΔE from the dispersion energy contribution (D only).

Compound	DFTB-D	DFTB only	D only
SWCNT-SWCNT			
LL	-155.89	5.73	-161.61
LS	-125.57	11.53	-137.10
SS	-105.39	3.12	-108.51
SWCNT-acetone-SWCNT (average)			
LacL	-48.16	12.88	-61.04
LacS	-46.08	0.89	-46.98
SacS	-47.25	5.77	-53.01

Placing acetone in the groove site, giving rise to structures LacL, LacS, or SacS, ("ac" denotes the groove-site acetone located between either L or S tubes) was performed by assuming initial coordinates where acetone is oriented either parallel (a) or perpendicular (b) to the tube axes, with planar parallel (PP), oxygen pointing away (UP) or oxygen pointing towards (DP) the tube surfaces. The latter had already been found to be energetically unfavorable, and thus optimized geometries correspond to either PP or UP type, or both (in the case of SL). Figure 23 shows representative optimized geometries for the acetone-groove structures. The obtained six optimized structures for each groove site were very similar in energy, so that we decided to average the energies and only list one interaction energy value for acetone interaction with each groove in Table 4. Remarkably, although the individual contributions from DFTB and dispersion term are somewhat different, we find a narrow range of total DFTB-D interaction

energies of acetone with the tube dimers from 46 to 48 kJ mol^{-1}, which is roughly 1.9 times the value of exohedral adsorption on a single tube. Since ΔE for groove site adsorption is much smaller than 100 kJ mol^{-1}, these sites cannot be responsible for the high temperature desorption observed following "high-pressure" gas exposure.

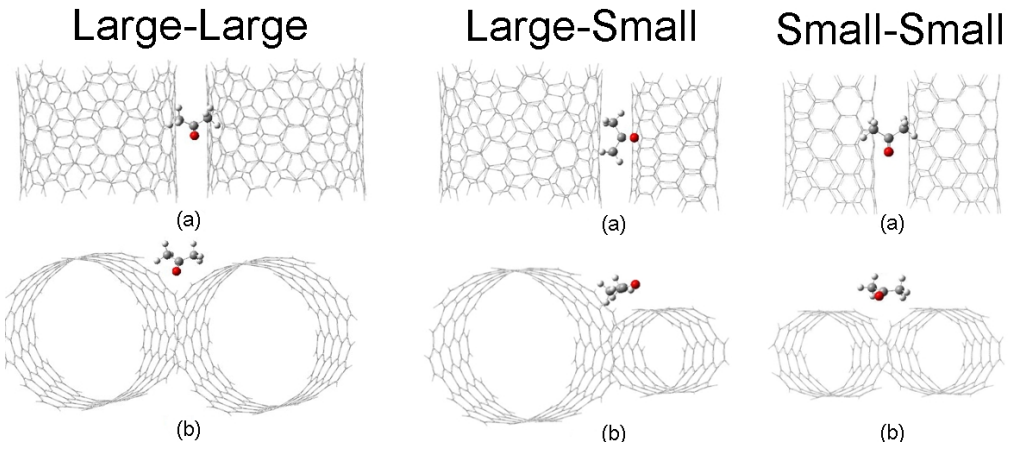

Figure 23: Representative optimized geometries for acetone adsorbed in LL, LS, and SS groove sites. (a) top view, (b) skewed front view.

Acetone adsorbed in interstitial sites. Interstitial sites of SWCNT bundles have been pronounced inaccessible for physisorbed adsorbate molecules, due to the narrow space.[110] However, theoretical simulations predict that, for bundles formed of carbon nanotubes of different diameter, the interstitial sites are accessible for molecules of a certain size.[111, 112] We attempted to compute optimized geometries for acetone adsorbed inside interstitial sites of the four different bundles comprised of L and S tubes, offering interstitial spaces as follows: LLL, LLS, LSS, and SSS. Out of these four, we found only local minima for acetone inside LLL and LLS bundles, while corresponding structures for LSS and SSS simply disintegrated during the course of geometry optimization. The interaction energy for acetone in the interstitial site of the LLL bundle is rather close to adsorption at a groove site with ΔE = -54.0 kJ mol^{-1}, which stems

from the fact that the tubes undergo substantial deformation in the complex with a deformation energy (DEF) of 16.7 kJ mol^{-1} relative to the geometry of the LLL bundle without acetone, while the interaction energy (INT) with the deformed tubes amounts to -70.7 kJ mol^{-1} (note that ΔE = DEF+INT). Nevertheless, acetone physisorption inside the interstitial channel of an LLL bundle seems energetically feasible. The deformation of the tubes due to the presence of the acetone molecule can be seen best in the case of the LLS system, depicted in Figure 24. Here, the interaction energy ΔE becomes positive (repulsive) with 2.2 kJ mol^{-1}, and corresponding values for DEF and INT are 82.4 and -80.2 kJ mol^{-1}, respectively. Clearly, this is a highly unfavorable situation, presumably not accessible under the experimental conditions of this study.

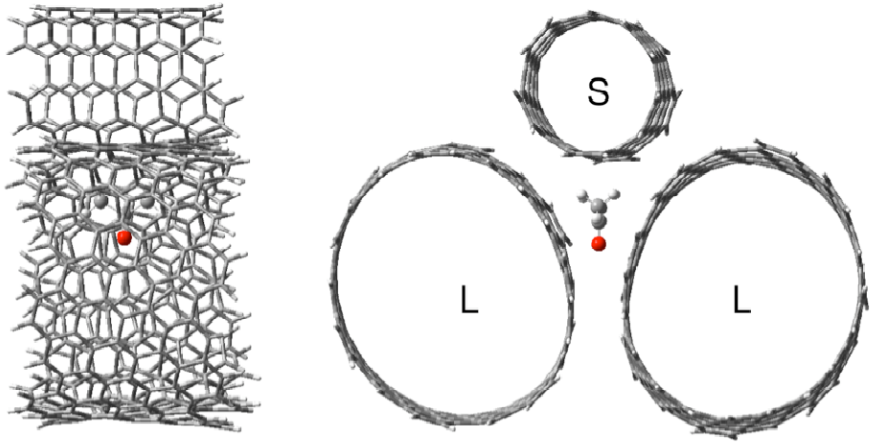

Figure 24: Optimized geometry for acetone adsorbed inside the interstitial site of an LLS bundle.

Any attempt to increase the distance between two tubes will cause a rapid loss of interaction energy, due to the r^{-6} dependence of the dispersion energy. Thus, release of acetone from the interstitial sites can be associated with energy barriers $\Delta E^{\#}$ in excess of 100 kJ mol^{-1} which are required to open up an "exit channel" between the tubes, for instance >156 kJ mol^{-1} nm^{-1} in case of L-bundles. Attempts to locate a corresponding transition state with longer tubes in the LLL bundle are underway; these calculations are difficult due to the fact that very long

SWCNT segments (at least > 20 Å) need to be considered to properly describe the deformation for the release of a single acetone molecule.

6.4 DISCUSSION

The results presented here suggest that heating of purified and as-produced SWCNTs releases multiple fragments that can be misinterpreted as fragments of ethanol, acetone, or other chemical species (Figure A1 and C3). We believe that those fragments belong to chemicals (presumably organics) that adsorbed from the ambient air prior to loading of the sample into the vacuum chamber. The ability of carbonaceous materials to adsorb organics from ambient is well known.[20, 175, 176] Carbon nanotubes can act as sorbents as well.[177, 178]

Carbon nanotubes can retain greater quantities (at least 50 times more) of strongly bound acetone than carbon black (Figure 20).[8] The carbon black (Cabot, CB-460) used in our experiments has a surface area of ~74 m^2/g and macro-porous structure (most of the pores >10 nm) (Figure C1). In turn, SWCNTs[9] have surface area ~400-1600 m^2/g,[45-47] and large fraction of micropores (Figure C1) defined by nanotube diameter (~1-2 nm). If the uptake of acetone is proportional to the surface area only then the difference in the uptake capacity between carbon black and SWCNTs should be at most 20 times. We suggest that the uptake capacity of

[8] We relate the amount of acetone strongly bound to SWCNTs after 7.6 Torr-300 K to the amount of acetone adsorbed by the same sample at 10^{-6} Torr-100 K. In such cases the mass of the sample deposited should not influence the amount of acetone bound under different T-P conditions. Instead the specific properties of the sample (surface area, porosity, etc.) will define the adsorption capacity.

[9] We do not have BET for the air/HCl samples used in present research: the amount of sample left after purification was not enough for BET analysis.

carbonaceous materials is defined primarily by microporous structure. We think that the observed desorption energies of ~110-123 kJ/mol (corresponding to the TPD peak at 450-490 K) are due to physical (e.g., diffusion) limitations for molecules to leave certain sites (endohedral, interstitial channels) in carbon nanotubes.

TPD-MS results suggest that both ethanol and acetone desorb upon heating as intact molecules. The TPD-MS does not provide information on the state of the ethanol on the surface, but based on the results of FTIR study[153] it follows that ethanol preserves it molecular structure when adsorbed from vapors on the SWCNTs at ambient temperature.

Chemical interactions of acetone were reported with the SWCNTs[121] and MWCNTs[122]. Chakrapani et al. suggested that acetone reacts with SWCNTs based on results of XPS, TPD-MS, and theoretical calculation.[121] Our experiments do not provide evidence of chemical transformation of acetone when it is adsorbed on SWCNTs, rather the absence of correlation between fragments observed by Chakrapani et al.[121] can originate from desorption of co-adsorbed organic compounds. Authors do not report a control experiment when their samples were not treated with acetone.[121]

One of the most intriguing facts discovered here is the existence of adsorption states with high binding energy after dosing molecules at "high pressure" ($\geq$7.6 Torr) and "high temperature" ($\geq$300 K). Note that exposure of the samples to "low" pressures (10^{-6} Torr) and temperatures (100 K) does allow access to sites with high binding energy (Figure 20 and Figure 22A).[159, 179] The limited access to sites with high binding energy for molecules dosed at low pressure and temperature can be explained by either activated adsorption or reversible chemical interaction that also requires some activation energy.

Our theoretical simulations of physisorbed acetone exohedrally and endohedrally bound to single intact and defective SWCNTs, grooves, and in interstitial sites of tube bundles show that binding energies never exceed ~80 kJ mol^{-1}, whereas the presented "high pressure/high temperature" experiments indicate the existence of barriers to desorption on the order of 100 to 225 kJ mol^{-1}. Strong SWCNT-SWCNT binding in bundles caused by dispersion forces was shown in our calculations to easily qualify as cause for high barriers required for an acetone molecule to leave interstitial sites. The important preliminary conclusion is that conventional techniques (e.g., TPD-MS) utilizing the adsorption of gases under low pressures and cryogenic temperatures do not probe all available sites in porous carbonaceous materials – especially in carbon nanotubes.

The amounts of acetone and ethanol retained in a strongly bound form on the purified SWCNTs exposed to 7.6 Torr (300 K, 10 min) of corresponding solvent differ significantly.[10] The estimated amount of strongly bound acetone corresponds to ~750 L of acetone adsorbed at 100 K (Figure 20B). However, the estimated amount of strongly bound ethanol corresponds to ~100 L of ethanol adsorbed at 100 K (Figure 22B). We suggest that more effective binding of acetone versus ethanol is due to the presence of the carbonyl (C=O) group in acetone, favoring π-π stacking[180] near the tube walls resulting in stronger binding. The results of gas adsorption experiments (see below and Figure C5) support this opinion.

Experiments on exchange of acetone-h6 strongly bound to the surface of SWCNTs with acetone-d6 from the gas phase allows an estimate of the exchange probability. Half (~350 L) of the molecules of acetone-h6 strongly bound to the surface can be replaced by acetone-d6 from the gas phase (Figure 19). From pressure and exposure time we can estimate the number of

[10] Assuming the sticking coefficients of ethanol and acetone to the SWCNTs are equal.

collision events, expressed as a maximum possible coverage (assuming a sticking probability of one): 7.6 Torr*600 sec*10^6 L/(Torr*sec) ~ 4.6* 10^9 L. Thus, the exchange probability is equal to 350 L/4.6*10^9 L ~7.6*10^{-8}. Only one collision out of 10 million leads to successful replacement of an acetone molecule strongly bound to the CNTs.

The strong binding of acetone and ethanol molecules to CNTs and carbon black is not unique property of these molecules. We explored interaction of the following gases with CNTs: 1,3-butadiene (1,3-C_4H_6), n-butane (n-C_4H_{10}), and methane (CH_4) (Figure C5). Both 1,3-C_4H_6 and n-C_4H_{10} bind strongly to SWCNTs upon exposure to 7.6 Torr of corresponding gas at 300 K. The amount of strongly bound 1,3-C_4H_6 significantly exceeds the amount of n-C_4H_{10} (1300 vs. 200 L, respectively). We think that higher capacity of SWCNTs of 1,3-C_4H_6 compared to n-C_4H_{10} is due to π-π stacking[180] that favors the interaction of molecules with CNT walls. Methane was almost completely desorbing by 300 K after dosing at 230 K. That suggests that interaction energy of molecules can also correlates with the mobility (size) of molecules within CNTs.

The pressure gap effect observed in our work can be explained by the following simplified model. Some CNT bundles have interstitial channels that are not accessible to gas molecules greater than a certain size (acetone, butane, etc.). When such molecules approach the CNT bundles, they may occasionally squeeze into interstitial channels and "debundle" nanotubes temporarily while moving along interstitial channels and filling them (Figure 25). Molecules that are close to the exit of CNT interstitial channels may desorb first, while molecules that are far away from the interstitial channel exit can be locked inside, because physisorption to the sidewalls decreases their mobility. The forces that hold CNTs in bundles are of van der Waals nature[174] and our calculations suggest that CNT can interact with energy of ~150 kJ/mol for every nanometer if interaction length. This is the energy that one would need supply to

temporarily open up a bundle and create an "exit" at the location of the acetone molecule inside the bundle. Simply put, the molecules that are squeezed between CNTs inside of the interstitial channel need to overcome the energy of the interaction between CNTs to escape from the interstitial channel.

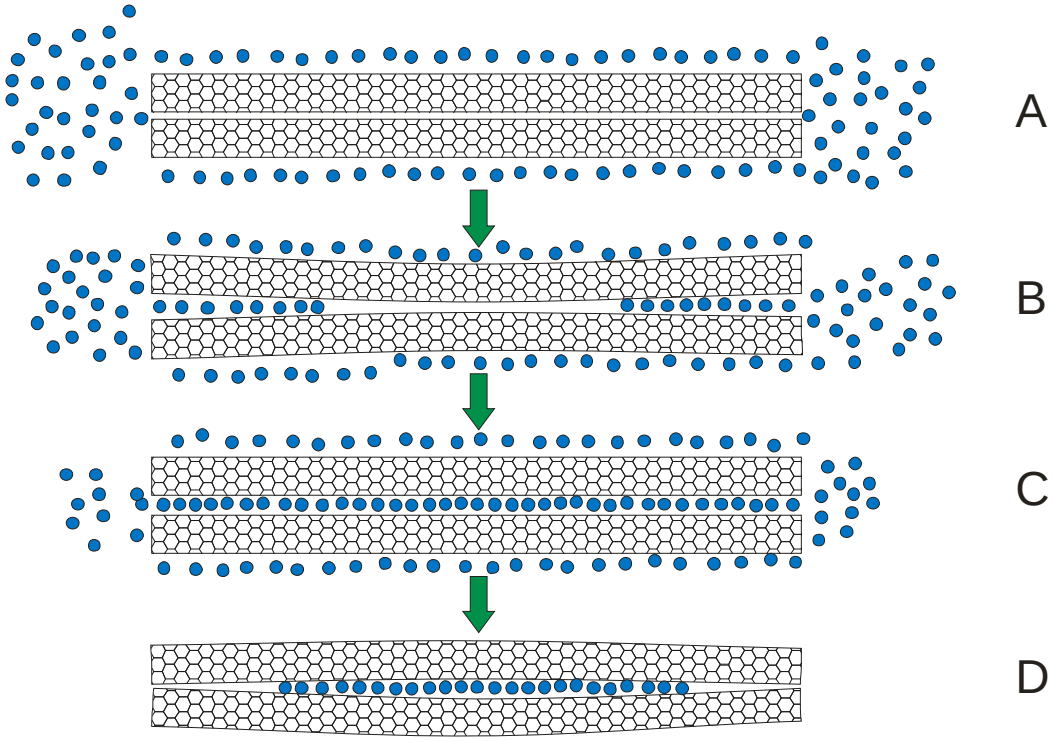

Figure 25: Model describing activated adsorption/desorption mechanism of molecules inside interstitial channels of SWCNT bundle. Molecules approach SWCNT bundle (side view shows only two nanotubes for simplification) (A) and start to penetrate the interstitial channel "debundling" nanotubes (B). Ultimately molecules can fill the whole interstitial channel (C). Upon evacuation molecules that are close to the "exits" will desorb first, while molecules that are in the middle of interstitial channels can be trapped inside (D). Elastic deformation of carbon nanotubes may assist trapping of the molecules (D).

The findings presented here have a number of implications. The developers of CNT based nanosensors, especially for organic molecule detection,[11, 12, 17, 116] should be aware of strong binding of those molecules to carbon nanotubes. Strongly bound molecules can deteriorate the performance of CNT based sensors by blocking the access to the sites responsible

for detector response. In particular the binding is irreversible at room temperature as temperatures >450-490 K are needed to remove the adsorbed gases in a reasonable amount of time. In order to keep SWCNTs "clean" it is advised to heat up them up to temperatures ≥600 K when most of the molecules studied here desorb from SWCNTs. Such temperature are reasonable for pure SWCNTs even in ambient air; the purified SWCNTs start to burn ~600-700 K (see Figure C1 in [159]).[181]

6.5 SUMMARY

As-produced and air/HCl purified SWCNTs contain impurities that decompose upon heating under vacuum producing multiple fragments that can be misinterpreted as fragments of other chemical species. Those impurities could possibly be adsorbed on SWCNTs from ambient air. Heating in inert atmosphere is suggested to remove these impurities.

The interaction of such solvents as acetone and ethanol with the air/HCl purified SWCNTs was studied after reflux, sonication, and exposure to corresponding solvent vapors. Results suggest that after contact with solvents SWCNTs can retain them up to high temperatures (400-900 K) corresponding to binding energies of 100-225 kJ mol^{-1}. The retained solvents desorb as intact molecules. Theoretical calculations find that adsorption of the molecules on pristine or defective SWCNT sidewalls or in grooves of SWCNT dimers never exceed 80 kJ mol^{-1}, and that physisorption of acetone inside interstitial sites of large-diameter SWCNT is energetically and sterically feasible. This result suggests that the observed high energies should be interpreted as desorption barriers for acetone escape from the inside of individual tubes or the interstitial sites

of tube bundles. Our study thus suggests the existence of a “pressure gap” to molecular encapsulation in carbon nanomaterials.

7.0 "STEALTH" MOLECULES INSIDE SINGLE WALL CARBON NANOTUBES: CAN FTIR DETECT MOLECULES ADSORBED IN CARBON NANOTUBE BUNDLES?

Results reported in this chapter require additional research to be done before submission for publication.

Abstract

Encapsulation of molecules inside of carbon nanotubes (endohedral adsorption) is key for CNT applications in such fields as drug delivery, storage of chemicals, catalyst development, etc. The detection of molecules inside of carbon nanotubes is important to estimation of the effectiveness of the encapsulation processes and for the characterization of encapsulated molecules. We chose acetone as a probe molecule to study its adsorption in the endohedral sites of SWCNTs by FTIR spectroscopy. Acetone has many advantages: acetone adsorbs on different sites of SWCNTs with different adsorption energies[159] and the C=O bond of acetone has a high extinction coefficient in the infrared region[182]. The results of FTIR studies suggest that acetone molecules adsorbed on the external walls of SWCNTs can be easily detected by FTIR spectroscopy, while acetone molecules adsorbed in more tightly bound sites, presumably inside of endohedral channels of SWCNTs, are not detectable by IR spectroscopy.

7.1 INTRODUCTION

Carbon nanotubes (CNTs) are promising materials for the encapsulation of chemical species for such applications as data storage,[183] drug delivery and cancer treatment,[184, 185] hydrogen storage,[18] catalysis,[186, 187] etc. Effective tools are required for the evaluation of the encapsulation process and the characterization of the encapsulated molecules.

Transmission electron microscopy (TEM),[188-191] infrared spectroscopy (FTIR),[10, 103, 158, 170, 189, 192-195] and Raman spectroscopy[189, 191, 196] are the most widely used experimental techniques to characterize encapsulated molecules. The only technique that provides direct evidence of encapsulated molecules is TEM.[188, 189, 191] The shifts or changes in intensity of Raman and FTIR features characteristic of encapsulated molecules, or of carbon nanotubes by themselves, are usually considered as evidence of molecules located inside CNTs.[10, 103, 158, 170, 189, 191-196] Vibrational frequency shifts observed for molecules adsorbed in the endohedral channels of CNTs are usually associated with changes that molecules undergo due to interaction with CNT walls or due to confinement of the molecules.[103, 194, 197]

Our experimental findings suggest that acetone molecules, adsorbed presumably in endohedral channels of air/HCl purified SWCNTs, can not be detected with FTIR spectroscopy. We discuss the implications of our findings for the use of FTIR for the characterization of molecules encapsulated inside CNTs and suggest directions for the investigation of factors that might influence the spectroscopic behavior of molecules adsorbed on/in CNTs.

7.2 EXPERIMENTAL

7.2.1 Materials

As-received single wall carbon nanotubes produced by HiPco method[43] were purified according to the air/HCl procedure described in detail in Chapter 4.2.[159] The same sample was used for TPD studies described in Chapter 6 and the FTIR studies described in this chapter. The residual iron content after purification was ~0.9 wt.% (Figure 6).

7.2.2 Sample preparation and acetone adsorption

For the FTIR experiment, the purified SWCNTs were sonicated in acetone and then deposited by drop-and-dry technique in a flow of preheated air (~60 °C) on the W-grid.[159] The amount of SWCNTs deposited on the W-grid was adjusted to obtain a uniform mat of SWCNTs (1 x 2 cm) with no holes visible in the mat. The optical density of SWCNT mats varied in ~1.4 - 2.2 O.D. range at 2000 cm^{-1}. After deposition of SWCNTs on the W-grid, the sample holder was placed inside the vacuum chamber and evacuated overnight to $<10^{-8}$ Torr. The SWCNT sample was annealed under high vacuum at 500 K for 2 h before adsorption experiments. Before acetone adsorption the SWCNT sample was cooled to ~100 K with liquid nitrogen and a background IR-spectrum was collected. Spectra were collected at 4 cm^{-1} resolution and 6400 scans were collected in 4000-400 cm^{-1} spectral range. Acetone (Fisher, ACS grade) was degassed by freeze-pump-thaw cycles (4-7) before dosing to the sample. The desired amount of acetone was dosed through a leak valve.

7.3 RESULTS AND DISCUSSION

To start, 500 L of acetone were dosed to SWCNT sample cooled to 100 K and after that spectrum was recorded (Figure 26A (—)). Characteristic IR-bands of physically adsorbed acetone appeared in the FTIR spectrum: an intense band at 1708 cm^{-1} characteristic of a C=O bond, and several less intense modes associated with stretching (~2900 cm^{-1}) and deformation (~1400 cm^{-1}) of C-H bonds in CH_3 groups. The sample with pre-adsorbed acetone was flash-heated to 200 K at 2 K sec^{-1}, while the pressure was monitored with the ion gauge (Figure 26B (- - -)). After the temperature reached 200 K the sample was held for 30 sec at that temperature and then it was cooled back to 100 K and a spectrum was recorded (Figure 26A (---)). The spectrum revealed no IR bands characteristic of physically adsorbed acetone, while the TPD-MS results (Figure 11B) suggest that acetone should be still at the surface of SWCNTs after flash heating to 200 K. The subsequent heating of the sample to 500 K, with pressure monitoring as a function of sample temperature, proved that acetone is still adsorbed on the SWCNTs: a broad desorption peak was observed at ~248 K (Figure 26B (•••)), in agreement with TPD-MS results (Figure 11B). After heating of the SWCNT sample to 500 K the sample was cooled to 100 K and an infrared spectrum was recorded; spectrum showed no bands characteristic of acetone adsorbed (Figure 26A (•••)).

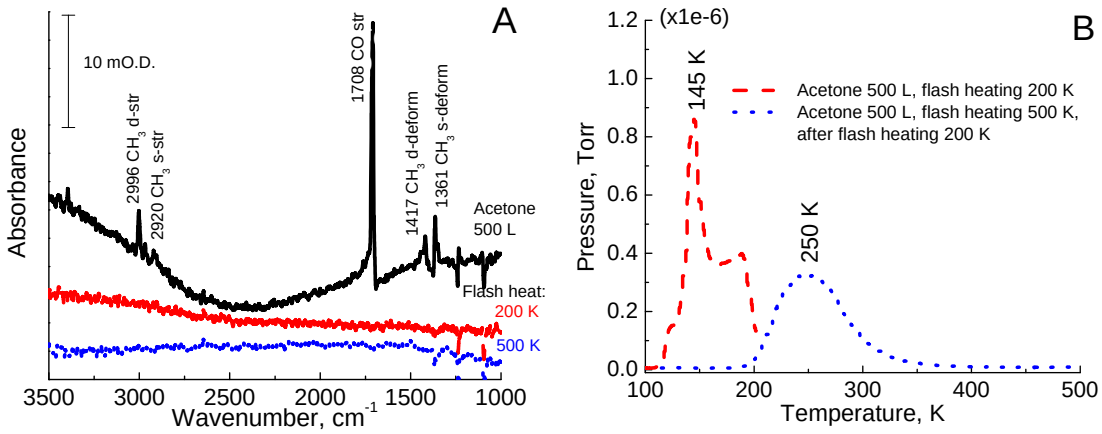

Figure 26: Infrared spectra of acetone adsorbed on SWCNTs (HiPco, Air/HCl) annealed to 500 K. **A**. Acetone (500 L) was adsorbed at 100 K (—). After adsorption of acetone, the sample was flash heated to 200 K (---) and then to 500 K (•••). After each flash heating step the FTIR spectrum was recorded. **B**. Pressure desorption profiles of acetone from SWCNT sample during each flash heating step.

Using the areas under the curves (Figure 26B) as a measure of the relative populations, we infer that the fraction of acetone desorbing below 200 K is similar to the amount of acetone desorbing above 200 K. According to TPD-MS results (Figure 11B), for a dose of 500 L to the sample annealed at 500 K, the ratio of acetone desorbing below 200 K to acetone desorbing above 200 K should be 1:8. However, in the TPD-MS experiment we detect mainly acetone desorbing from the sample that is positioned right in front of RGA cone that collects desorbing molecules from a sample area of a few square millimeter. In the case of the FTIR experiment the pressure profiles (Figure 26B) are recorded with the ion gauge which measures total pressure not just the fraction associated with acetone. Furthermore the ion gauge pressure profile reflects desorption of molecules from both sample (~15x10 mm) and from the W-grid (25 x 20 mm) that is not covered with SWCNTs. The W-grid can adsorb acetone revealing desorption peak at ~140 K (Figure B2). However, there is no evidence for acetone desorbing above 200 K from the W-grid (Figure B2). The ratio between acetone desorbing below 200 K and above 200 K should therefore be different for FTIR and TPD experimental setups. While the quantitatively the TPD-

MS experiment is more accurate, the results of the ion gauge measurement clearly indicate that significant a amount of acetone remains adsorbed on the SWCNTs even after flash heating to 200 K.

It would seem reasonable therefore that, after flash heating of the sample to 200 K, the IR peaks should decrease at most by a factor of two (considering ion gauge results (Figure 26B)) or just by ~10-20% (considering TPD-MS results (Figure 11B)). However, all acetone related peaks disappear completely from the FTIR spectrum after flash heating to 200 K. It appears that FTIR can detect only acetone adsorbed on SWCNTs that desorbs below 200 K. According to the results of Chapter 5 and 6, acetone desorbing at 140 K can be assigned to acetone adsorbed on the W-grid (Figure B2), adsorbed on external walls of carbon nanotubes, and to multilayers of adsorbed acetone (Figure 15). The desorption energy from grooves and interstitial channels (~50 kJ/mol) is close to 200 K that we used in the flash heating experiment; some of the molecules adsorbed in grooves and interstitial sites can also be desorbed upon flash heating to 200 K. After flash-heating to 200 K, there should be no molecules adsorbed on external walls of carbon nanotubes, the W-grid, or grooves and interstitial sites. FTIR clearly reveals the disappearance of molecules from those sites. However, FTIR does not seem to detect the considerable amounts of acetone that remain after flash heating of the sample to 200 K.

Our findings appear to contradict the results of several papers where the successful detection of molecules inside endohedral channels of SWCNTs with FTIR was reported.[10, 103, 158, 170, 189, 192-195] Of the papers that reported successful detection of molecules trapped inside of endohedral channels by FTIR technique[10, 103, 158, 170, 189, 192-195] only one work presented direct evidence (results of TEM) of molecules encapsulated inside the endohedral channels of CNTs[189].

The results of successful FTIR detection of molecules, either trapped or physically adsorbed, inside of endohedral channels of carbon nanotubes are summarized in Table 5. The shifts in IR frequencies of molecules adsorbed endohedrally vary from - 8 cm^{-1} for CO[158] to -292 cm^{-1} for NO_2[195]. There are some inconsistencies in reported results present; for NH_3 adsorbed on SWCNTs different frequency shifts are reported -46[10] and -180[195] cm^{-1}.

While assignment of vibrational features to molecules adsorbed in the endohedral channels of CNTs may be reasonable, other possibilities need to be considered. As-produced CNTs normally contain admixtures of carbonaceous impurities that may survive purification procedures.[63, 198] A question that arises is whether molecules adsorbed inside of micropores of, carbonaceous impurities could be responsible for the spectroscopic features assigned to molecules adsorbed in the endohedral channels of CNTs? How can we differentiate spectroscopically between molecules adsorbed on carbonaceous impurities and molecules adsorbed on/in CNTs? Moreover, even after purification, catalytically produced CNTs contain metal admixtures on the order of 0.4-6 wt% (Figure 6).[46, 47, 61, 70, 78] This raises another question, how do metal impurities influence the spectroscopic features of adsorbed molecules?

Table 5: The frequency shifts in IR spectra of molecules reportedly adsorbed on CNT exohedral and endohedral sites (table was adapted from [199]).

	Vibrational Frequency (cm^{-1}) for various sites			
Molecule	Gas phase frequency	Endohedral	Exohedral	Endohedral Shift wrt gas phase
CO[158]	2143	2135	2140	–8
$(NO)_2$[193]	1868	1853	----	–15
CO_2[197]	2349	2329	2342	–20
SF_6[170]	947	927	----	–20
H_2O[103]	3657 sym	3507	3255	-150
	3756 anti			-249
CF_4[194]	1282	1247	1267	–35
$H_8Si_8O_{12}$[189]	2277 (Si–H solution)	2262	----	–15
NH_3[195]	3336	3156	3205	–180
NH_3[10]	3336	3290	3290	-46
NO_2[195]	1318	1026	1026	–292

The results reported in the literature[10, 103, 158, 170, 189, 192-195] cause concern and require scrupulous analysis. For example, the FTIR results on NO adsorption on SWCNTs produced by laser vaporization technique[73] suggest that NO adsorbed endohedrally exists in the form of dimers.[193] In the laser vaporization technique Co and Ni are used as catalysts for SWCNT synthesis and TGA analysis shows that purified samples contain non-combustible ash (presumably, CoO_x and NiO_x).[73] It is well known from the literature that NO adsorbs both on Ni and Co, both in single crystal form and supported nanoparticles.[200-203] The frequency and relative intensity of the symmetric and asymmetric vibrations of the NO bonds in dimer depend on the oxidation state of the metal, the particle support material, and the orientation of NO molecules in metal-$(NO)_2$ dimers.[200, 201, 203] We can not exclude the possibility that the NO observed was adsorbed on Ni or Co moieties left on carbon nanotubes after purification.[73]

The presence of metal residuals may also influence the adsorption behavior of other molecules: CO (HiPco and Rice Tubes, 4 wt.% (Fe) and 8wt.% (Co and Ni) according to TGA,

respectively),[158, 204] CO_2 (nanotubes were produced and purified according to the procedure described elsewhere[73]).[192] The experiment that reported the trapping of SF_6 and CO_2 molecules in CNTs use SWCNTs (HiPco) with 18 wt.% of iron content. [170] The opening of the nanotubes and removal of carbonaceous impurities was done *in situ* by ozonation, while iron was not removed.[170]

In the present work we do not provide direct evidence for acetone molecules adsorbed inside the endohedral channels of SWCNTs, but by using the flash heating approach we exclude the possibility of acetone adsorbed on sites with low binding energy – exohedral sites having desorption temperature of 140 K. From the literature it is well known that endohedral sites have the maximum energy for adsorption.[110, 159, 205, 206] It is logical to suggest that molecules that persist above 200 K, and that we do not see in our experiments with FTIR, are adsorbed inside of endohedral channels.

According to literature the screening of molecules adsorbed in/on carbon nanotubes is possible due to the high polarizability of CNTs.[207, 208] However, screening of vibrational modes is most likely to occur if the transition dipoles are parallel to the CNT walls.[208] In the case of acetone adsorbed on/in SWCNTs all the vibrational transition dipoles of the multiple modes (CH and CO) of acetone can not be parallel to the CNT wall simultaneously. Therefore we should observe some IR features even after flash heating to 200 K.

The results of our work are in contrast to results reported elsewhere.[10, 103, 158, 170, 189, 192-195] At the present moment we do not have a clear explanation for the effect of screening of acetone molecules that desorb from SWCNTs above 200 K and that can possibly be adsorbed in the endohedral channels of CNTs. Theoretical calculations aiming to provide an explanation for our

experimental findings are under way. Other molecules will be investigated as well, to make sure that acetone spectroscopic behavior on SWCNTs is not unique.

8.0 CONCLUSIONS AND FUTURE DIRECTIONS

In the course of this work it was established that the air/HCl purification introduces oxygen functionalities to the as-produced SWCNTs. No evidence of carboxylic (carbonyl) group introduction (thermal decomposition) was found from the FTIR study. We tentatively assigned the introduced functionalities to hydroxyls (OH) on the sidewalls of carbon nanotubes. These findings are in contrast with the findings by other authors who reported introduction of carboxylic (carbonyl) groups after air/HCl purification.[69, 70] It is highly desirable to address the effect of water vapors addition to the air mixture during the oxidation step. At this step water vapors might be responsible for the formation of OH groups at the surface of CNTs. It is also desirable to study the effect of HCl step on introduction and/or modification of surface functionalities; HCl might act as a catalyst and facilitate hydrolysis of, e.g., ether bonds.

Interaction of molecules with carbon nanotubes under variable conditions should be investigated in more details. It would be interesting to find out whether there are chemical interactions of carbon nanotubes with different solvents and gases at high temperatures. The question on the nature of the sites that retain molecules in a strongly bound form is still open. The answer to this question might help to design CNT based materials for effective molecular storage applications.

Adsorbed (both physically and chemically) molecules can introduce electronic modifications to carbon nanotubes (due to electronic density redistribution, polarization, etc.).

The understanding of the electronic modification trends will benefit the development of CNT based chemical sensors and CNT based electronics where tuning of the electronic properties is desirable.[10-17] This topic should be considered in the future works.

APPENDIX A

SUPPORTING INFORMATION FOR CHAPTER 4

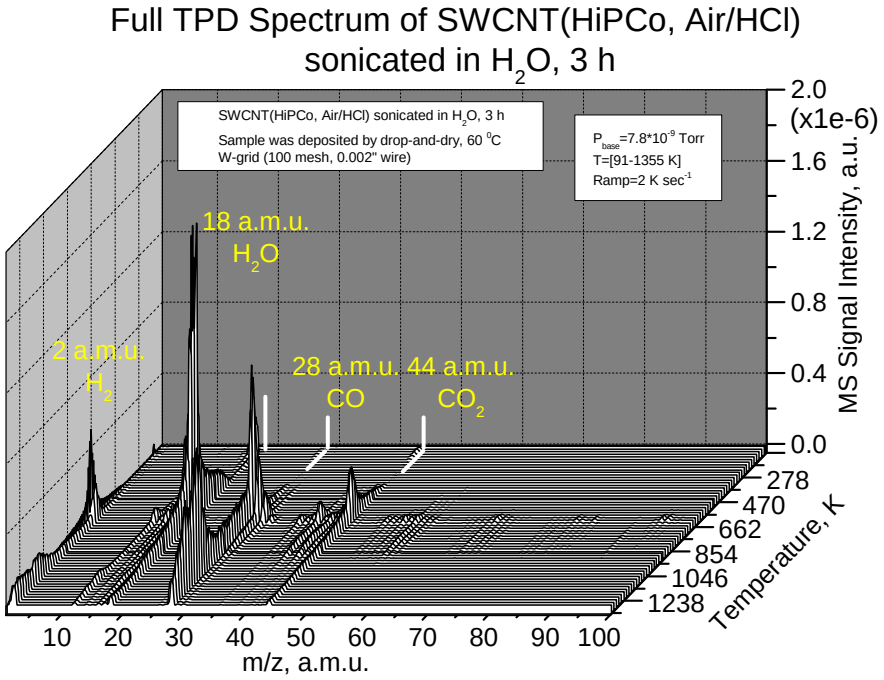

Figure A1B: Full TPD spectrum from air/HCl SWCNTs produced by HiPco method. The dominant fragment that release upon heating are 2 amu (H_2), 18 amu (H_2O), 28 amu (CO) and 44 amu (CO_2). There are multiple fragments that can be misinterpreted as arising from acetone, ethanol, or other compounds.

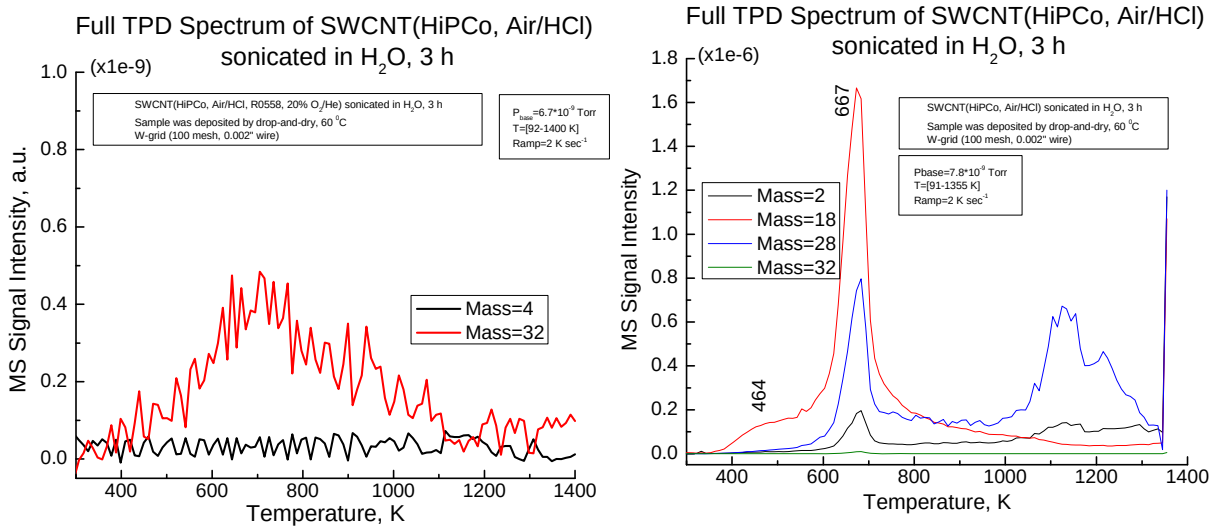

Figure A2: Profiles of mass 4 and 32 amu releasing from air/HCl purified SWCNTs are shown. Profiles suggest no increase in signal intensity for 4 amu signal (He) and extremely low intensity for 32 amu signal (O_2). Signals 2 (H_2), 18 (H_2O), 28 (CO), and 32 amu (O_2) are shown on the same scale. Note that sample was oxidized with 20% O_2/He and then sonicated in HCl under 20% O_2/He environment.

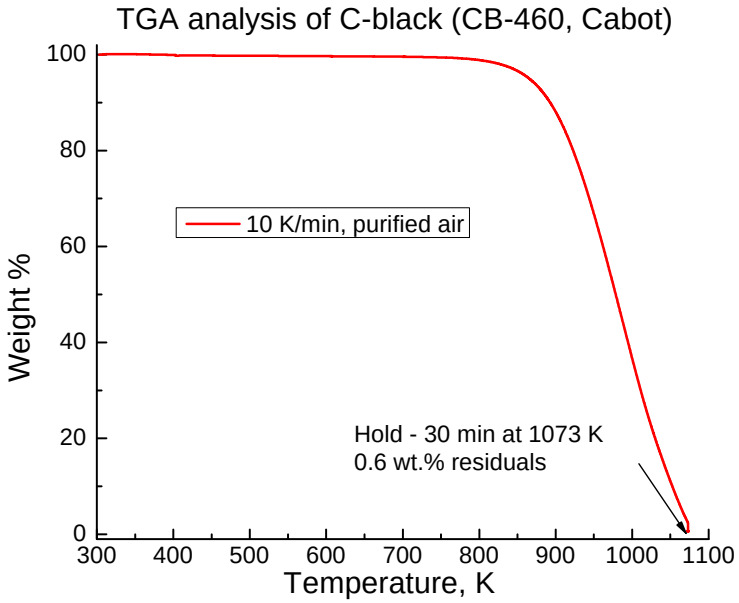

Figure A3: Results of TGA experiment for carbon black. Carbon black starts to burn in a flow of air at ~800 K. [Author acknowledges the assistance of the Baran group (Temple University) for TGA analysis.]

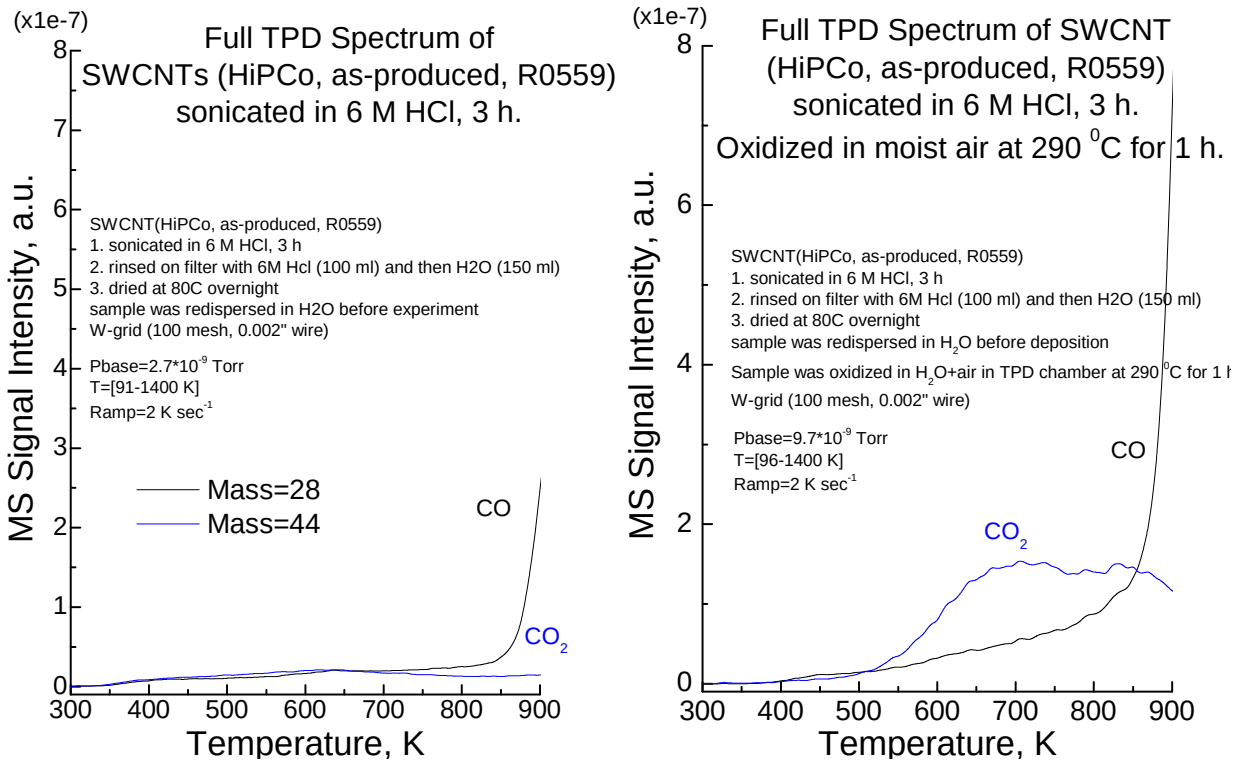

Figure A4: Release of CO and CO_2 fragments from SWCNTs (HiPco) that (A) were sonicated in 6 M HCl solution (B) were sonicated in 6 M HCl solution and then were oxidized at 290 °C. The TPD profile of CO releasing from both samples does not change, while profile of CO_2 for sample oxidized at 290 °C is different suggesting formation of a new oxygen functionalities after oxidation step that decompose at ~ 700 K.

APPENDIX B

SUPPORTING INFORMATION FOR CHAPTER 5

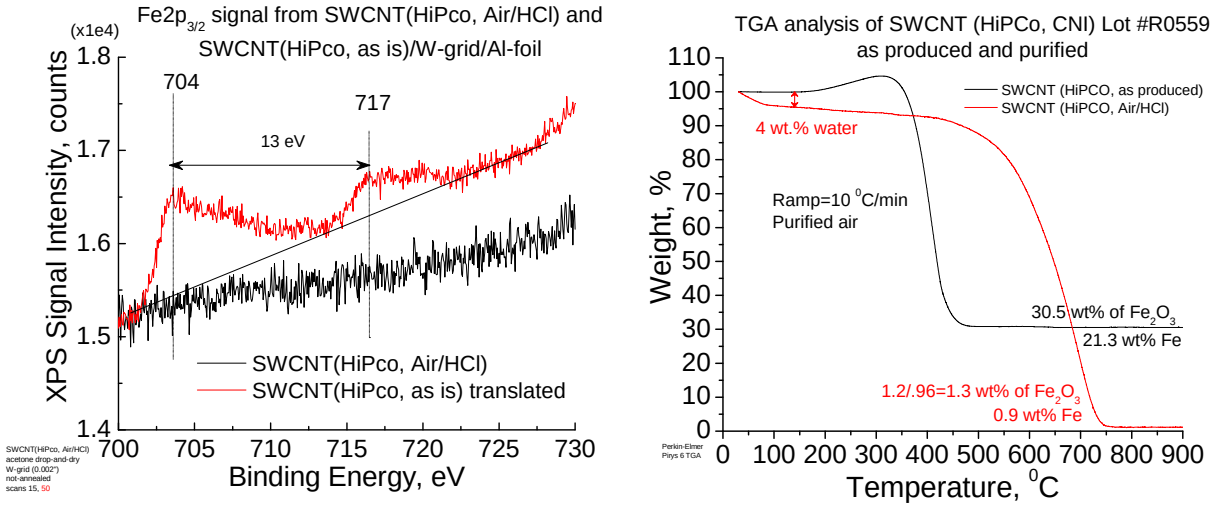

Figure B1. (Left) Results of XPS Analysis of SWCNTs (HiPco). As produced SWCNT show a distinct Fe(2p) signal, while the purified sample shows no signal from catalyst. (Right) Results of TGA analysis: as produced SWCNTs contain ~21 wt.% of Fe, while air-HCl purification reduces the Fe content to ~1 wt.%

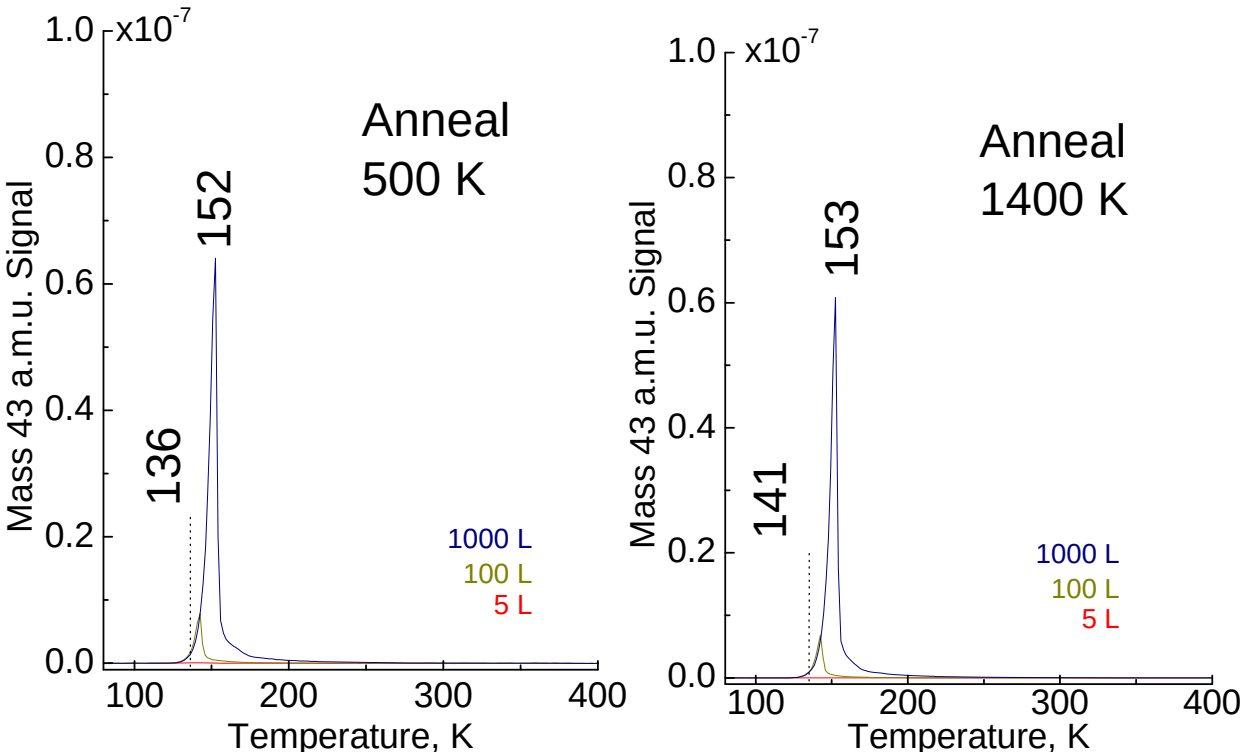

Figure B2. Control experiment: acetone adsorption on W-grid (0.002", AlfaAesar) used in our experiments. Before acetone adsorption W-grid was annealed to 500 K and then to 1400 K. Acetone physisorbs on the W-grid desorbing below 200 K independent of anneal temperature.

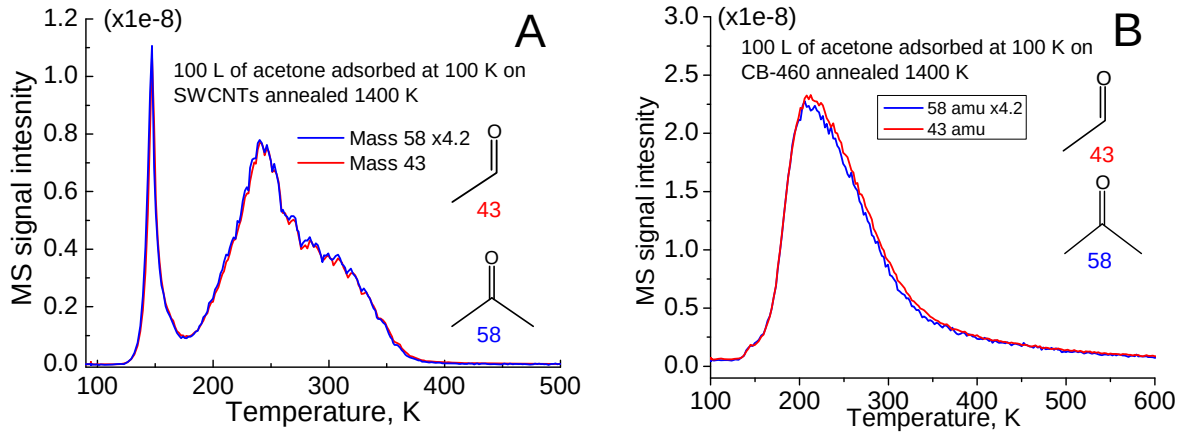

Figure B3. TPD of acetone dosed (1000 L) to purified SWCNTs-1400K (A) and 100 L dosed to carbon black (CB-460) annealed to 1400 K (B). Profiles for masses 43 amu (e.g. CH_3CO) and 58 amu ($CH_3C(O)CH_3$) coincide as an evidence that acetone desorbed as an intact molecule.

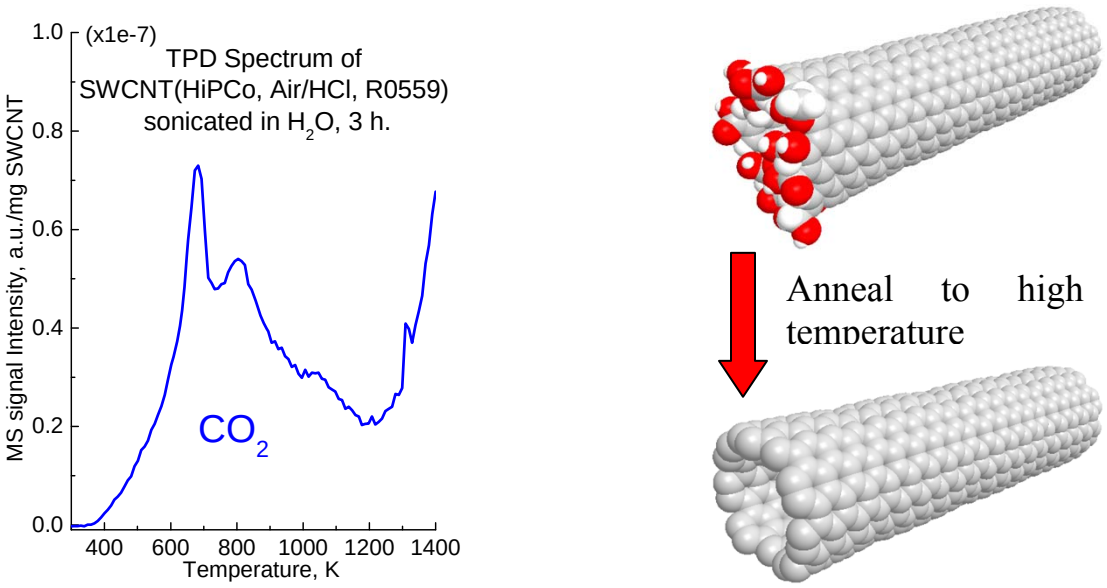

Figure B4. TPD profile of 28 and 44 amu during anneal of SWCNT (HiPco, air/HCl) purified. Mass 44 amu can be assigned to CO_2 that forms during decomposition of oxygen containing functionalities, e.g. carboxylic groups. That sample was sonicated in H_2O before deposition on the W-grid.

APPENDIX C

SUPPORTING INFORMATION FOR CHAPTER 6

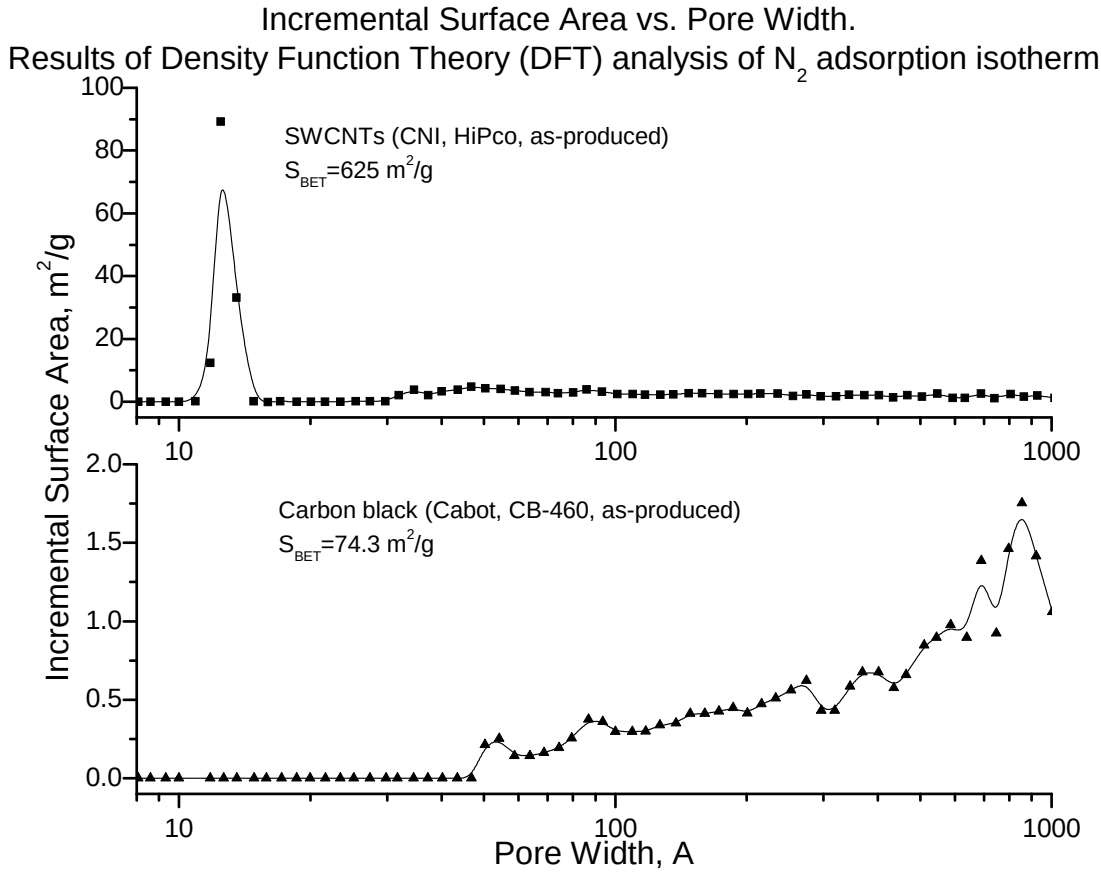

Figure C1: Results of DFT analysis of N_2 adsorption isotherm obtained by volumetric adsorption (Micromeritics, ASAP 2020) method for as-produced SWCNTs (HiPco, CNI) and for carbon black (CB-460, Cabot company). SWCNTs have a large amount of micropores (<20 nm), while carbon black has mainly meso- (20-500 A) and macro-pores (>500 A).

SWCNTs (HiPco, as-produced) sonicated in H_2O, deposited by drop-and-dry at 60 °C

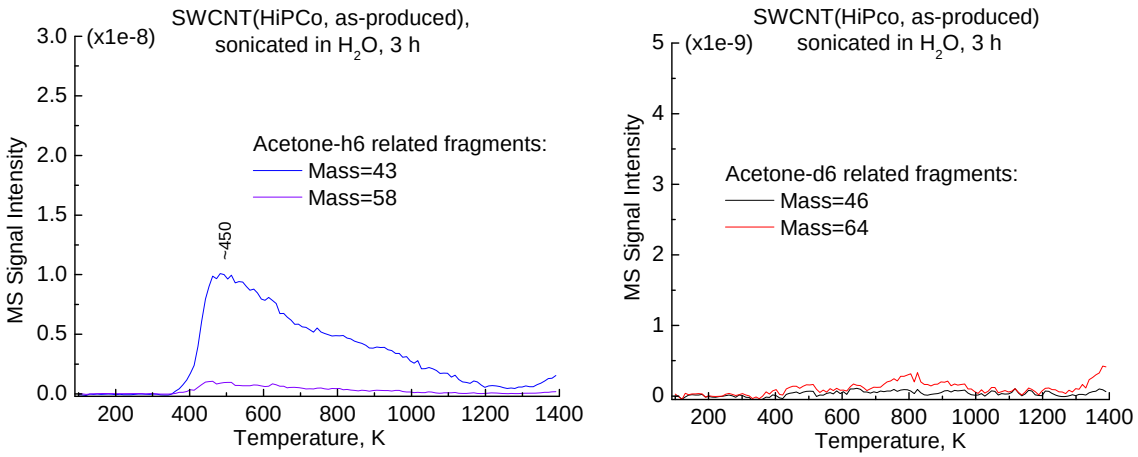

SWCNTs (HiPco, Air/HCl purified) sonicated in H_2O, deposited by drop-and-dry at 60 °C.

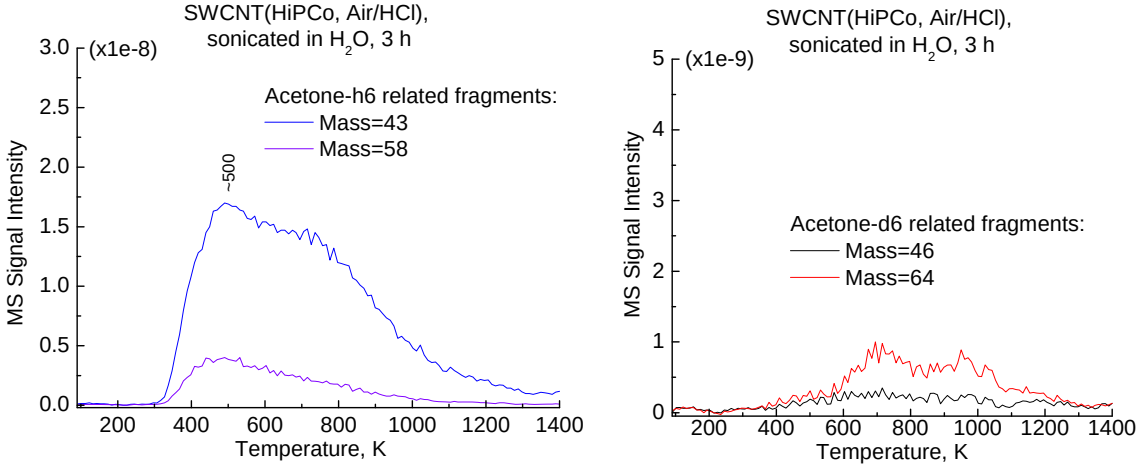

Figure C3: Both as-produced and air/HCl purified SWCNTs upon heating release fragments that have the same masses as fragments that could be assigned to acetone-h6 or acetone-d6 molecules. Presumably, those fragments are due to organics that adsorb from the ambient air on SWCNTs.

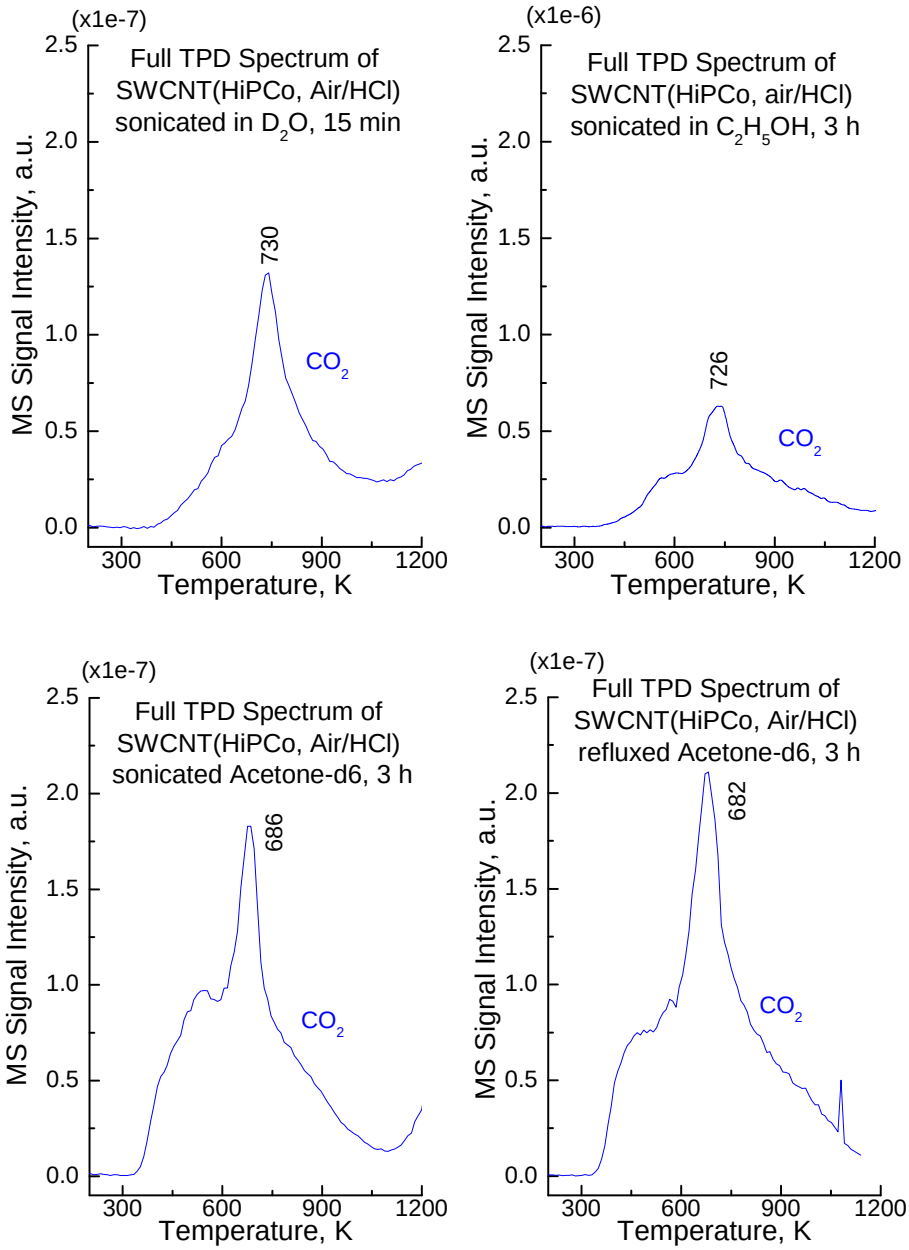

Figure C4: 44 amu signal (CO_2) intensity could serve as an internal standard to compare the signal intensity variation from SWCNT samples pretreated in different ways. Acetone-d6 and ethanol slightly contribute to intensity of 44 amu signal in region 400-600 K, but contribution of from either from acetone-d6 or ethanol to mass 44 amu is negligible in comparison with intensity of CO_2 signal. By comparing the intensity of the CO_2 signals for samples sonicated in acetone we can conclude that the amount of CO_2 released is approximately the same for the two different samples. Signals for CO_2 released from samples treated in D_2O and ethanol have the same order of magnitude to signal of CO_2 released from samples treated in acetone

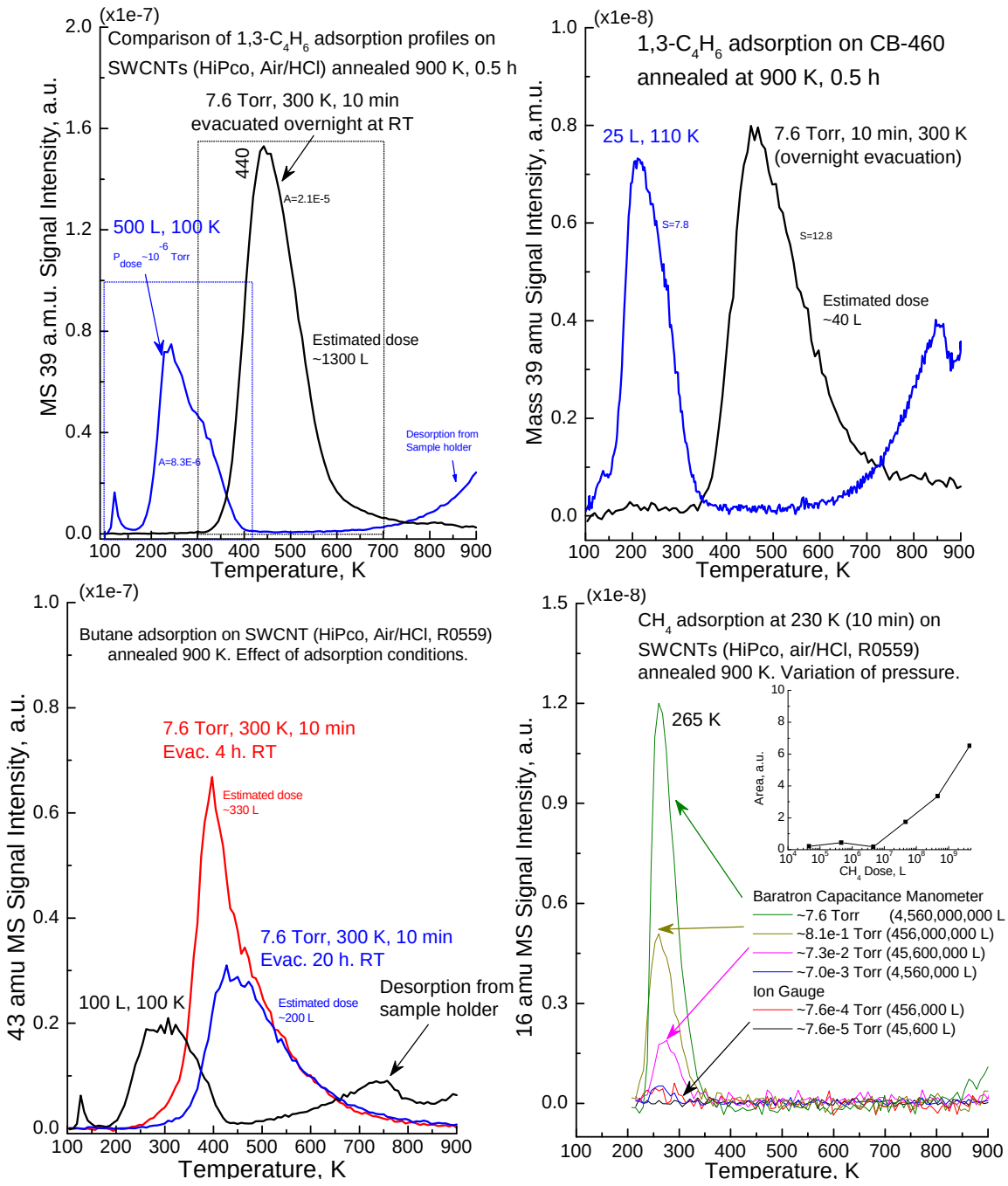

Figure C5: Adsorption of 1,3-butadiene (1,3-C_4H_6), n-butane (n-C_4H_{10}) and methane (CH_4) on carbonaceous materials. Top row shows adsorption of 1,3-C_4H_6 on SWCNTs (HiPco, air/HCl) and carbon black (CB-460, as-received). Both SWCNTs and carbon black retain 1,3-C_4H_6 dosed at "7.6 Torr-300 K" up to high temperatures (~450 K). Adsorption capacity of SWCNTs with respect to strongly bound 1,3-C_4H_6 significantly exceeds adsorption capacity of carbon black, 1300L and 40 L, respectively. The bottom row shows adsorption of n-butane (C) and methane on SWCNTs (D). The example of n-C_4H_{10} adsorption on SWCNTs clearly shows that time of evacuation plays a crucial role in the amount of gas retained by SWCNTs. After 4 hours of evacuation the amount of n-C_4H_{10} retained is ~300 L, while after 20 hours of evacuation the amount of n-C_4H_{10} decreases to 200 L (compare red and blue curves on graph C). Graph D shows the amount of methane that binds to SWCNTs upon exposure at 230 K. Almost all methane desorbs from SWCNTs by 300 K.

APPENDIX D

LIST OF PUBLICATIONS

1. "Effect of Cu/Pt ratio on a selectivity of $PtCu_n/SiO_2$ catalysts in the reaction of monochloroethane selective hydrodechlorination to ethylene", D. Kazachkin, V. Kovalchuk, J. d'Itri (in preparation)

2. "Infrared study of molecules adsorbed in CNTs. Screening effect of CNTs." D. Kazachkin, Y. Nishimura, S. Irle, R. Vidic, E. Borguet (in preparation)

3. "Temperature and pressure dependence of solvent molecule adsorption on single wall carbon nanotubes and the existence of a "pressure gap", D. V. Kazachkin, Y. Nishimura, S. Irle, X. Feng, R. Vidic, and E. Borguet (submitted)

4. "Impact of Synthesis Conditions on Surface Chemistry and Structure of Carbide-Derived Carbons", C. Portet, D. Kazachkin, S. Osswald, E. Borguet, Y. Gogotsi (submitted)

5. "Hydrogen-Assisted 1,2-Dichloroethane Dechlorination Catalyzed by Pt-Cu/SiO_2: Insights into the Nature of Ethylene-Selective Active Sites", D. Kazachkin, D. Luebke, V. Kovalchuk, J. d'Itri (Accepted to Journal of Siberian Federal University.)

6. "Interaction of acetone with single wall carbon nanotubes at cryogenic temperatures: A combined temperature programmed desorption and theoretical study", D. Kazachkin, Y. Nishimura, S. Irle, Keiji Morokuma, R. Vidic, E. Borguet (Langmuir, 24 (15) (2008) 7848–7856)

7. "Characterization and catalytic activity of differently pretreated Pd/Al_2O_3 catalysts: the role of acid sites and of palladium-alumina interactions", M. Skotak, Z. Karpinski, W. Juszczyk, J. Pielaszek, L. Kepinski, D. Kazachkin, V. Kovalchuk, J. d'Itri (Journal of Catalysis (2004), 227(1), 11-25)

BIBLIOGRAPHY

1. Reibold, M.; Paufler, P.; Levin, A. A.; Kochmann, W.; Paetzke, N.; Meyer, D. C., Materials: Carbon nanotubes in an ancient Damascus sabre. *Nature (London, United Kingdom)* **2006,** 444, (7117), 286.

2. Radushkevich, L. V.; Luk'yanovich, V. M., Structure of the carbon produced in the thermal decomposition of carbon monoxide on an iron catalyst. *Zhurnal Fizicheskoi Khimii* **1952,** 26, 88-95.

3. *The Science and Technology of Carbon Nanotubes*. Elsevier Science Ltd: Oxford, 1999; p 191.

4. Burchell, T. D., *Carbon Materials for Advanced Technologies*. 1999; p 540.

5. Ajayan, P. M.; Zhou, O. Z., Applications of carbon nanotubes. In *Carbon Nanotubes*, 2001; Vol. 80, pp 391-425.

6. Science of Fullerenes and Carbon Nanotubes. In Dresselhaus, M. S.; Dresselhaus, G.; Eklund, P. C., Eds. Academic Press: New York, 1996.

7. Pierson, H. O., *Handbook of carbon, graphite, diamond, and fullerenes*. Noyes Publications: Park Ridge, New Jersey, U.S.A., 1993.

8. O'Connell, M. J., *Carbon Nanotubes. Properties and Applications*. CRC Press/Taylor & Francis: Boca Raton, 2006; p 319.

9. Osawa, E., *Perspectives of Fullerene Nanotechnology*. Springer: 2002; p 400.

10. Feng, X.; Irle, S.; Witek, H.; Morokuma, K.; Vidic, R.; Borguet, E., Sensitivity of Ammonia Interaction with Single-Walled Carbon Nanotube Bundles to the Presence of Defect Sites and Functionalities. *Journal of the American Chemical Society* **2005,** 127, (30), 10533-10538.

11. Robinson, J. A.; Snow, E. S.; Badescu, S. C.; Reinecke, T. L.; Perkins, F. K., Role of Defects in Single-Walled Carbon Nanotube Chemical Sensors. *Nano Letters* **2006,** 6, (8), 1747-1751.

12. Parikh, K.; Cattanach, K.; Rao, R.; Suh, D.-S.; Wu, A.; Manohar, S. K., Flexible vapour sensors using single walled carbon nanotubes. *Sensors and Actuators, B: Chemical* **2006,** B113, (1), 55-63.

13. Lu, Y.; Partridge, C.; Meyyappan, M.; Li, J., A carbon nanotube sensor array for sensitive gas discrimination using principal component analysis. *Journal of Electroanalytical Chemistry* **2006,** 593, (1-2), 105-110.

14. Kong, J.; Franklin, N. R.; Zhou, C. W.; Chapline, M. G.; Peng, S.; Cho, K. J.; Dai, H. J., Nanotube molecular wires as chemical sensors. *Science* **2000,** 287, (5453), 622-625.

15. Snow, E. S.; Perkins, F. K.; Houser, E. J.; Badescu, S. C.; Reinecke, T. L., Chemical detection with a single-walled carbon nanotube capacitor. *Science* **2005,** 307, (5717), 1942-1945.

16. Li, J.; Lu, Y. J.; Ye, Q.; Cinke, M.; Han, J.; Meyyappan, M., Carbon nanotube sensors for gas and organic vapor detection. *Nano Letters* **2003,** 3, (7), 929-933.

17. Penza, M.; Tagliente, M. A.; Aversa, P.; Cassano, G., Organic-vapor detection using carbon-nanotubes nanocomposite microacoustic sensors. *Chemical Physics Letters* **2005,** 409, (4-6), 349-354.

18. Dillon, A. C.; Jones, K. M.; Bekkedahl, T. A.; Kiang, C. H.; Bethune, D. S.; Heben, M. J., Storage of hydrogen in single-walled carbon nanotubes. *Nature* **1997,** 386, (6623), 377-379.

19. Gadiou, R.; Saadallah, S. E.; Piquero, T.; David, P.; Parmentier, J.; Vix-Guterl, C., The influence of textural properties on the adsorption of hydrogen on ordered nanostructured carbons. *Microporous and Mesoporous Materials* **2005,** 79, (1-3), 121-128.

20. Sircar, S.; Golden, T. C.; Rao, M. B., Activated carbon for gas separation and storage. *Carbon* **1996,** 34, (1), 1-12.

21. Fletcher, B. L.; Retterer, S. T.; McKnight, T. E.; Melechko, A. V.; Fowlkes, J. D.; Simpson, M. L.; Doktycz, M. J., Actuatable Membranes Based on Polypyrrole-Coated Vertically Aligned Carbon Nanofibers. *ACS Nano* **2008,** 2, (2), 247-254.

22. Sznejer, G. A.; Efremenko, I.; Sheintuch, M., Carbon membranes for high temperature gas separations: Experiment and theory. *AIChE Journal* **2004,** 50, (3), 596-610.

23. Hinds, B. J.; Chopra, N.; Rantell, T.; Andrews, R.; Gavalas, V.; Bachas, L. G., Aligned Multiwalled Carbon Nanotube Membranes. *Science* **2004,** 303, (5654), 62-65.

24. Shaikh, S.; Li, L.; Lafdi, K.; Huie, J., Thermal conductivity of an aligned carbon nanotube array. *Carbon* **2007,** 45, (13), 2608-2613.

25. Edwards, B. C., Design and Deployment of a Space Elevator. *Acta Astronautica* **2000,** 47, (10), 735-744.

26. Mhuircheartaigh, E. M. N.; Blau, W. J.; Prat, M.; Giordani, S., Sonication of porphyrin-nanotube composites: A cautionary tale. *Physica Status Solidi B-Basic Solid State Physics* **2007,** 244, (11), 4227-4230.

27. Deng, J. N.; Zhang, X. Q.; Wang, K.; Zou, H.; Zhang, Q.; Fu, Q., Synthesis and properties of poly(ether urethane) membranes filled with isophorone diisocyanate-grafted carbon nanotubes. *Journal Of Membrane Science* **2007,** 288, (1-2), 261-267.

28. Owens, F. J.; Jayakody, J. R. P.; Greenbaum, S. G., Characterization of single walled carbon nanotube: Polyvinylene difluoride composites. *Composites Science and Technology* **2006,** 66, (10), 1280-1284.

29. Lee, H.; Mall, S.; Nalladega, V.; Sathish, S.; Roy, A.; Lafdi, K., Characterization of carbon nanofibre reinforced epoxy composite using nanoindentation and AFM/UFM techniques. *Polymers & Polymer Composites* **2006,** 14, (6), 549-562.

30. Koshio, A.; Yudasaka, M.; Zhang, M.; Iijima, S., A Simple Way to Chemically React Single-Wall Carbon Nanotubes with Organic Materials Using Ultrasonication. *Nano Letters* **2001,** 1, (7), 361-363.

31. Huang, W. J.; Lin, Y.; Taylor, S.; Gaillard, J.; Rao, A. M.; Sun, Y. P., Sonication-assisted functionalization and solubilization of carbon nanotubes. *Nano Letters* **2002,** 2, (3), 231-234.

32. Suslick, K. S., Sonochemistry. *Science* **1990,** 247, (4949, Pt. 1), 1439-45.

33. Kwon, S. Environmentally Relevant Adsorption on Carbonaceous Surfaces Studied by Optical Differential Reflectance and Temperature Programmed Desorption. Dissertation, University of Pittsburgh, Pittsburgh, 2002.

34. Brunauer, S.; Emmett, P. H.; Teller, E., Adsorption of Gases in Multimolecular Layers. *Journal of the American Chemical Society* **1938,** 60, (2), 309-319.

35. Kostarelos, K., The long and short of carbon nanotube toxicity. *Nat Biotech* **2008,** 26, (7), 774-776.

36. Zhao, Y.; Xing, G.; Chai, Z., Nanotoxicology: Are carbon nanotubes safe? *Nat Nano* **2008,** 3, (4), 191-192.

37. Krupke, R.; Hennrich, F.; Lohneysen, H. v.; Kappes, M. M., Separation of Metallic from Semiconducting Single-Walled Carbon Nanotubes. *Science* **2003,** 301, (5631), 344-347.

38. Maeda, Y.; Kanda, M.; Hashimoto, M.; Hasegawa, T.; Kimura, S.-I.; Lian, Y.; Wakahara, T.; Akasaka, T.; Kazaoui, S.; Minami, N.; Okazaki, T.; Hayamizu, Y.; Hata, K.; Lu, J.; Nagase, S., Dispersion and Separation of Small-Diameter Single-Walled Carbon Nanotubes. *Journal of the American Chemical Society* **2006,** 128, (37), 12239-12242.

39. Krishnan, A.; Dujardin, E.; Ebbesen, T. W.; Yianilos, P. N.; Treacy, M. M. J., Young's modulus of single-walled nanotubes. *Physical Review B* **1998,** 58, (20), 14013.

40. Fonseca, I.; Benito, J. A.; Mejia, I.; Jorba, J.; Roca, A., Changes on Young's modulus of steel C45E (EN 10083) by thermal treatment. *Revista De Metalurgia* **2002,** 38, (4), 249-255.

41. Berber, S.; Kwon, Y.-K.; Tomбnek, D., Unusually High Thermal Conductivity of Carbon Nanotubes. *Physical Review Letters* **2000,** 84, (20), 4613.

42. Lide, D. R., *CRC Handbook of Chemistry and Physics*. 83rd ed.; CRC Press LLC: Boca Raton, 2002; p 2664.

43. Nikolaev, P.; Bronikowski, M. J.; Bradley, R. K.; Rohmund, F.; Colbert, D. T.; Smith, K. A.; Smalley, R. E., Gas-phase catalytic growth of single-walled carbon nanotubes from carbon monoxide. *Chemical Physics Letters* **1999,** 313, (1-2), 91-97.

44. Pan, Z. W.; Xie, S. S.; Chang, B. H.; Wang, C. Y.; Lu, L.; Liu, W.; Zhou, W. Y.; Li, W. Z.; Qian, L. X., Very long carbon nanotubes. *Nature* **1998,** 394, (6694), 631-632.

45. Yang, C. M.; Kanoh, H.; Kaneko, K.; Yudasaka, M.; Iijima, S., Adsorption Behaviors of HiPco Single-Walled Carbon Nanotube Aggregates for Alcohol Vapors. *J. Phys. Chem. B* **2002,** 106, (35), 8994-8999.

46. Yang, C. M.; Kaneko, K.; Yudasaka, M.; Iijima, S., Effect of Purification on Pore Structure of HiPco Single-Walled Carbon Nanotube Aggregates. *Nano Letters* **2002,** 2, (4), 385-388.

47. Cinke, M.; Li, J.; Chen, B.; Cassell, A.; Delzeit, L.; Han, J.; Meyyappan, M., Pore structure of raw and purified HiPco single-walled carbon nanotubes. *Chemical Physics Letters* **2002,** 365, (1-2), 69-74.

48. Frank, S.; Poncharal, P.; Wang, Z. L.; Heer, W. A.; nbsp; de, Carbon Nanotube Quantum Resistors. *Science* **1998,** 280, (5370), 1744-1746.

49. Yao, Z.; Kane, C. L.; Dekker, C., High-Field Electrical Transport in Single-Wall Carbon Nanotubes. *Physical Review Letters* **2000,** 84, (13), 2941.

50. Iijima, S., Helical microtubules of graphitic carbon. *Nature* **1991,** 354, (6348), 56-8.

51. Thess, A.; Lee, R.; Nikolaev, P.; Dai, H.; Petit, P.; Robert, J.; Xu, C.; Lee, Y. H.; Kim, S. G.; Rinzler, A. G.; Colbert, D. T.; Scuseria, G. E.; Tomanek, D.; Fischer, J. E.; Smalley, R. E., Crystalline ropes of metallic carbon nanotubes. *Science (Washington, D. C.)* **1996,** 273, (5274), 483-487.

52. Ivanov, V.; Fonseca, A.; Nagy, J. B.; Lucas, A.; Lambin, P.; Bernaerts, D.; Zhang, X. B., Catalytic production and purification of nanotubules having fullerene-scale diameters. *Carbon* **1995,** 33, (12), 1727-1738.

53. Kang, Z.; Wang, E.; Mao, B.; Su, Z.; Chen, L.; Xu, L., Obtaining carbon nanotubes from grass. *Nanotechnology* **2005,** 16, (8), 1192-1195.

54. Derycke, V.; Martel, R.; Radosavljevic, M.; Ross, F.; Avouris, P., Catalyst-Free Growth of Ordered Single-Walled Carbon Nanotube Networks. *Nano Letters* **2002,** 2, (10), 1043-1046.

55. Bethune, D. S.; Klang, C. H.; de Vries, M. S.; Gorman, G.; Savoy, R.; Vazquez, J.; Beyers, R., Cobalt-catalysed growth of carbon nanotubes with single-atomic-layer walls. *Nature* **1993,** 363, (6430), 605-607.

56. Ebbesen, T. W.; Ajayan, P. M., Large-scale synthesis of carbon nanotubes. *Nature* **1992,** 358, (6383), 220-222.

57. Journet, C.; Maser, W. K.; Bernier, P.; Loiseau, A.; de la Chapelle, M. L.; Lefrant, S.; Deniard, P.; Lee, R.; Fischer, J. E., Large-scale production of single-walled carbon nanotubes by the electric-arc technique. *Nature* **1997,** 388, (6644), 756-758.

58. Kong, J.; Cassell, A. M.; Dai, H., Chemical vapor deposition of methane for single-walled carbon nanotubes. *Chemical Physics Letters* **1998,** 292, (4-6), 567-574.

59. Peng, X.; Koczkur, K.; Chen, A., Synthesis of well-aligned bamboo-like carbon nanotube arrays from ethanol and acetone. *Journal of Physics D-Applied Physics* **2008,** 41, (9), 6.

60. Bronikowski, M. J.; Willis, P. A.; Colbert, D. T.; Smith, K. A.; Smalley, R. E., Gas-phase production of carbon single-walled nanotubes from carbon monoxide via the HiPco process: A parametric study. *Journal of Vacuum Science & Technology A: Vacuum, Surfaces, and Films* **2001,** 19, (4), 1800–1805.

61. Chiang, I. W.; Brinson, B. E.; Huang, A. Y.; Willis, P. A.; Bronikowski, M. J.; Margrave, J. L.; Smalley, R. E.; Hauge, R. H., Purification and Characterization of Single-Wall Carbon Nanotubes (SWNTs) Obtained from the Gas-Phase Decomposition of CO (HiPco Process). *Journal of Physical Chemistry B* **2001,** 105, (35), 8297-8301.

62. Chiang, I. W.; Brinson, B. E.; Smalley, R. E.; Margrave, J. L.; Hauge, R. H., Purification and Characterization of Single-Wall Carbon Nanotubes. *Journal of Physical Chemistry B* **2001,** 105, (6), 1157-1161.

63. Hou, P.-X.; Liu, C.; Cheng, H.-M., Purification of carbon nanotubes. *Carbon* **2008,** 46, (15), 2003-2025.

64. Bandow, S.; Rao, A. M.; Williams, K. A.; Thess, A.; Smalley, R. E.; Eklund, P. C., Purification of Single-Wall Carbon Nanotubes by Microfiltration. *Journal of Physical Chemistry B* **1997,** 101, (44), 8839-8842.

65. Ebbesen, T. W.; Ajayan, P. M.; Hiura, H.; Tanigaki, K., Purification of nanotubes. *Nature* **1994,** 367, (6463), 519-519.

66. Erik Dujardin, T. W. E. A. K. M. M. J. T., Purification of Single-Shell Nanotubes. *Advanced Materials* **1998,** 10, (8), 611-613.

67. Ziegler, K. J.; Gu, Z.; Peng, H.; Flor, E. L.; Hauge, R. H.; Smalley, R. E., Controlled Oxidative Cutting of Single-Walled Carbon Nanotubes. *Journal of the American Chemical Society* **2005,** 127, (5), 1541-1547.

68. Wang, Y. H.; Shan, H.; Hauge, R. H.; Pasquali, M.; Smalley, R. E., A Highly Selective, One-Pot Purification Method for Single-Walled Carbon Nanotubes. *J. Phys. Chem. B* **2007,** 111, (6), 1249-1252.

69. Yang, C.-M.; Kaneko, K.; Yudasaka, M.; Iijima, S., Surface chemistry and pore structure of purified HiPco single-walled carbon nanotube aggregates. *Physica B: Condensed Matter* **2002,** 323, (1-4), 140-142.

70. Feng, X.; Matranga, C.; Vidic, R.; Borguet, E., A Vibrational Spectroscopic Study of the Fate of Oxygen-Containing Functional Groups and Trapped CO_2 in Single-Walled Carbon Nanotubes During Thermal Treatment. *Journal of Physical Chemistry B* **2004,** 108, (52), 19949-19954.

71. Kim, U. J.; Furtado, C. A.; Liu, X.; Chen, G.; Eklund, P. C., Raman and IR Spectroscopy of Chemically Processed Single-Walled Carbon Nanotubes. *Journal of the American Chemical Society* **2005,** 127, (44), 15437-15445.

72. Tanaka, K.; Yamabe, T.; Fukui, K.; Editors, *The Science and Technology of Carbon Nanotubes*. 1999; p 191 pp.

73. Rinzler, A. G.; Liu, J.; Dai, H.; Nikolaev, P.; Huffman, C. B.; Rodríguez-Macías, F. J.; Boul, P. J.; Lu, A. H.; Heymann, D.; Colbert, D. T.; Lee, R. S.; Fischer, J. E.; Rao, A. M.; Eklund, P. C.; Smalley, R. E., Large-scale purification of single-wall carbon nanotubes: process, product, and characterization. *Applied Physics A: Materials Science & Processing* **1998,** 67, (1), 29-37.

74. Martinez, M. T.; Callejas, M. A.; Benito, A. M.; Cochet, M.; Seeger, T.; Anson, A.; Schreiber, J.; Gordon, C.; Marhic, C.; Chauvet, O.; Maser, W. K., Modifications of single-wall carbon nanotubes upon oxidative purification treatments. *Nanotechnology* **2003,** 14, (7), 691-695.

75. Kuznetsova, A.; Popova, I.; Yates, J. T., Jr.; Bronikowski, M. J.; Huffman, C. B.; Liu, J.; Smalley, R. E.; Hwu, H. H.; Chen, J. G., Oxygen-Containing Functional Groups on Single-Wall Carbon Nanotubes: NEXAFS and Vibrational Spectroscopic Studies. *Journal of the American Chemical Society* **2001,** 123, (43), 10699-10704.

76. Martinez, M. T.; Callejas, M. A.; Benito, A. M.; Cochet, M.; Seeger, T.; Anson, A.; Schreiber, J.; Gordon, C.; Marhic, C.; Chauvet, O.; Fierro, J. L. G.; Maser, W. K., Sensitivity of single wall carbon nanotubes to oxidative processing: structural modification, intercalation and functionalisation. *Carbon* **2003,** 41, (12), 2247-2256.

77. Xu, Y. Q.; Peng, H.; Hauge, R. H.; Smalley, R. E., Controlled Multistep Purification of Single-Walled Carbon Nanotubes. *Nano Letters* **2005,** 5, (1), 163-168.

78. Strong, K. L.; Anderson, D. P.; Lafdi, K.; Kuhn, J. N., Purification process for single-wall carbon nanotubes. *Carbon* **2003,** 41, (8), 1477-1488.

79. Najafi, E.; Kim, J.-Y.; Han, S.-H.; Shin, K., UV-ozone treatment of multi-walled carbon nanotubes for enhanced organic solvent dispersion. *Colloids and Surfaces, A: Physicochemical and Engineering Aspects* **2006,** 284+285, 373-378.

80. Watts, P. C. P.; Mureau, N.; Tang, Z. N.; Miyajima, Y.; Carey, J. D.; Silva, S. R. P., The importance of oxygen-containing defects on carbon nanotubes for the detection of polar and non-polar vapours through hydrogen bond formation. *Nanotechnology* **2007,** 18, (17).

81. Hu, C.-C.; Su, J.-H.; Wen, T.-C., Modification of multi-walled carbon nanotubes for electric double-layer capacitors: Tube opening and surface functionalization. *Journal of Physics and Chemistry of Solids* **2007,** 68, (12), 2353-2362.

82. Kovtyukhova, N. I.; Mallouk, T. E.; Pan, L.; Dickey, E. C., Individual Single-Walled Nanotubes and Hydrogels Made by Oxidative Exfoliation of Carbon Nanotube Ropes. *Journal of the American Chemical Society* **2003,** 125, (32), 9761-9769.

83. Cai, L.; Bahr, J. L.; Yao, Y.; Tour, J. M., Ozonation of Single-Walled Carbon Nanotubes and Their Assemblies on Rigid Self-Assembled Monolayers. *Chem. Mater.* **2002,** 14, (10), 4235-4241.

84. Guo, D.-J.; Li, H.-L., High dispersion and electrocatalytic properties of palladium nanoparticles on single-walled carbon nanotubes. *Journal of Colloid and Interface Science* **2005,** 286, (1), 274-279.

85. Ramanathan, T.; Fisher, F. T.; Ruoff, R. S.; Brinson, L. C., Amino-Functionalized Carbon Nanotubes for Binding to Polymers and Biological Systems. *Chemistry of Materials* **2005,** 17, (6), 1290-1295.

86. Feng, X.; Dementev, N.; Feng, W.; Vidic, R.; Borguet, E., Detection of low concentration oxygen containing functional groups on activated carbon fiber surfaces through fluorescent labeling. *Carbon* **2006,** 44, (7), 1203-1209.

87. Xing, Y.; Borguet, E., Specificity and Sensitivity of Fluorescence Labeling of Surface Species. *Langmuir* **2007,** 23, (2), 684-688.

88. Figueiredo, J. L.; Pereira, M. F. R.; Freitas, M. M. A.; Orfao, J. J. M., Modification of the surface chemistry of activated carbons. *Carbon* **1999,** 37, (9), 1379-1389.

89. Figueiredo, J. L.; Pereira, M. F. R.; Freitas, M. M. A.; Orfao, J. J. M., Characterization of Active Sites on Carbon Catalysts. *Industrial and Engineering Chemistry Research* **2007,** 46, (12), 4110-4115.

90. Zielke, U.; Huttinger, K. J.; Hoffman, W. P., Surface-oxidized carbon fibers: I. Surface structure and chemistry. *Carbon* **1996,** 34, (8), 983-998.

91. Muckenhuber, H.; Grothe, H., The heterogeneous reaction between soot and NO2 at elevated temperature. *Carbon* **2006,** 44, (3), 546-559.

92. Muckenhuber, H.; Grothe, H., The reaction between soot and NO2 - investigation on functional groups using TPD-MS. *Topics in Catalysis* **2004,** 30/31, (1-4), 287-291.

93. Kim, U. J.; Liu, X. M.; Furtado, C. A.; Chen, G.; Saito, R.; Jiang, J.; Dresselhaus, M. S.; Eklund, P. C., Infrared-Active Vibrational Modes of Single-Walled Carbon Nanotubes. *Physical Review Letters* **2005,** 95, (15), 157402-4.

94. Sbai, K.; Rahmani, A.; Chadli, H.; Bantignies, J. L.; Hermet, P.; Sauvajol, J. L., Infrared Spectroscopy of Single-Walled Carbon Nanotubes. *Journal of Physical Chemistry B* **2006,** 110, (25), 12388-12393.

95. Bantignies, J. L.; Sauvajol, J. L.; Rahmani, A.; Flahaut, E., Infrared-active phonons in carbon nanotubes. *Physical Review B (Condensed Matter and Materials Physics)* **2006,** 74, (19), 195425-5.

96. Yumura, T.; Nozaki, D.; Bandow, S.; Yoshizawa, K.; Iijima, S., End-Cap Effects on Vibrational Structures of Finite-Length Carbon Nanotubes. *Journal of the American Chemical Society* **2005,** 127, (33), 11769-11776.

97. Furtado, C. A.; Kim, U. J.; Gutierrez, H. R.; Pan, L.; Dickey, E. C.; Eklund, P. C., Debundling and Dissolution of Single-Walled Carbon Nanotubes in Amide Solvents. *Journal of the American Chemical Society* **2004,** 126, (19), 6095-6105.

98. Dementev, N.; Feng, X.; Borguet, E., Fluorescence Labeling and Quantification of Oxygen-Containing Functionalities on the Surface of Single Walled Carbon Nanotubes. *submitted for publication*.

99. Kwon, S.; Borguet, E.; Vidic, R. D., Impact of Surface Heterogeneity on Mercury Uptake by Carbonaceous Sorbents under UHV and Atmospheric Pressure. *Environmental Science and Technology* **2002,** 36, (19), 4162-4169.

100. Feng, X. Application of single walled carbon nanotubes in environmental engineering: adsorption and desorption of environmentally relevant species studied by infrared spectroscopy and temperature programmed desorption. University of Pittsburgh, **2005**.

101. Kuznetsova, A.; Mawhinney, D. B.; Naumenko, V.; Yates, J. T.; Liu, J.; Smalley, R. E., Enhancement of adsorption inside of single-walled nanotubes: opening the entry ports. *Chemical Physics Letters* **2000,** 321, (3,4), 292-296.

102. Kuznetsova, A.; Yates, J. T., Jr.; Liu, J.; Smalley, R. E., Physical adsorption of xenon in open single walled carbon nanotubes. Observation of a quasi-one-dimensional confined Xe phase. *Journal of Chemical Physics* **2000,** 112, (21), 9590-9598.

103. Byl, O.; Liu, J. C.; Wang, Y.; Yim, W. L.; Johnson, J. K.; Yates, J. T., Unusual hydrogen bonding in water-filled carbon nanotubes. *Journal of the American Chemical Society* **2006,** 128, (37), 12090-12097.

104. Kuhlmann, U.; Jantoljak, H.; Pfander, N.; Bernier, P.; Journet, C.; Thomsen, C., Infrared active phonons in single-walled carbon nanotubes. *Chemical Physics Letters* **1998,** 294, (1-3), 237-240.

105. Kastner, J.; Pichler, T.; Kuzmany, H.; Curran, S.; Blau, W.; Weldon, D. N.; Delamesiere, M.; Draper, S.; Zandbergen, H., Resonance Raman and infrared spectroscopy of carbon nanotubes. *Chemical Physics Letters* **1994,** 221, (1-2), 53-58.

106. Branca, C.; Frusteri, F.; Magazu, V.; Mangione, A., Characterization of Carbon Nanotubes by TEM and Infrared Spectroscopy. *Journal of Physical Chemistry B* **2004,** 108, (11), 3469-3473.

107. Mawhinney, D. B.; Naumenko, V.; Kuznetsova, A.; Yates, J. T., Jr.; Liu, J.; Smalley, R. E., Infrared Spectral Evidence for the Etching of Carbon Nanotubes: Ozone Oxidation at 298 K. *Journal of the American Chemical Society* **2000,** 122, (10), 2383-2384.

108. Hamon, M. A.; Stensaas, K. L.; Sugar, M. A.; Tumminello, K. C.; Allred, A. K., Reacting soluble single-walled carbon nanotubes with singlet oxygen. *Chemical Physics Letters* **2007,** 447, (1-3), 1-4.

109. Zhou, J.-H.; Sui, Z.-J.; Zhu, J.; Li, P.; Chen, D.; Dai, Y.-C.; Yuan, W.-K., Characterization of surface oxygen complexes on carbon nanofibers by TPD, XPS and FT-IR. *Carbon* **2007,** 45, (4), 785-796.

110. Kondratyuk, P.; Yates, J., Molecular Views of Physical Adsorption Inside and Outside of Single-Wall Carbon Nanotubes. *Acc. Chem. Res.* **2007**.

111. Shi, W.; Johnson, J. K., Gas Adsorption on Heterogeneous Single-Walled Carbon Nanotube Bundles. *Physical Review Letters* **2003,** 91, (1), 015504.

112. LaBrosse, M. R.; Shi, W.; Johnson, J. K., Adsorption of Gases in Carbon Nanotubes: Are Defect Interstitial Sites Important? *Langmuir* **2008,** 24, (17), 9430-9439.

113. Kirk-Othmer Encyclopedia of Chemical Technology. In 5 ed.; Kirk, R. E.; Othmer, D. F.; Kroschwitz, J. I., Eds. John Wiley & Sons: New York, 2007.

114. Singh, H. B.; Ohara, D.; Herlth, D.; Sachse, W.; Blake, D. R.; Bradshaw, J. D.; Kanakidou, M.; Crutzen, P. J., Acetone in the atmosphere: distribution, sources, and sinks. *Journal of Geophysical Research, [Atmospheres]* **1994,** 99, (D1), 1805-19.

115. VanItallie, T. B.; Nufert, T. H., Ketones: Metabolism's ugly duckling. *Nutrition Reviews* **2003,** 61, (10), 327-341.

116. Snow, E. S.; Perkins, F. K., Capacitance and Conductance of Single-Walled Carbon Nanotubes in the Presence of Chemical Vapors. *Nano Letters* **2005,** 5, (12), 2414-2417.

117. Guirado-Lopez, R. A.; Sanchez, M.; Rincon, M. E., Interaction of Acetone Molecules with Carbon-Nanotube-Supported TiO_2 Nanoparticles: Possible Applications as Room Temperature Molecular Sensitive Coatings. *Journal of Physical Chemistry C* **2007,** 111, (1), 57-65.

118. Federici, M. O.; Benedetti, M. M., Ketone bodies monitoring. *Diabetes Research and Clinical Practice* **2006,** 74, (Supplement 2), S77-S81.

119. Kwon, S.; Russell, J.; Zhao, X.; Vidic, R. D.; Johnson, J. K.; Borguet, E., Combined Experimental and Theoretical Investigation of Polar Organic Adsorption/Desorption from Model Carbonaceous Surfaces: Acetone on Graphite. *Langmuir* **2002,** 18, (7), 2595-2600.

120. Kwon, S.; Vidic, R.; Borguet, E., The effect of surface chemical functional groups on the adsorption and desorption of a polar molecule, acetone, from a model carbonaceous surface, graphite. *Surface Science* **2003,** 522, (1-3), 17-26.

121. Chakrapani, N.; Zhang, Y. M.; Nayak, S. K.; Moore, J. A.; Carroll, D. L.; Choi, Y. Y.; Ajayan, P. M., Chemisorption of Acetone on Carbon Nanotubes. *Journal of Physical Chemistry B* **2003,** 107, (35), 9308-9311.

122. Shih, Y.-h.; Li, M.-s., Adsorption of selected volatile organic vapors on multiwall carbon nanotubes. *Journal of Hazardous Materials* **2008,** 154, (1-3), 21-28.

123. Redhead, P. A., Thermal desorption of gases. *Vacuum* **1962,** 12, 203-11.

124. Elstner, M.; Hobza, P.; Frauenheim, T.; Suhai, S.; Kaxiras, E., Hydrogen bonding and stacking interactions of nucleic acid base pairs: A density-functional-theory based treatment. *Journal of Chemical Physics* **2001,** 114, 5149-5155.

125. Elstner, M.; Porezag, D.; Jungnickel, G.; Elsner, J.; Haugk, M.; Frauenheim, T.; Suhai, S.; Seifert, G., Self-consistent-charge density-functional tight-binding method for simulations of complex materials properties. *Physical Review B* **1998,** 58, 7260-7268.

126. Weigend, F.; Koehn, A.; Haettig, S., Efficient use of the correlation consistent basis sets in resolution of the identity MP2 calculations. *Journal of Chemical Physics* **2002,** 116, (8), 3175-3183.

127. Schäfer, A.; Horn, H.; Ahlrichs, R., Fully optimized contracted Gaussian basis sets for atoms Li to Kr. *Journal of Chemical Physics* **1992,** 97, (4), 2571-2577.

128. Schäfer, A.; Huber, C.; Ahlrichs, R., Fully optimized contracted Gaussian basis sets of triple zeta valence quality for atoms Li to Kr. *Journal of Chemical Physics* **1994,** 100, (8), 5829-5835.

129. Weigend, F.; Furche, F.; Ahlrichs, R., Gaussian basis sets of quadruple zeta valence quality for atoms H-Kr. *Journal of Chemical Physics* **2003,** 119, 12753-12762.

130. Boys, S. F.; Bernardi, F., The calculation of small molecular interactions by the differences of separate total energies. Some procedures with reduced errors. *Molecular Physics* **1970,** 19, (4), 553-566.

131. Lin, C. S.; Zhang, R. Q.; Lee, S. T.; Elstner, M.; Frauenheim, T.; Wan, L. J., Simulation of Water Cluster Assembly on a Graphite Surface. *J. Phys. Chem. B* **2005,** 109, 14183-14188.

132. Pankewitz, T.; Klopper, W., Ab Initio Modeling of Methanol Interaction with Single-Walled Carbon Nanotubes *J. Phys. Chem. C* **2007,** 111, (51), 18917-18926.

133. Zhechkov, L.; Heine, T.; Patchkovskii, S.; Seifert, G.; Duarte, H. A., An Efficient a Posteriori Treatment for Dispersion Interaction in Density-Functional-Based Tight Binding. *Journal of Chemical Theory and Computation* **2005,** 1, (5), 841-847.

134. Kubar, T.; Hanus, M.; Ryjacek, F.; Hobza, P., Binding of cationic and neutral phenanthridine Intercalators to a DNA oligomer is controlled by dispersion energy: Quantum chemical calculations and molecular mechanics simulations. *Chemistry-a European Journal* **2006,** 12, (1), 280-290.

135. Ajayan, P. M.; Ebbesen, T. W., Nanometre-size tubes of carbon. *Reports on Progress in Physics* **1997,** 60, (10), 1025-1062.

136. Girifalco, L. A.; Hodak, M.; Lee, R. S., Carbon nanotubes, buckyballs, ropes, and a universal graphitic potential. *Physical Review B: Condensed Matter and Materials Physics* **2000,** 62, (19), 13104-13110.

137. Maniwa, Y.; Kataura, H.; Abe, M.; Suzuki, S.; Achiba, Y.; Kira, H.; Matsuda, K., Phase transition in confined water inside carbon nanotubes. *Journal of the Physical Society of Japan* **2002,** 71, (12), 2863-2866.

138. Talapatra, S.; Zambano, A. Z.; Weber, S. E.; Migone, A. D., Gases Do Not Adsorb on the Interstitial Channels of Closed-Ended Single-Walled Carbon Nanotube Bundles. *Physical Review Letters* **2000,** 85, (1), 138.

139. Rols, S.; Johnson, M. R.; Zeppenfeld, P.; Bienfait, M.; Vilches, O. E.; Schneble, J., Argon adsorption in open-ended single-wall carbon nanotubes. *Physical Review B (Condensed Matter and Materials Physics)* **2005,** 71, (15), 155411.

140. Burghaus, U.; Bye, D.; Cosert, K.; Goering, J.; Guerard, A.; Kadossov, E.; Lee, E.; Nadoyama, Y.; Richter, N.; Schaefer, E.; Smith, J.; Ulness, D.; Wymore, B., Methanol adsorption in carbon nanotubes. *Chemical Physics Letters* **2007,** 442, (4-6), 344-347.

141. Krasheninnikov, A. V.; Nordlund, K.; Keinonen, J., Production of defects in supported carbon nanotubes under ion irradiation. *Physical Review B* **2002,** 65, (16), 165423.

142. Zheng, G.; Irle, S.; Elstner, M.; Morokuma, K., Quantum Chemical Molecular Dynamics Model Study of Fullerene Formation from Open-Ended Carbon Nanotubes. *Journal of Physical Chemistry A* **2004,** 108, (15), 3182-3194.

143. Geng, H. Z.; Zhang, X. B.; Mao, S. H.; Kleinhammes, A.; Shimoda, H.; Wu, Y.; Zhou, O., Opening and closing of single-wall carbon nanotubes. *Chemical Physics Letters* **2004,** 399, (1-3), 109-113.

144. Fang, S. L.; Rao, A. M.; Eklund, P. C.; Nikolaev, P.; Rinzler, A. G.; Smalley, R. E., Raman scattering study of coalesced single walled carbon nanotubes. *Journal of Materials Research* **1998,** 13, (9), 2405-2411.

145. Kim, U. J.; Gutierrez, H. R.; Kim, J. P.; Eklund, P. C., Effect of the Tube Diameter Distribution on the High-Temperature Structural Modification of Bundled Single-Walled Carbon Nanotubes. *Journal of Physical Chemistry B* **2005,** 109, (49), 23358-23365.

146. Do, D. D., *Adsorption Analysis: Equilibria and Kinetics*. Imperial College Press: 1998.

147. Gregg, S. J.; Sing, K. S., *Adsorption, Surface Area, and Porosity*. Second ed.; Academic Press: 1982.

148. Khazaei, M.; Dean, K. A.; Farajian, A. A.; Kawazoe, Y., Field Emission Signature of Pentagons at Carbon Nanotube Caps. *J. Phys. Chem. C* **2007,** 111, (18), 6690-6693.

149. Kowalska, E.; Kowalczyk, P.; Radomska, J.; Czerwosz, E.; Wronka, H.; Bystrzejewski, M., Influence of high vacuum annealing treatment on some properties of carbon nanotubes. *Journal of Thermal Analysis and Calorimetry* **2006,** 86, (1), 115-119.

150. Mulliken, R. S., *Journal of Chemical Physics* **1949,** 46, 497.

151. Mulliken, R. S., *Journal of Chemical Physics* **1949,** 46, 675.

152. Heinzmann, R.; Ahlrichs, R., *Theoretical Chemical Acta* **1976,** 42, 33.

153. Ellison, M. D.; Morris, S. T.; Sender, M. R.; Brigham, J.; Padgett, N. E., Infrared and Computational Studies of the Adsorption of Methanol and Ethanol on Single-Walled Carbon Nanotubes. *Journal of Physical Chemistry C* **2007,** 111, (49), 18127-18134.

154. Zheng, G. S.; Wang, Z.; Irle, S.; Morokuma, K., Origin of the linear relationship between CH_2/NH/O-SWNT reaction energies and sidewall curvature: Armchair nanotubes. *Journal of the American Chemical Society* **2006,** 128, (47), 15117-15126.

155. Noy, A.; Park, H. G.; Fornasiero, F.; Holt, J. K.; Grigoropoulos, C. P.; Bakajin, O., Nanofluidics in carbon nanotubes. *Nano Today* **2007,** 2, (6), 22-29.

156. Holt, J. K.; Park, H. G.; Wang, Y.; Stadermann, M.; Artyukhin, A. B.; Grigoropoulos, C. P.; Noy, A.; Bakajin, O., Fast Mass Transport Through Sub-2-Nanometer Carbon Nanotubes. *Science* **2006,** 312, (5776), 1034-1037.

157. Lee, J.; Park, J.; Kim, J.; Yi, W., Efficient visible photoluminescence from encapsulation of fluorescent materials inside single-walled carbon nanotubes. *Colloids and Surfaces A: Physicochemical and Engineering Aspects* **2008,** 313-314, 296-299.

158. Matranga, C.; Bockrath, B., Hydrogen-bonded and physisorbed CO in single-walled carbon nanotube bundles. *Journal of Physical Chemistry B* **2005,** 109, (11), 4853.

159. Kazachkin, D.; Nishimura, Y.; Irle, S.; Morokuma, K.; Vidic, R. D.; Borguet, E., Interaction of Acetone with Single Wall Carbon Nanotubes at Cryogenic Temperatures: A Combined Temperature Programmed Desorption and Theoretical Study. *Langmuir* **2008,** 24, (15), 7848-7856.

160. Lu, L.; Shao, Q.; Huang, L.; Lu, X., Simulation of adsorption and separation of ethanol-water mixture with zeolite and carbon nanotube. *Fluid Phase Equilibria* **2007,** 261, (1-2), 191-198.

161. Shao, Q.; Huang, L.; Zhou, J.; Lu, L.; Zhang, L.; Lu, X.; Jiang, S.; Gubbins, K. E.; Zhu, Y.; Shen, W., Molecular Dynamics Study on Diameter Effect in Structure of Ethanol Molecules Confined in Single-Walled Carbon Nanotubes. *J. Phys. Chem. C* **2007,** 111, (43), 15677-15685.

162. Carmo, M.; Paganin, V. A.; Rosolen, J. M.; Gonzalez, E. R., Alternative supports for the preparation of catalysts for low-temperature fuel cells: the use of carbon nanotubes. *Journal of Power Sources* **2005,** 142, (1-2), 169-176.

163. Contreras-Torres, F. F.; Basiuk, V. A., ONIOM Studies of Esterification at Oxidized Carbon Nanotube Tips. *Journal of Physics: Conference Series* **2007,** 61, (1), 85.

164. Basiuk, V. A., Reactivity of Carboxylic Groups on Armchair and Zigzag Carbon Nanotube Tips: A Theoretical Study of Esterification with Methanol. *Nano Letters* **2002,** 2, (8), 835-839.

165. Fu, K.; Kitaygorodskiy, A.; Rao, A. M.; Sun, Y. P., Deuterium Attachment to Carbon Nanotubes in Solution. *Nano Letters* **2002,** 2, (10), 1165-1168.

166. Fu, K.; Li, H.; Zhou, B.; Kitaygorodskiy, A.; Allard, L. F.; Sun, Y. P., Deuterium Attachment to Carbon Nanotubes in Deuterated Water. *Journal of the American Chemical Society* **2004,** 126, (14), 4669-4675.

167. Goering, J.; Kadossov, E.; Burghaus, U., Adsorption Kinetics of Alcohols on Single-Wall Carbon Nanotubes: An Ultrahigh Vacuum Surface Chemistry Study. *J. Phys. Chem. C* **2008,** 112, (27), 10114-10124.

168. Donnet, J. B.; Bansai, R. C.; Wang, M. J.; Editors, *Carbon Black: Science and Technology, Second Edition*. 1993; p 461 pp.

169. Bradley, R. H.; Sutherland, I.; Sheng, E., Carbon surface: area, porosity, chemistry, and energy. *Journal of Colloid and Interface Science* **1996,** 179, (2), 561-569.

170. Matranga, C.; Bockrath, B., Controlled Confinement and Release of Gases in Single-Walled Carbon Nanotube Bundles. *Journal of Physical Chemistry B* **2005,** 109, (19), 9209-9215.

171. Zhuang, Q. L.; Kyotani, T.; Tomita, A., DRIFT and TK/TPD Analyses of Surface Oxygen Complexes Formed during Carbon Gasification. *Energy Fuels* **1994,** 8, (3), 714-718.

172. Grimme, S., Accurate description of van der Waals complexes by density functional theory including empirical corrections. *Journal of Computational Chemistry* **2004,** 25, (12), 1463-1473.

173. Hashimoto, A.; Suenaga, K.; Gloter, A.; Urita, K.; Iijima, S., Direct evidence for atomic defects in graphene layers. *Nature* **2004,** 430, (7002), 870-873.

174. Szabados, A.; Biro, L. P.; Surjan, P. R., Intertube interactions in carbon nanotube bundles. *Physical Review B (Condensed Matter and Materials Physics)* **2006,** 73, (19), 195404-9.

175. Huang, C.-C.; Lin, Y.; Lu, F., Dynamic Adsorption of Organic Solvent Vapors onto a Packed Bed of Activated Carbon Cloth. *Separation Science & Technology* **1999,** 34, (4), 555.

176. Khan, F. I.; Kr. Ghoshal, A., Removal of Volatile Organic Compounds from polluted air. *Journal of Loss Prevention in the Process Industries* **2000,** 13, (6), 527-545.

177. Li, Q.-L.; Yuan, D.-X.; Lin, Q.-M., Evaluation of multi-walled carbon nanotubes as an adsorbent for trapping volatile organic compounds from environmental samples. *Journal of Chromatography, A* **2004,** 1026, (1-2), 283-288.

178. Liu, J.-M.; Li, L.; Fan, H.-L.; Ning, Z.-W.; Zhao, P., Evaluation of Single-walled Carbon Nanotubes as Novel Adsorbent for Volatile Organic Compounds. *Chinese Journal of Analytical Chemistry* **2007,** 35, (6), 830-834.

179. Ulbricht, H.; Zacharia, R.; Cindir, N.; Hertel, T., Thermal desorption of gases and solvents from graphite and carbon nanotube surfaces. *Carbon* **2006,** 44, (14), 2931-2942.

180. Tournus, F.; Charlier, J. C., Ab initio study of benzene adsorption on carbon nanotubes. *Physical Review B (Condensed Matter and Materials Physics)* **2005,** 71, (16), 165421.

181. Brukh, R.; Sae-Khow, O.; Mitra, S., Stabilizing single-walled carbon nanotubes by removal of residual metal catalysts. *Chemical Physics Letters* **2008,** 459, (1-6), 149-152.

182. Silverstein, R. M.; Webster, F. X., *Spectrometric Identification of Organic Compounds, 6th Edition*. 1997; p 496 pp.

183. Leonhardt, A.; Ritschel, M.; Kozhuharova, R.; Graff, A.; Muhl, T.; Huhle, R.; Monch, I.; Elefant, D.; Schneider, C. M., Synthesis and properties of filled carbon nanotubes. *Diamond and Related Materials* **2003,** 12, (3-7), 790-793.

184. Kam, N. W. S.; O'Connell, M.; Wisdom, J. A.; Dai, H. J., Carbon nanotubes as multifunctional biological transporters and near-infrared agents for selective cancer cell destruction. *Proceedings of the National Academy of Sciences of the United States of America* **2005,** 102, (33), 11600-11605.

185. Bianco, A.; Kostarelos, K.; Partidos, C. D.; Prato, M., Biomedical applications of functionalised carbon nanotubes. *Chemical Communications* **2005**, (5), 571-577.

186. Serp, P.; Corrias, M.; Kalck, P., Carbon nanotubes and nanofibers in catalysis. *Applied Catalysis A: General* **2003,** 253, (2), 337-358.

187. Planeix, J. M.; Coustel, N.; Coq, B.; Brotons, V.; Kumbhar, P. S.; Dutartre, R.; Geneste, P.; Bernier, P.; Ajayan, P. M., Application of Carbon Nanotubes as Supports in Heterogeneous Catalysis. *Journal of the American Chemical Society* **1994,** 116, (17), 7935-7936.

188. Gogotsi, Y.; Naguib, N.; Libera, J. A., In situ chemical experiments in carbon nanotubes. *Chemical Physics Letters* **2002,** 365, (3-4), 354-360.

189. Jiawei Wang; Marina K. Kuimova; Martyn Poliakoff; G. Andrew D. Briggs; Khlobystov, A. N., Encapsulation and IR Probing of Cube-Shaped Octasilasesquioxane $H_8Si_8O_{12}$ in Carbon Nanotubes. *Angewandte Chemie International Edition* **2006,** 45, (31), 5188-5191.

190. Smith, B. W.; Monthioux, M.; Luzzi, D. E., Carbon nanotube encapsulated fullerenes: a unique class of hybrid materials. *Chemical Physics Letters* **1999,** 315, (1-2), 31-36.

191. Li, Y. F.; Hatakeyama, R.; Kaneko, T.; Izumida, T.; Okada, T.; Kato, T., Synthesis and electronic properties of ferrocene-filled double-walled carbon nanotubes. *Nanotechnology* **2006,** 17, (16), 4143-4147.

192. Matranga, C.; Chen, L.; Smith, M.; Bittner, E.; Johnson, J. K.; Bockrath, B., Trapped CO_2 in Carbon Nanotube Bundles. *J. Phys. Chem. B* **2003,** 107, (47), 12930-12941.

193. Byl, O.; Kondratyuk, P.; Yates, J. T., Adsorption and Dimerization of NO Inside Single-Walled Carbon Nanotubes-An Infrared Spectroscopic Study. *Journal of Physical Chemistry B* **2003,** 107, (18), 4277-4279.

194. Byl, O.; Kondratyuk, P.; Forth, S. T.; FitzGerald, S. A.; Chen, L.; Johnson, J. K.; Yates, J. T., Jr., Adsorption of CF_4 on the Internal and External Surfaces of Opened Single-Walled Carbon Nanotubes: A Vibrational Spectroscopy Study. *Journal of the American Chemical Society* **2003,** 125, (19), 5889-5896.

195. Ellison, M. D.; Crotty, M. J.; Koh, D.; Spray, R. L.; Tate, K. E., Adsorption of NH_3 and NO_2 on Single-Walled Carbon Nanotubes. *Journal of Physical Chemistry B* **2004,** 108, (23), 7938-7943.

196. Nishide, D.; Dohi, H.; Wakabayashi, T.; Nishibori, E.; Aoyagi, S.; Ishida, M.; Kikuchi, S.; Kitaura, R.; Sugai, T.; Sakata, M.; Shinohara, H., Single-wall carbon nanotubes encaging linear chain C10H2 polyyne molecules inside. *Chemical Physics Letters* **2006,** 428, (4-6), 356-360.

197. Yim, W.-L.; Byl, O.; Yates, J. T., Jr.; Johnson, J. K., Vibrational behavior of adsorbed CO2 on single-walled carbon nanotubes. *Journal of Chemical Physics* **2004,** 120, (11), 5377-5386.

198. Itkis, M. E.; Perea, D. E.; Niyogi, S.; Rickard, S. M.; Hamon, M. A.; Hu, H.; Zhao, B.; Haddon, R. C., Purity Evaluation of As-Prepared Single-Walled Carbon Nanotube Soot by Use of Solution-Phase Near-IR Spectroscopy. *Nano Letters* **2003,** 3, (3), 309-314.

199. Britz, D. A.; Khlobystov, A. N., Noncovalent interactions of molecules with single walled carbon nanotubes. *Chemical Society Reviews* **2006,** 35, (7), 637-659.

200. Akolekar, D. B.; Bhargava, S. K., NO and CO adsorption studies on transition metal-exchanged silico-aluminophosphate of type 34 catalysts. *Applied Catalysis a-General* **2001,** 207, (1-2), 355-365.

201. Li, Y. J.; Slager, T. L.; Armor, J. N., Selective Reduction of NOx by Methane on Co-Ferrierites : II. Catalyst Characterization. *Journal of Catalysis* **1994,** 150, (2), 388-399.

202. Erley, W., Infrared spectroscopy of NO adsorbed on Ni(111) at 85 K. *Surface Science* **1988,** 205, (1-2), L771-L776.

203. Mihaylov, M.; Hadjiivanov, K., FTIR Study of CO and NO Adsorption and Coadsorption on Ni-ZSM-5 and Ni/SiO2. *Langmuir* **2002,** 18, (11), 4376-4383.

204. Penkova, A.; Dzwigaj, S.; Kefirov, R.; Hadjiivanov, K.; Che, M., Effect of the Preparation Method on the State of Nickel Ions in BEA Zeolites. A Study by Fourier Transform Infrared Spectroscopy of Adsorbed CO and NO, Temperature-Programmed Reduction, and X-Ray Diffraction. *The Journal of Physical Chemistry C* **2007,** 111, (24), 8623-8631.

205. Kondratyuk, P.; Wang, Y.; Johnson, J. K.; Yates, J. T., Jr., Observation of a One-Dimensional Adsorption Site on Carbon Nanotubes: Adsorption of Alkanes of Different Molecular Lengths. *Journal of Physical Chemistry B* **2005,** 109, (44), 20999-21005.

206. Kondratyuk, P.; Yates, J. T., Desorption kinetic detection of different adsorption sites on opened carbon single walled nanotubes: The adsorption of n-nonane and CCl_4. *Chemical Physics Letters* **2005,** 410, (4-6), 324-329.

207. Li, Y.; Lu, D.; Schulten, K.; Ravaioli, U.; Rotkin, S. V., Screening of water dipoles inside finite-length armchair carbon nanotubes. *Journal of Computational Electronics* **2005,** 4, (1/2), 161-165.

208. Setyowati, K.; Piao, M. J.; Chen, J.; Liu, H., Carbon nanotube surface attenuated infrared absorption. *Applied Physics Letters* **2008,** 92, (4), 043105-3.